博士論文

Characterization of AAG8 as an oncoprotein

（がん蛋白質 AAG8 の機能解析）

Department of Bioengineering

SUN Bing

孫　兵

July 28, 2014

Contents

Chapter 1 General Introduction

1. Background

1.1 Cancer

The systematic translation of fundamental cancer research data into knowledge of tumor biology and therapeutic possibilities still remains challenging. Such efforts should be greatly aided by robust preclinical investigation systems that reflect the intrinsic property of cancer and for which detailed molecular mechanisms and pharmacological annotations are available. Cancer also links to the other diseases. For example, senescence-associated secretory phenotype has crucial roles in promoting obesity-associated

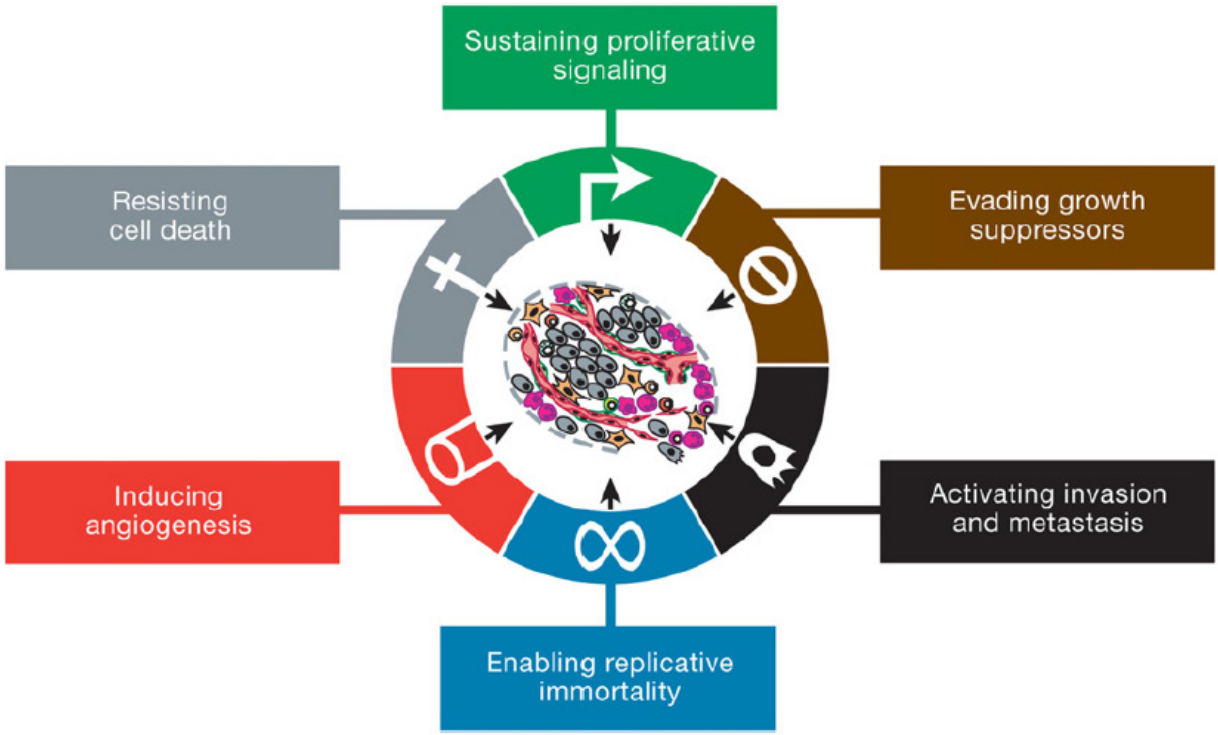

Figure 1-1 The Hallmarks of Cancer. The past decade has witnessed remarkable progress toward understanding the mechanistic underpinnings of each hallmark. (Hanahan, D. & Weinberg, R. A., Cell, 2011)

hepatocellular carcinoma development, providing valuable new insights into the development of obesity-associated cancer.[1] The six hallmarks of cancer—distinctive and complementary capabilities that enable tumor growth and metastatic dissemination—continue to provide a solid foundation for understanding carcinogenesis (Figure 1-1).[2] The intracellular integrated circuits can be segmented into distinct subcircuits, each of which is specialized to support a discrete cell-biological property in normal cells and is

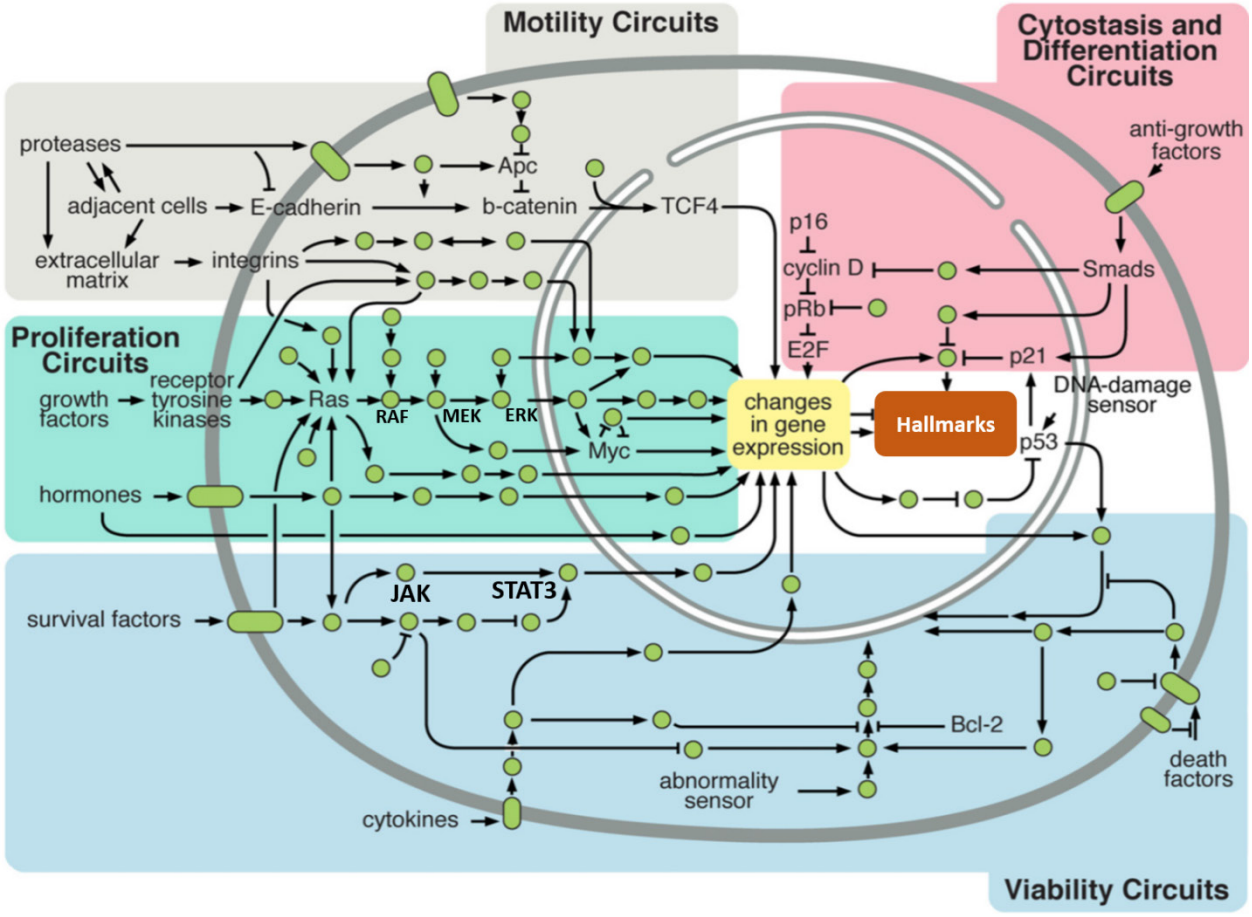

Figure 1-2 Intracellular signaling networks regulate the operations of the cancer cell. An elaborate integrated circuit operates within normal cells and is reprogrammed to regulate hallmark capabilities within cancer cells. Separate subcircuits, depicted here in differently colored fields, are specialized to orchestrate the various capabilities. At one level, this depiction is simplistic, as there is considerable crosstalk between such subcircuits. (Modified from Hanahan, D. & Weinberg, R. A., Cell, 2011)

reprogrammed in order to implement the hallmarks in cancer cells (Figure 1-2).[2] Importantly, changes in gene expression play central roles in these networks formed by various of distinct circuits and contribute to cancer hallmarks. Comprehensive knowledge of the genes underlying cancer is a critical foundation for cancer therapy. Now the major international projects are underway aimed at creating a comprehensive catalogue of all the genes responsible for the initiation and progression of cancer.[3] Previous cancer studies have led to the identification of scores of cancer-associated genes, including both tumor suppressor genes and oncogenes. Substantially, large-scale analysis of the cancer genome has provided an unprecedentedly detailed picture of cancer, which has been, and continues to serve as, a blueprint for the development of molecular-targeted therapies.[4]

Tumor suppressor genes encode a broad class of molecules whose downregulation (lost or markedly reduced or mutational attenuation) contributes to malignant progression. As a well-known instance, a mouse model demonstrated that deleted in colorectal carcinoma (DCC) functions as a tumor suppressor via its ability to trigger tumor cell apoptosis[5] and limits survival of disseminated tumor cells[6]. In addition, the well-established p53 tumor suppressor has been attractive during the past decades. The latest report found that transient p53-p21 activation and cell-cycle arrest promoted cell survival by efficiently channeling depleted serine stores to glutathione synthesis, thus preserving cellular anti-oxidant capacity. Cells lacking p53 failed to complete the response to serine depletion, resulting in oxidative stress, reduced viability and severely impaired proliferation, indicating that serine depletion has a potential role in the treatment of p53-deficient tumors.[7]

Targeted therapies directed against amplified or mutant-activated key driver oncoproteins have demonstrated efficacy against specific subsets of molecularly defined cancers and provided encouraging clinical implications. Oncoprotein triggers the activation of oncogenetic signaling pathways, such as mTOR signalling[8] and AMP-activated protein kinase (AMPK) pathways[9], during carcinogenesis and metastasis. For instance, as a typical oncoprotein, COUP transcription factor II (COUP-TFII), a member of the nuclear receptor superfamily, serves as a key regulator to inhibit SMAD4-dependent transcription, and consequently overrides the TGFβ-dependent checkpoint for PTEN-null indolent tumors (Figure 1-3).[10]

Some oncogenes even exert the tumor-promoting effects by their RNA format after transcription. An outstanding study demonstrated that HMGA2 (a well-known oncoprorein) mRNA promotes lung cancer progression by operating as a competing endogenous RNA (ceRNA) for the let-7 microRNA (miRNA) family. HMGA2 can promote the transformation of lung cancer cells independent of protein-coding function but dependent upon the presence of let-7 sites; mechanistically, TGFBR3 serves as a putative target of HMGA2 ceRNA function.[11] These findings highlight the vital roles of oncogenes in their functions as ceRNAs and emphasize the ceRNAs as novel pools of therapeutic targets.

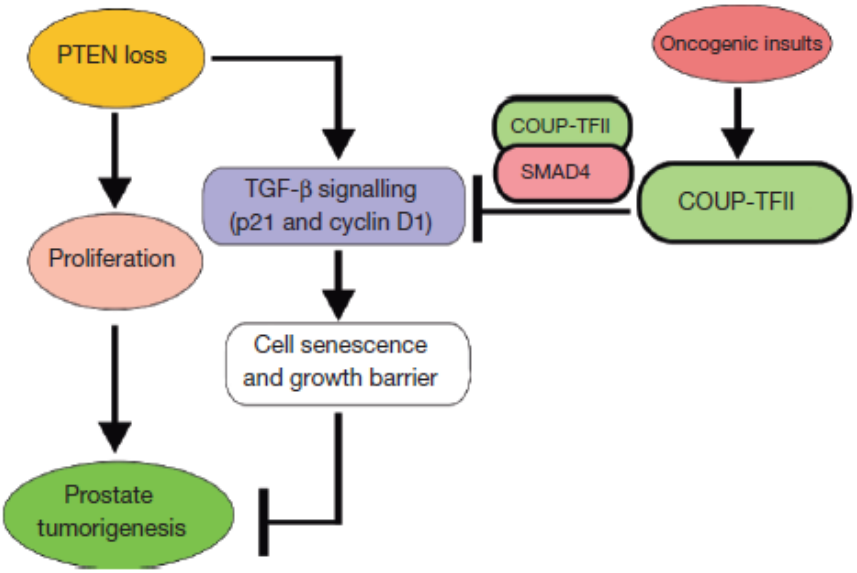

Figure 1-3 Model of COUP-TFII in prostate tumorigenesis. PTEN inactivation drives prostate tumor initiation and progression. However, it also elicits the activation of TGFβ signalling that induces cellular senescence to constrain the indolent tumor from becoming aggressive. To develop metastasis-prone tumors, alternative oncogenic signals stimulate COUP-TFII expression, which counteracts the TGFβ-dependent checkpoint through direct association with SMAD4. Thus, COUP-TFII serves as a crucial regulator that counteracts the TGFβ-dependent growth barrier to enable indolent prostate cancer tumors to acquire metastatic potential. (Qin, J. *et al.* Nature, 2013)

1.2 Aging-associated gene 8 (AAG8)

AAG8, encoded by the *SIGMAR1* gene, was originally considered an enigmatic polypeptide and has recently been identified as a unique ligand-regulated chaperone protein. AAG8 is widely expressed with higher expression in liver, colon, prostate, placenta, small intestine, heart and pancreas (Figure 1-4, 1-5). It is also expressed in the retina by retinal pigment epithelial cells (Figure 1-5).

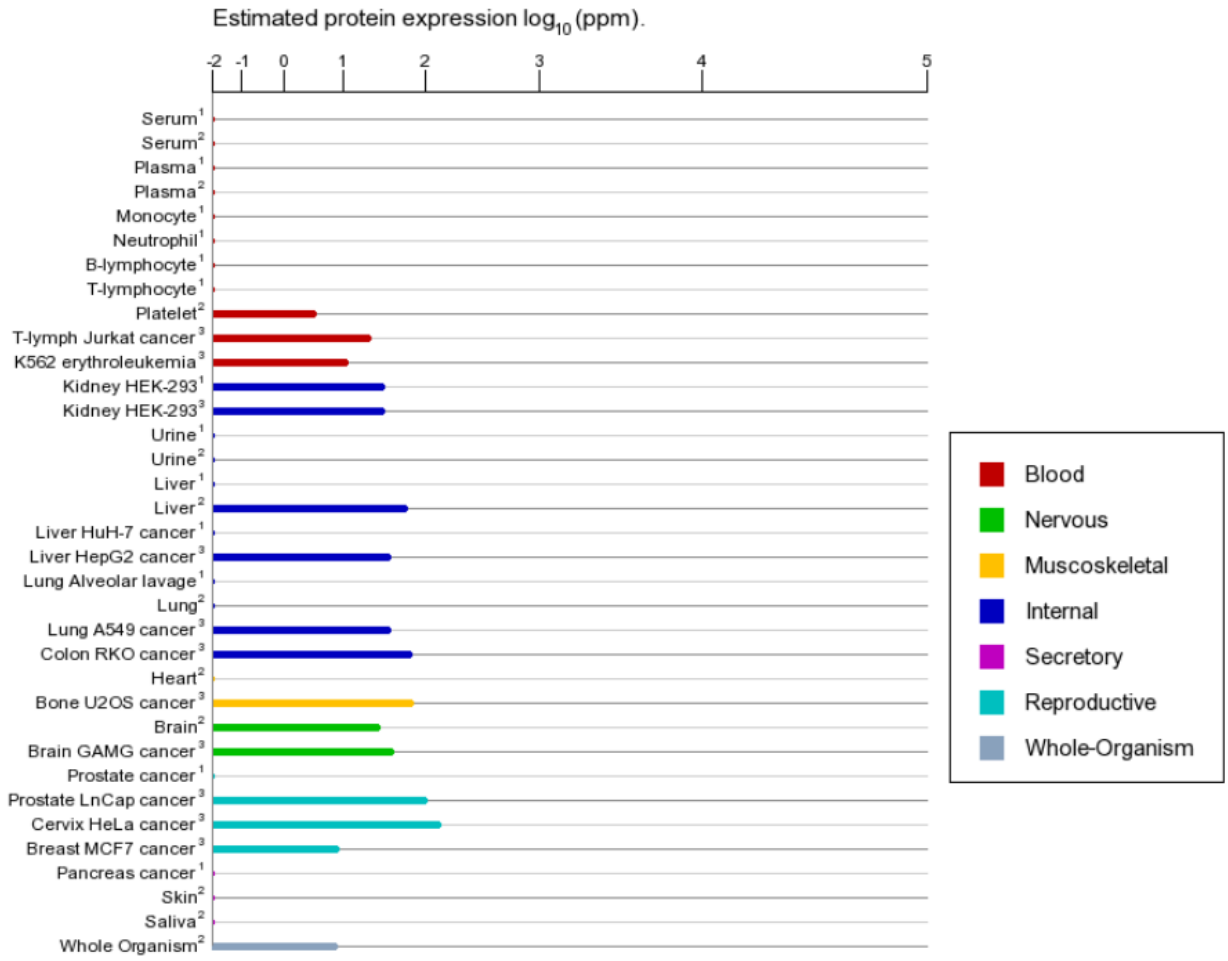

Figure 1-4 AAG8 expression pattern in normal and cancer cells. (Data from Genecard databases. 1: MOPED database; 2: PaxDb database; 3: MAXQB database. http://www.genecards.org/cgi-bin/carddisp.pl?gene=SIGMAR1)

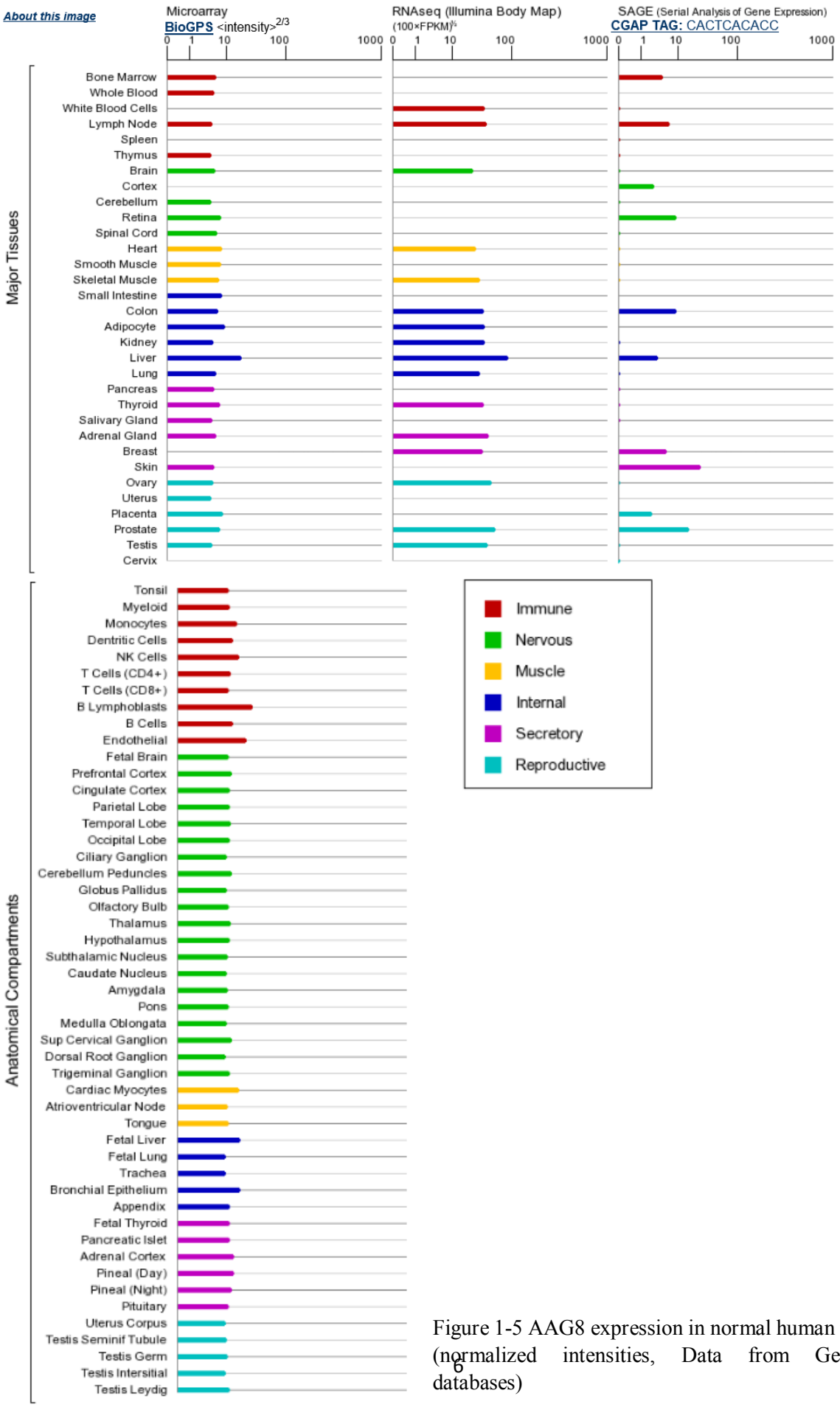

Figure 1-5 AAG8 expression in normal human tissues (normalized intensities, Data from Genecard databases)

The chaperone domain of AAG8 is C-terminal to two putative transmembrane domains (residues 11-29 and 80-100) but contains a predicted membrane associated region (residues ~176-204) containing two cholesterol recognition motifs (CRM) (Figure 1-6). Solution NMR spectroscopy studies found that the chaperone domain contains a helix at the N terminus followed by a largely dynamic region and a structured, helical C-terminal region that encompasses a membrane associated domain containing four helices. The helical region at residues ~198-206 is amphipathic and proposed to anchor the chaperone domain to micelles and membranes. Three of the helices in the C-terminal region closely correspond to cholesterol and drug recognition sites. In addition, the chaperone domain interacts with HSP70 binding immunoglobulin protein (BiP) and regulates the inositol triphosphate receptor calcium channel.[12] AAG8 may exist naturally in equilibrium among monomeric, dimeric, and/or oligomeric forms according to an AAG8 ligand-based structural prediction study (Figure 1-7).[13]

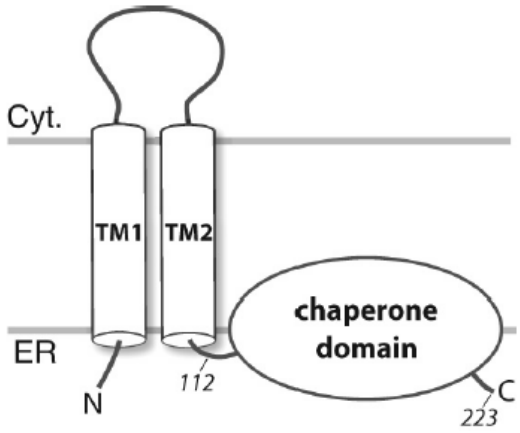

Figure 1-6 Full-length AAG8 topology schematic showing two predicted transmembrane helices (TM1 and TM2) and the membrane-associated domain. The N and C termini and the approximate positions of residues 112 and 223 (the C-terminal residue) are indicated. TM1, transmembrane domain 1; TM2, transmembrane domain 2; Cyt., cytosol. (Ortega-Roldan, J. L., *et al*. J Biol Chem, 2013)

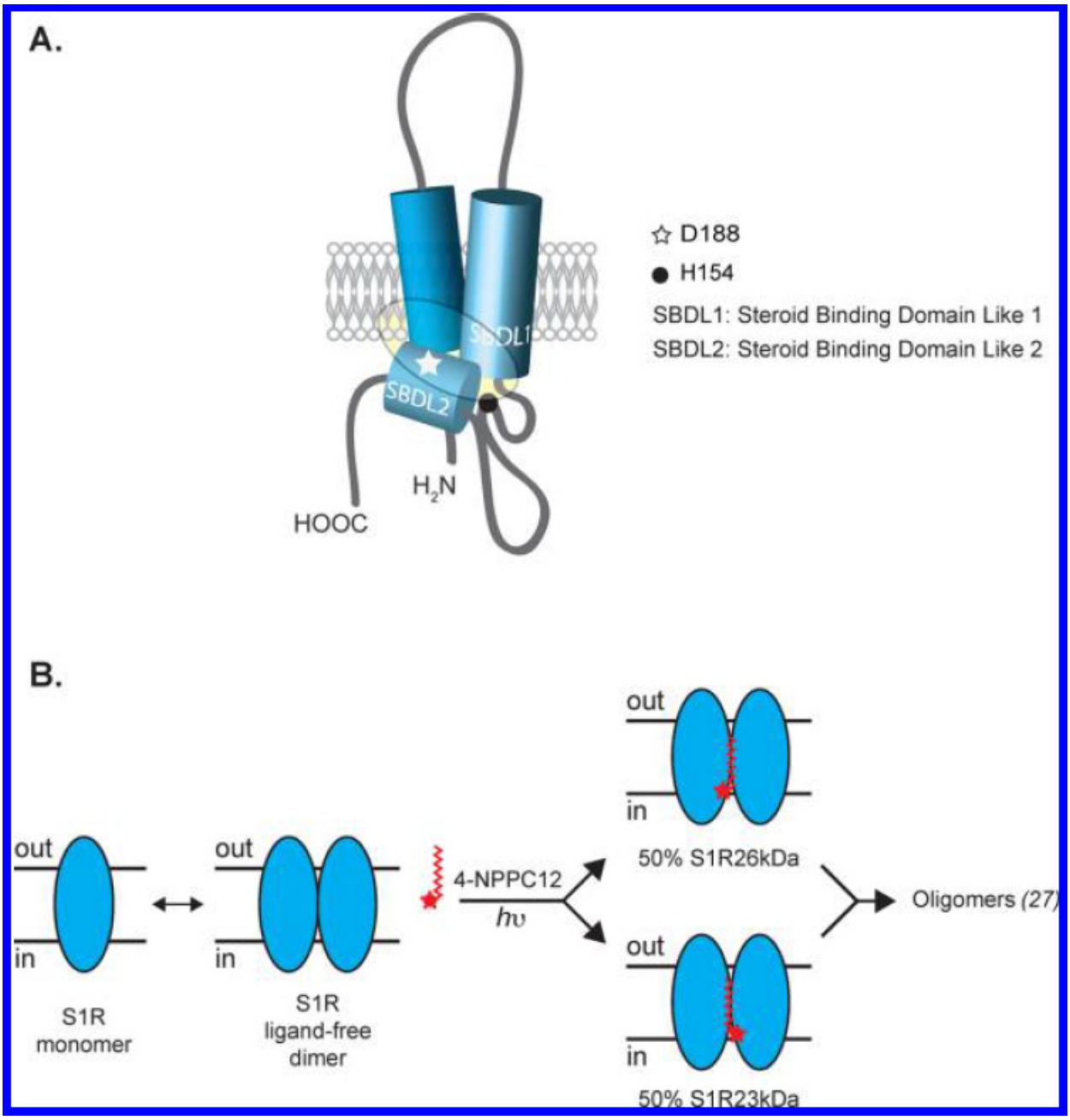

Figure 1-7 Models of the AAG8 (S1R) ligand binding region. (A) Model of the sigma-1 receptor binding region from previous photolabeling studies and from the results with the derivatization by its ligand 4-NPPC12. D188, aspartate 188; H154, histidine 154. The shaded area represents the ligand binding region. (B) Proposed model of AAG8 in the presence of 4-NPPC12. (Chu, U. B, *et al.* Biochemistry-Us, 2013)

AAG8 is predominantly expressed at the mitochondria-associated endoplasmic reticulum (ER) membrane (MAM) and distributes dynamically (Figure 1-8). The MAM, highly capable of accumulating ceramides, is a small section of the outer mitochondrial membrane tethered to the ER by lipid and protein filaments and is enriched with both cholesterol and simple sphingolipids. A lipid overlay assay found that AAG8 preferentially associates with simple sphingolipids such as ceramides. AAG8 associates with MAM-derived detergent-resistant membranes (DRMs) which play an important role in anchoring AAG8 to the MAM. Disrupting DRMs by lowering cholesterol or inhibiting de novo synthesis of ceramides at the ER largely decreases AAG8 at DRMs and causes translocation of AAG8 from the MAM to ER cisternae, suggesting that the MAM, bearing cholesterol and ceramide-enriched microdomains at the ER, may use the microdomains to anchor AAG8 to the location; thus, it serves to stage AAG8 at ER-mitochondria junctions.[14]

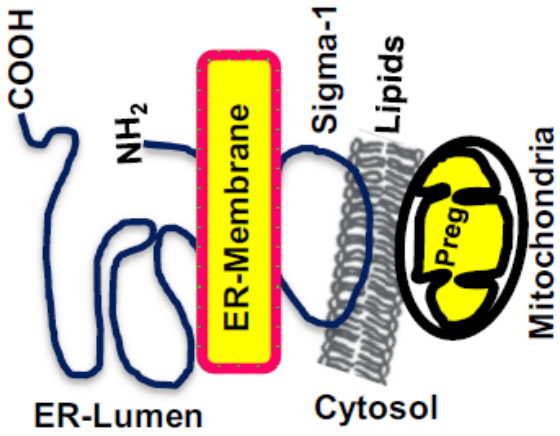

Figure 1-8 Proposed model of interaction between ER and mitochondria through the MAM resident AAG8 (Sigma-1). (Hayashi, T. *et al.* Mol Pharmacol, 2010)

Due to its localization, AAG8 modulates both MAM-specific and plasma membrane proteins and mitochondrial metabolisms. AAG8 at the MAM coordinates with steroidogenic acute regulatory protein for cholesterol trafficking into the mitochondria for metabolic regulation.[15] Furthermore, AAG8 promotes degradation of UDP-galactose:ceramide galactosyltransferase (CGalT), a glycoprotein that synthesizes galactosylceramides at ER, by forming a complex with Insig (Figure 1-9), suggesting that AAG8 is involved

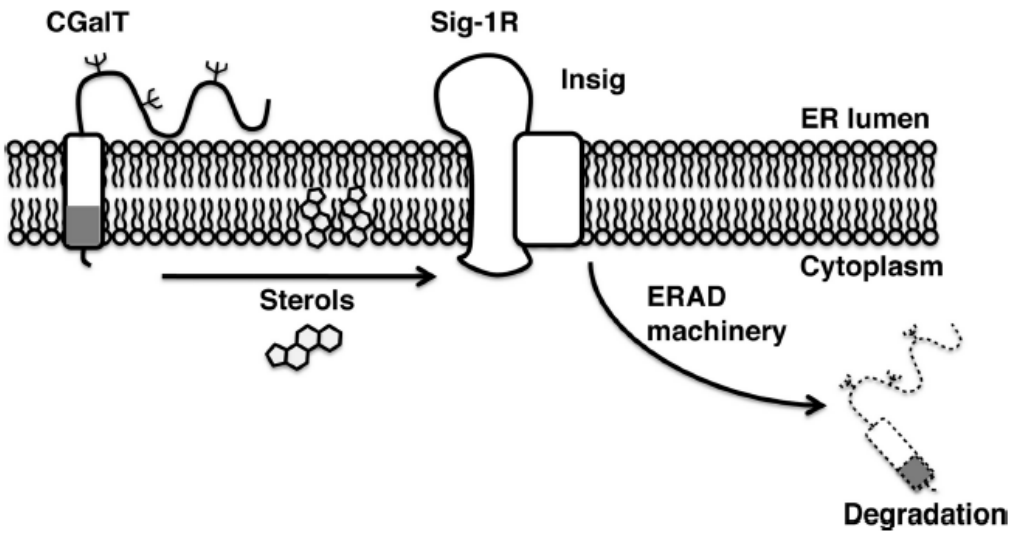

Figure 1-9 A scheme depicting a putative molecular action of AAG8 (Sig-1R) regulating the CGalT level. The second transmembrane domain of the AAG8 associates with Insig to form an ERAD complex at the ER membrane. In the presence of high sterols (e.g. 25-hydroxysterol), CGalT is recruited to the AAG8-Insig machinery for degradation. Other components involved in the AAG8-regulated ERAD machinery (e.g. ubiquitin ligases) are not defined. The transmembrane domain of CGalT (a gray box) contains a putative sterol-binding motif that, upon binding to sterols, might be recognized by the Insig-mediated ERAD complex. (Hayashi, T. *et al*. J Biol Chem, 2012)

in post-translationally regulation and ER-associated degradation.[16] Importantly, AAG8 chaperones the ER stress sensor inositol-requiring protein 1 (IRE1), which is enriched at the MAM, to facilitate inter-organelle signaling for survival. IRE1 is stabilized at the MAM by AAG8 when cells are under ER stress. AAG8 stabilize IRE1 and thus allow for conformationally correct IRE1 to dimerize into the long-lasting, activated endonuclease (Figure 1-10). The IRE1 at the MAM also responds to reactive oxygen species derived from mitochondria. Therefore, the ER-mitochondrion interface serves as an important subcellular entity in the regulation of cellular survival by enhancing the stress-responding signalling between mitochondria, ER, and nucleus.[17]

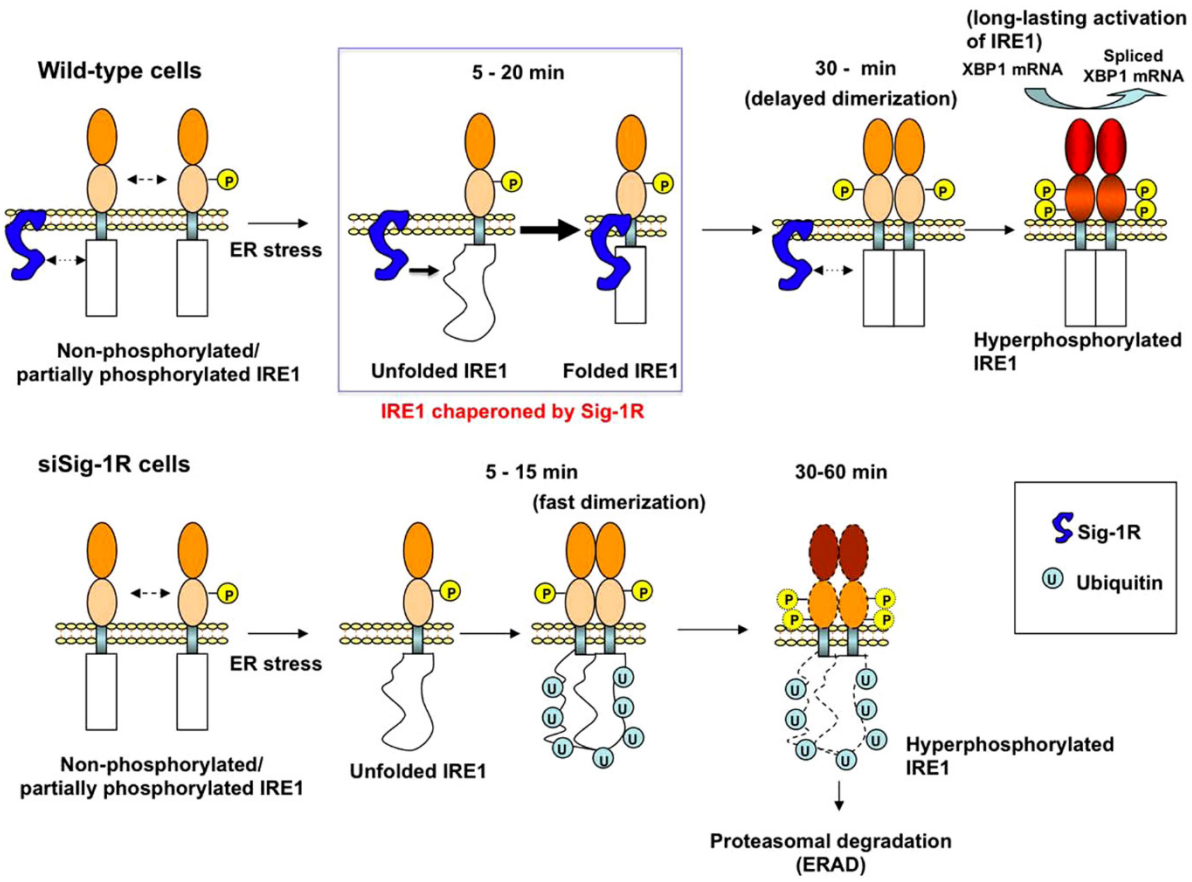

Figure 1-10. Schematic model depicting the role of AAG8 (Sig-1R) in the activation of IRE1. AAG8 enhances its association with IRE1 to correct or stabilize the conformation of IRE1 when cells are facing ER stress (i.e., as indicated in the blue-lined rectangle). This transient association of the AAG8 with IRE1 interferes with the dimerization of IRE1, leading to a delay in the transautophosphorylation of IRE1. This delayed dimerization/phosphorylation, however, ensures a long-lasting active form of IRE1 (the cytoplasmic domain filled in red) which splices the XBP1 mRNA. In lower panels, when AAG8 knockdown cells encounter ER stress, IRE1, although being misfolded, can still quickly dimerize and transautophosphorylate. The conformationally awry pIRE1, which may still possess endonuclease activity albeit being less compared to controls, is however readily ubiquitinated and degraded by proteasomes. (Mori, T. *et al.* Plos one, 2013)

AAG8 has been intensively elaborated in neuroscience and mutations of AAG8 have been shown to cause neurodegenerative diseases such as amyotrophic lateral sclerosis.[18-32] AAG8 is an interorganelle signaling modulator that potentially plays a role in drug-seeking behaviors. Spinal AAG8-induced sensitization is mediated by an increase in nNOS activity, which is associated with an NO-induced increase in PKC-dependent pGluN1 expression (Figure 1-11).[33] In the brain, it interacts functionally with a variety of ion channels and regulates their activities. Cocaine exposure can trigger an AAG8-dependent upregulation of D-type K^+ current in the nucleus accumbens that results in neuronal hypoactivity and thereby enhances behavioral cocaine response. Combined ex vivo and in vitro studies demonstrated that this neuroadaptation is caused by a persistent protein-protein association between AAG8 and Kv1.2 channels, a phenomenon that is associated to a redistribution of both proteins from intracellular compartments to the plasma membrane. In conclusion, the dynamic AAG8-Kv1.2 complex represents a mechanism that shapes neuronal and behavioral response to cocaine. Functional consequences of AAG8 binding to K^+ channels may have implications for other chronic diseases where maladaptive intrinsic plasticity and AAG8 are engaged (Figure 1-12).[34] In addition to Kv1.2 channels, AAG also binds to the Nav1.5 Na^+ channels. Atomic force microscopy imaging of complexes between AAG8 and Nav1.5 Na^+ channels reveals a 4-fold symmetry, i.e., each of the four sets of six transmembrane regions in Nav1.5 constitutes an AAG8 binding site. As a result, AAG8 knockdown strongly reduces the voltage-dependent Na^+ current (Figure 1-13).[35] Besides ion channels, a study using atomic force microscopy (AFM) imaging found that AAG8 bound directly to GluN1/GluN2A NMDA receptor (NMDAR) heterotetramers. In situ proximity ligation assays demonstrated that the Sig1R interacts with GluN1 within intact cells and also that its C terminus is extracellular (Figure 1-14). Therefore AAG8 binds to the GluN1/GluN2A NMDAR specifically via the GluN1 subunit.[36] This interaction likely accounts for at least some of the modulatory effects of Sig1R ligands on the NMDAR.

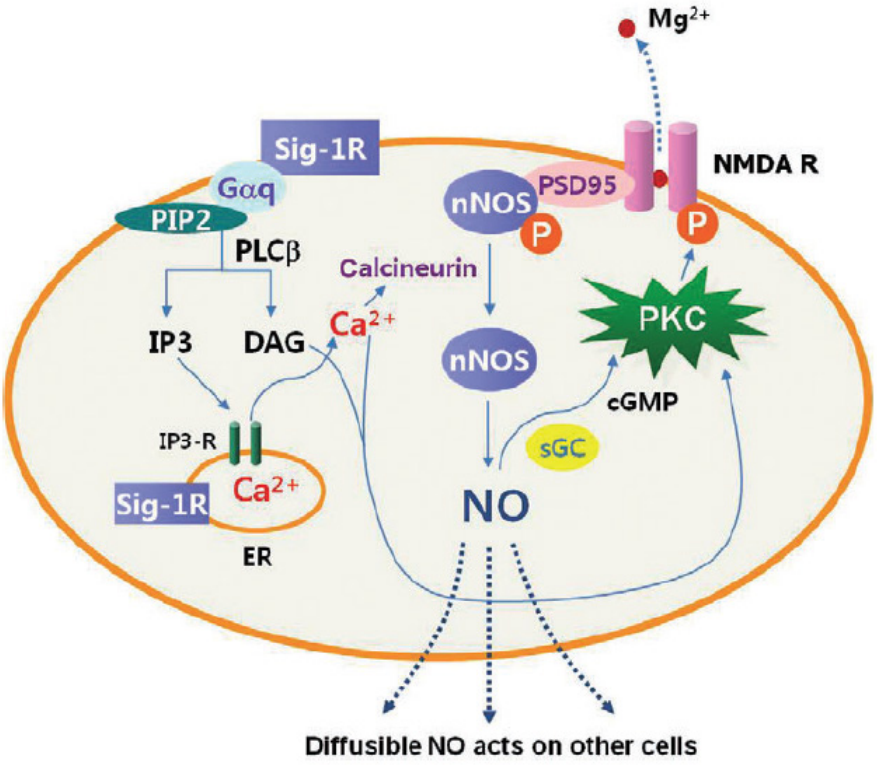

Figure 1-11 Schematic diagram that summarizes the proposed mechanism for how activation of AAG8 (Sig-1R) in turn activates nitric oxide (NO), which then stimulates pGluN1(NMDA R) via a protein kinase C (PKC) mechanism to ultimately facilitate pain. AAG8 activation stimulates PLC to hydrolyze PIP2 to produce diacyl glycerol (DAG) and IP3. IP3 then binds to IP3 receptors (IP3-R) in the endoplasmic reticulum to promote the efflux of Ca^{2+} to the cytoplasm. Increased cytosolic Ca^{2+} then influences calcineurin activity and via this mechanism reduces the phosphorylation of nNOS (i.e. resulting in an increase in nNOS activity). The NO generated from nNOS stimulates cGMP production via sGC, which in turn leads to an increase in PKC activity. The increase in cGMP is likely to produce the PKC activation, which induces the phosphorylation of the PKC-dependent NMDA receptor GluN1 subunit, resulting in the initiation of the pain facilitatory effect. In addition, the diffusible NO produced AAG8 activation can also contribute to the pain facilitatory effect by diffusion from the cell to affect other cells. AAG8 activation leads to an increase in activated nNOS, which plays a key role in AAG8-mediated mechanical and thermal hypersensitivity and PKC-dependent, but not PKA-dependent, pGluN1 expression. (Roh, D. H. *et al.* Brit J Pharmacol, 2013)

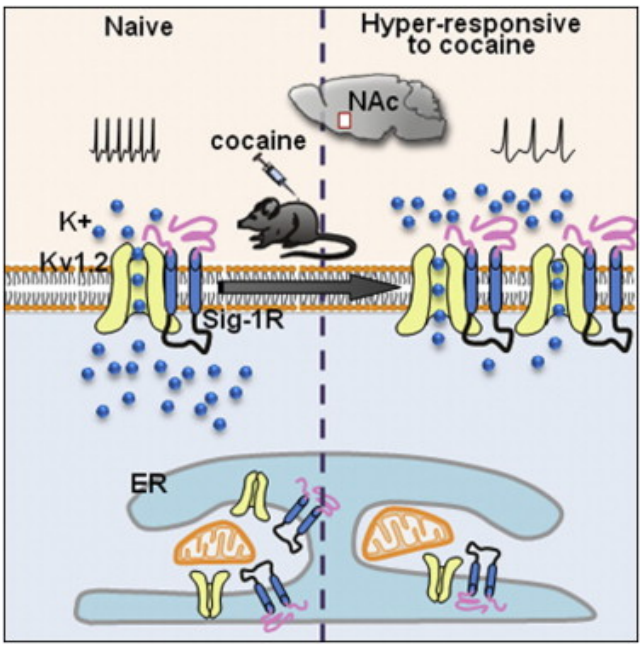

Figure 1-12 Dynamic interaction between AAG8 (Sig-1R) and Kv1.2 shapes neuronal and behavioral responses to cocaine. (Kourrich, S. et al. Cell, 2013)

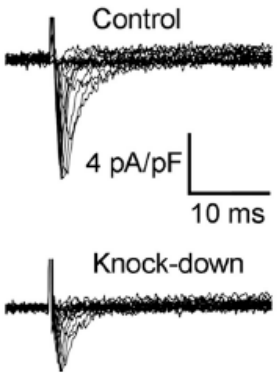

Figure 1-13 AAG8 regulates Nav1.5 current density inMDA-MB-231 cells. Figure shows the representative Na^+ currents elicited in Sig1R knockdown or control MDA-MB-231 cells. (Balasuriya, D. *et al*. J Biol Chem, 2012)

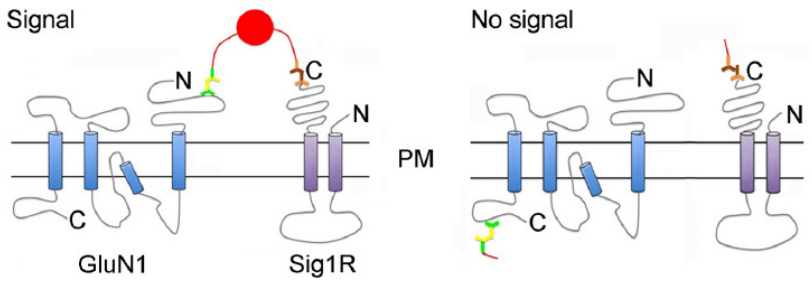

Figure 1-14 Schematic illustration of the in situ proximity ligation assay for AAG8 (Sig1R) plus GluN1. PM, plasma membrane. (Balasuriya, D. *et al.* J Neurosci, 2013)

A plethora of ligands of AAG8 has been synthesized.[37,38] A methodology for monitoring AAG8 activation switch in living cells was developed recently (Figure 1-15). This biosensor uncovered the intrinsic nature of AAG8 ligands by recording the ligand-mediated conformational changes. The change triggered by each ligand correlated well with its ability to attenuate formalin induced nociception in an animal model of pain.[39] With the use of these ligands, functions of AAG8 in the central nervous system (CNS) have been evaluated. Importantly, AAG8 was found to mediate pain hypersensitivity in mice and neuropathic pain in rats. Direct activation of the spinal AAG8 with PRE084, a specific AAG8 agonist, produces mechanical allodynia and induced an increase in NOX2 activation and reactive oxygen species (ROS) production in

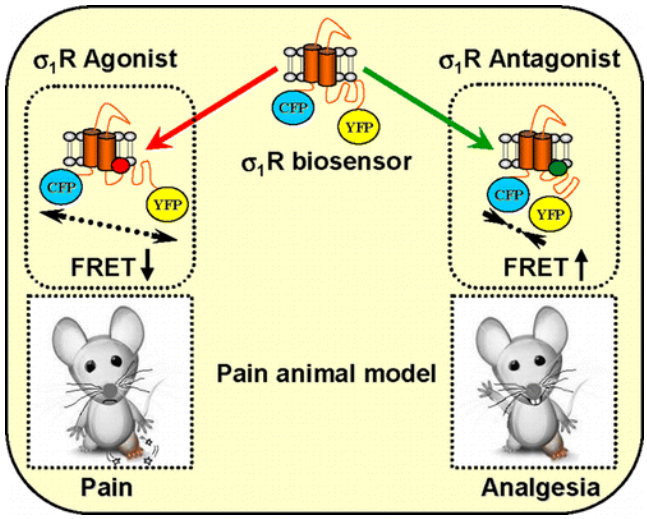

Figure 1-15 Predicting the antinociceptive efficacy of AAG8 (σ1R) ligands by a receptor FRET-based biosensor. (Gomez-Soler, M. *et al.* J Med Chem, 2014)

mice, which can be attenuated by pretreatment with the selective AAG8 antagonist, BD1047. This demonstrates that spinal AAG8 modulate NOX2 activation and ROS production in the spinal cord, and ultimately contribute to the AAG8-induced pain hypersensitivity and the peripheral nerve injury-induced induction of chronic neuropathic pain (Figure 1-16).[40] On the other hand, intrathecal injection of PRE084 into naïve mice time-dependently increases the expression of p-p38, which can be blocked by pretreatment with BD1047. Intrathecal pretreatment with SB203580, a p38 inhibitor also dose-dependently inhibited PRE084-induced mechanical allodynia, demonstrating that the increase in spinal p-p38 is closely associated with the induction of AAG8 mediated mechanical allodynia.[41] AAG8 stimulation with its specific agonist SA4503 ameliorates cardiac hypertrophy and dysfunction by restoring both mitochondrial Ca^{2+} mobilization and ATP production, suggesting that AAG8 stimulation represents a strategy to rescue the heart from hypertrophic dysfunction (Figure 1-17).[42] A research group recently argued that treatment with some AAG8 ligands induces ER stress and activates the unfolded protein response (UPR). Autophagy is engaged after extended treatment with AAG8 ligands, which suggests that protracted

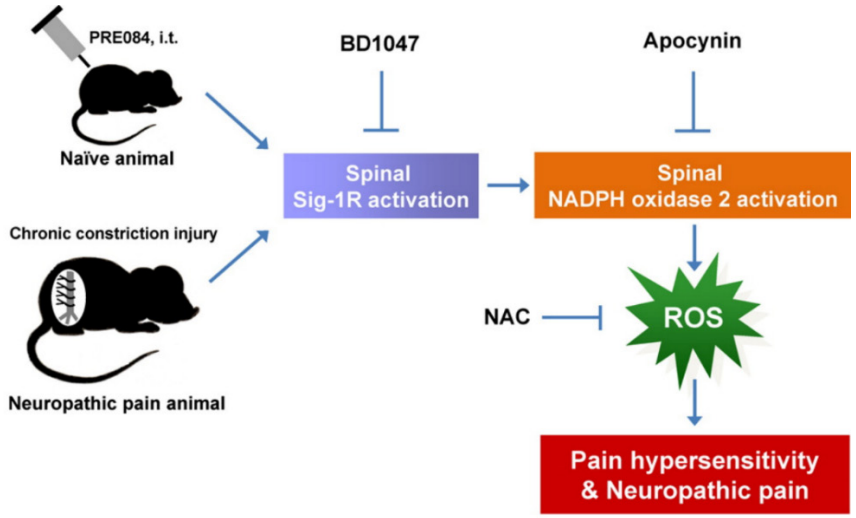

i.t., intrathecal; Sig-1R, sigma-1 receptor; ROS, reactive oxygen species

Figure 1-16 Spinal AAG8 (Sig-1R) activate NADPH oxidase 2 leading to the induction of pain hypersensitivity in mice and mechanical allodynia in neuropathic rats. (Choi, S. R. *et al*. Pharmacol Res, 2013)

UPR results in autophagy as a secondary response. In addition, UPR activation precedes autophagosome formation and autophagy precedes apoptosis in AAG8 ligand-treated cells, suggesting that UPR and autophagy are engaged as primary and secondary cytoprotective responses, respectively, to AAG8 ligand-induced disruption of cell protein homeostasis.[43]

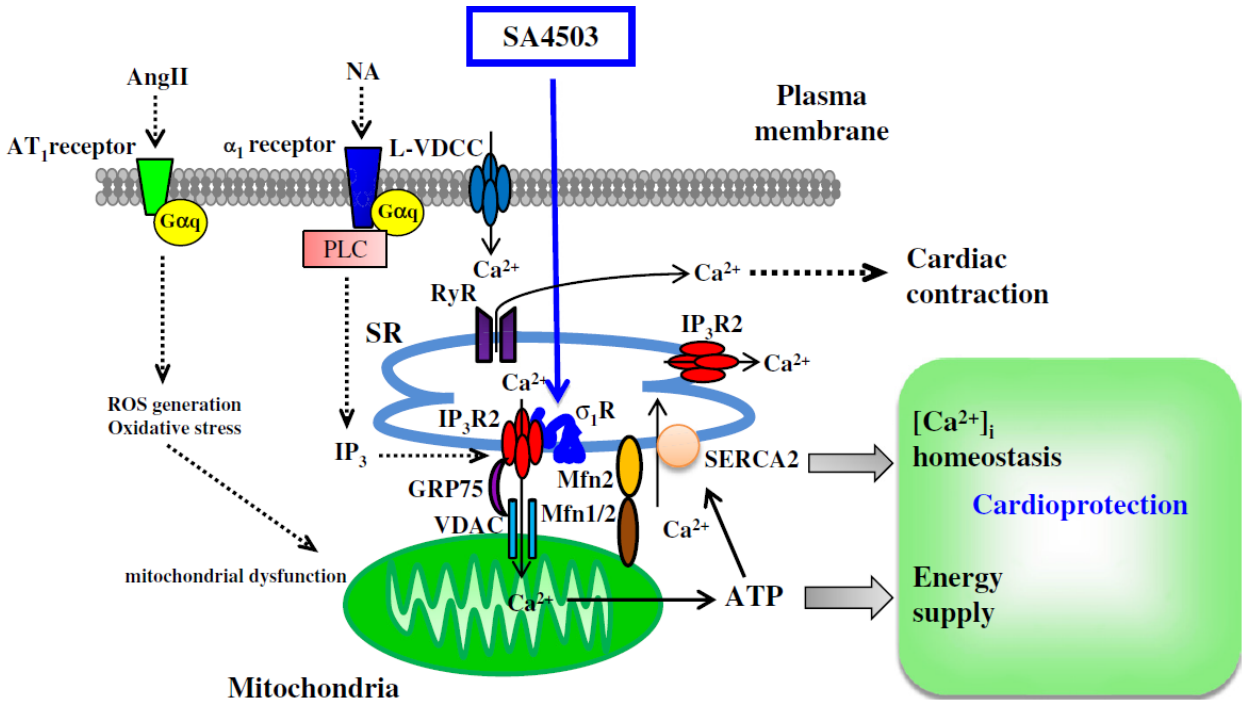

Figure 1-17 Shown is a model of regulation of Ca^{2+} homeostasis and ATP production by SA4503 through AAG8 (σ1R) stimulation. AAG8 stimulation with SA4503 promotes mitochondrial Ca^{2+} influx and mitochondrial Ca^{2+}-dependent ATP production. AAG8-induced regulation of Ca^{2+} homeostasis and ATP production is crucial for the cardioprotective activity of SA4503 against heart failure. VDAC: voltage-dependent anion channel. (Tagashira, H. *et al.* Bba-Gen Subjects, 2013)

2. Objective

Despite the notable advantages described above, people have only just begun to define the underlying mechanisms of AAG8, even in the field of neurology. Although recent emerging in vitro and in vivo evidences have implied AAG8 as a pharmacological target for the treatment of neurological disorders, little has been investigated regarding the roles of AAG8 in cancinogenesis. In contrast to the intensive use of AAG8 ligand for investigation of AAG8 in neurology, few ligands have been tested for their anti-cancer property. Growth-inhibitory effects of the novel selective AAG8 antagonists in a breast cancer cell line has been solely reported, however, molecular explanation was absent.[44] More importantly, since drug resistance and great side effects has largely impeded the efficient curable therapy for cancer, especially for MAPK-hyperactivated melanoma, it is necessary to discover the novel and potential inhibitors that target the important oncogenetic signalling cascades.

Despite the previously described findings of AAG8 in neuroscience, the importance of AAG8 in cancer has rarely been noticed, and the lack of gain- or loss-of-function studies has so far precluded a clear understanding of the rationale of AAG8 in carcinogenesis. This study therefore focuses on the molecular mechanisms of AAG8 and its ligands especially the antagonists and aims at characterization of its intrinsic functions in cancer.

3. Dissertation composition

This dissertation is composed of five chapters. In Chapter 1, general introduction including background (cancer and AAG8) and objective of this dissertation is described. In Chapter 2, I investigated the effects and mechanisms of AAG8 antagonism in melanoma cells, and proposed a novel strategy for melanoma therapy through tandem AAG8-MEK inhibition. Though this study, AAG8 antagonists have been discovered as novel MEK inhibitors. Finally, based on the experimental data, critical discussions are made regarding the several important arguable topics. In Chapter 3, I explored the intrinsic roles of AAG8 in cancer cells and found that AAG8 promoted carcinogenesis both in vitro and in vivo. I further characterized AAG8, for the first time to our knowledge, as a STAT3 activator, and demonstrated that it alternatively activated STAT3 in addition to IL6/JAK pathway. Finally, based on the experimental data, critical discussions are made regarding the several important arguable topics. In the last chapter, final conclusion is obtained and future perspective is proposed.

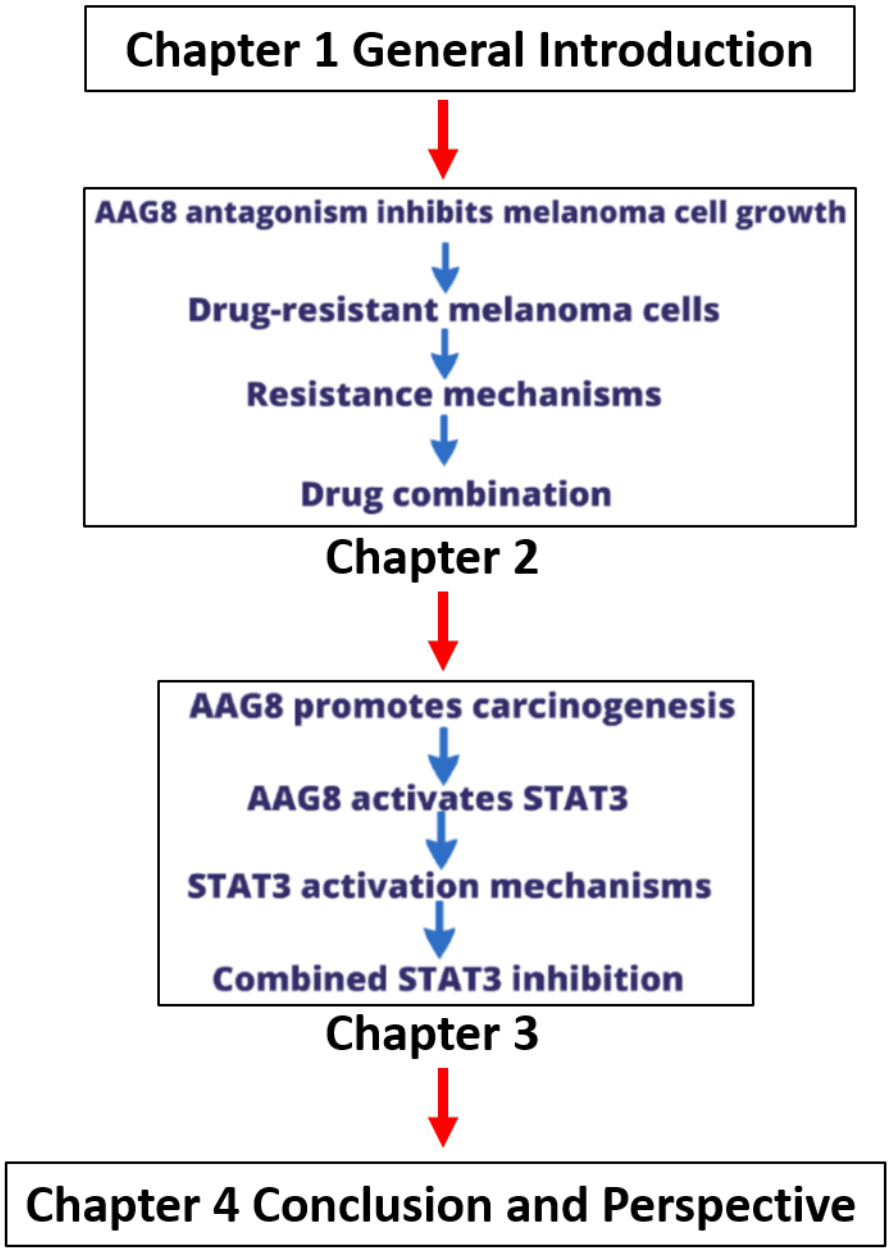
Chapter 1 General Introduction
AAG8 antagonism inhibits melanoma cell growth
Drug-resistant melanoma cells
Resistance mechanisms
Drug combination
Chapter 2
AAG8 promotes carcinogenesis
AAG8 activates STAT3
STAT3 activation mechanisms
Combined STAT3 inhibition
Chapter 3
Chapter 4 Conclusion and Perspective

4. Abbreviation

AAG8	Aging-associated gene 8
MAPK	Mitogen-activated protein kinase
STAT3	Signal transducer and activator of transcription 3
API4	Apoptosis inhibitor 4
ER	Endoplasmic reticulum
MAM	Mitochondria-associated endoplasmic reticulum membrane
JAK	Janus kinases

Chapter 2 Modeling Tandem AAG8-MEK Inhibition in Melanoma Cells

1 Introduction

1.1 MEK signalling

The cellular kinase-signalling network is a major regulator in pathogenesis, and kinase mutations are common and potent drivers of oncogenesis. The mitogen-activated protein kinase (MAPK), i.e. RAS-RAF-MEK-ERK signaling pathway, is a key modulator of cellular proliferation, differentiation and survival downstream of RAS activation. Upregulation of this pathway occurs in a large fraction of tumors, frequently owing to oncogenic activating mutations in KRAS, NRAS, HRAS and BRAF.[45] Somatic mutations in the small GTPase RAS family proteins are the most common activating lesions found in cancer, and are generally associated with poor response to standard therapies. Oncogenic mutations result in functional activation of RAS by impairing GTP hydrolysis. With diminished regulation by GTPase activity, the nucleotide state of RAS becomes more dependent on relative nucleotide affinity and concentration. This gives GTP an advantage over GDP and increases the proportion of active GTP-bound RAS.

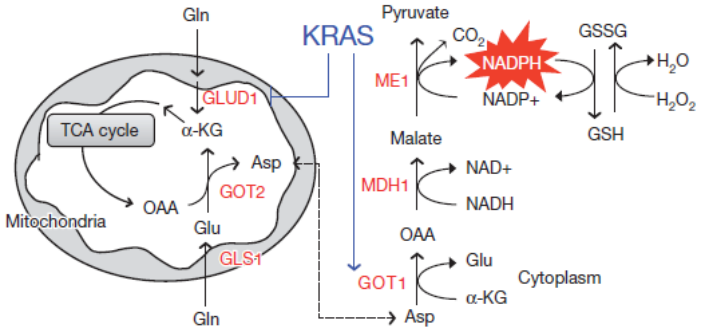

Figure 2-1 Model depicting the KRAS-regulated Glutamine metabolic reprogramming used to maintain redox and support growth. (Son, J. *et al*. Nature, 2013)

The Cancer Cell Line Encyclopedia (CCLE), a compilation of gene expression, chromosomal copy number and massively parallel sequencing data from 947 human cancer cell lines, enabled identification of genetic, lineage, and gene-expression-based predictors of drug sensitivity. Within CCLE, AHR gene (which encodes the aryl hydrocarbon receptor) expression was found to be associated with MEK inhibitor efficacy in NRAS-mutant lines.[46] Sleeping Beauty transposon-mediated insertional mutagenesis studies in a mouse model of pancreatic ductal preneoplasia identified genes, especially the X-linked deubiquitinase USP9X, that cooperate with oncogenic KRAS-G12D to accelerate tumorigenesis and promote progression.[47] In pancreatic ductal adenocarcinoma cells, a non-canonical pathway of glutamine use was identified to be required for tumor growth, and this reprogramming of glutamine metabolism is mediated by oncogenic KRAS (Figure 2-1).[48] Targeting a single kinase has proven successful in some cases. Ostrem, J. M. *et al.* reported the development of small molecules that irreversibly bind to a common oncogenic mutant, KRAS-G12C and decreased its association with BRAF and CRAF.[49] Interfering with binding of mammalian PDEδ to KRAS by means of small molecules provides a novel opportunity to suppress oncogenic RAS signalling by altering its localization to endomembranes (Figure 2-2).[50]

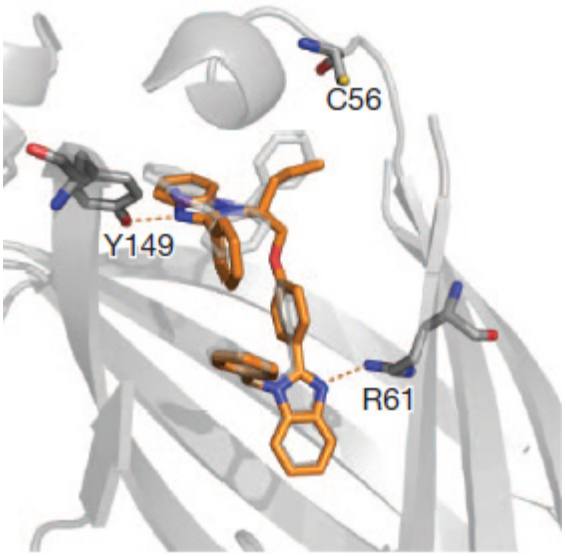

Figure 2-2 Structure of a small molecule (orange sticks) in complex with PDEδ. (Zaidi, M. R. *et al.* Nature, 2011)

1.2 Melanoma

Melanoma is a lethal cancer notable for its aggressive, metastatic and chemoresistant propensity. The known environmental and genetic risk factors include ultraviolet radiation exposure[51], pigmentation and nevus phenotypes.[52] Intermittent intense ultraviolet (UV) exposure represents an important aetiological factor in the development of malignant melanoma. The ability of UV radiation to cause tumour-initiating DNA mutations in melanocytes is now firmly established. Repetitive UV exposure of primary cutaneous melanomas in a genetically engineered mouse model promotes metastatic progression, independent of its tumour-initiating effects. UV irradiation enhanced the expansion of tumor cells along abluminal blood vessel surfaces and increased the number of lung metastases. The UV-induced neutrophilic inflammatory response stimulated angiogenesis and promoted the ability of melanoma cells to migrate towards endothelial cells and use selective motility cues on their surfaces. UV irradiation of epidermal keratinocytes is sensed by the innate immune system, but also show that the resulting inflammatory response catalyses reciprocal melanoma-endothelial cell interactions leading to perivascular invasion, a phenomenon originally described as angiotropism in human melanomas by histopathologists. Angiotropism represents a hitherto underappreciated mechanism of metastasis that also increases the likelihood of intravasation and haematogenous dissemination. Ulcerated primary human melanomas with abundant neutrophils and reactive angiogenesis frequently show angiotropism and a high risk for metastases.[53]

Recent efforts employing whole-genome sequencing or chemical genetic screen methods have identified a panel of candidate molecules, including both recurrently mutated or wild-type proteins[54,55] and RNAs[56,57], which contribute to melanomagenesis. Nevertheless, more than half of melanomas express the mutationally activated BRAF (V600E, the most prevalent genetic alteration) oncoprotein, which triggers the BRAF-MEK-ERK signaling pathway (MAPK pathway), a key regulator of proliferation and differentiation. Consequently, inhibitors targeting the clinically validated class of molecular components of MAPK cascade have been developed and shown to have notable clinical effects for melanoma chemotherapy. RNAi-based genetic screen was performed to search for kinases whose knockdown synergizes with BRAF (V600E)

inhibition. With this method, it was found that blockade of the epidermal growth factor receptor (EGFR) shows strong synergy with BRAF (V600E) inhibition. Mechanistically, BRAF (V600E) inhibition causes a rapid feedback activation of EGFR, which supports continued proliferation in the presence of BRAF (V600E) inhibition. Our data suggest that BRAF (V600E) mutant colon cancers, for which there are currently no targeted treatment options available, might benefit from combination therapy consisting of BRAF and EGFR inhibitors.[58]

For instance, Das Thakur and colleagues argued that vemurafenib-resistant melanoma cells exhibit similar resistance to the MEK inhibitor AZD6244, due to elevated BRAF (V600E) expression.[59] In addition, melanoma even elicits resistance to adoptive T-cell transfer therapies through the proinflammatory cytokine tumor necrosis factor (TNF)-induced reversible dedifferentiation, hinting strategies to sustain T-cell effector functions through minimizing immune-inhibitory effects in the melanoma microenvironment.[60] These studies present an embarrassed situation in dealing with the drug resistance of melanoma.

A recent study pinpointed a critical role of pyruvate dehydrogenase (PDH) in BRAF (V600E)-driven senescence of melanoma, showing that BRAF (V600E)-induced senescence was accompanied by simultaneous suppression of the PDH-inhibitory enzyme pyruvate dehydrogenase kinase 1 (PDK1) and induction of the PDH-activating enzyme pyruvate dehydrogenase phosphatase 2 (PDP2).[61]

1.3 Drug resistance

Efforts of cancer drug development have been mixed. Difficulties include rapidly emerging resistance as well as considerable toxicity that can limit dosing to levels that are insufficient for blocking tumor growth.[62] Clinical responses to anticancer therapies are often restricted to a subset of patients.[63] Cancers acquire resistance to systemic treatment as a result of clonal evolution and selection.[64] Drug resistance frequently results in relapse and presents a challenge for curable therapy. Proteomic analysis showed that stromal cell secretion of hepatocyte growth factor (HGF) resulted in activation of the HGF receptor MET, reactivation of the MAPK and phosphatidylinositol-3-OH kinase (PI3K)-AKT signalling pathways, and immediate resistance to RAF inhibitors.[3,65]

Genetically engineered mouse models have been used for conducting a 'co-clinical' trial that mirrors an ongoing human clinical trial in patients with KRAS-mutant lung cancers. This trial aimed to determine if the MEK inhibitor selumetinib (AZD6244) increases the efficacy of docetaxel, a standard of care chemotherapy. Concomitant loss of either p53 or LKB1 (also known as STK11), two clinically relevant tumour suppressors, markedly impaired the response of KRAS-mutant cancers to docetaxel monotherapy. Addition of selumetinib provided substantial benefit for mice with lung cancer caused by KRAS and KRAS and p53 mutations, but mice with KRAS and LKB1 mutations had primary resistance to this combination therapy.[66] To uncover biomarkers of sensitivity and resistance to cancer therapeutics, a panel of several hundred cancer cell lines, which represent much of the tissue-type and genetic diversity of human cancers, was screened with 130 drugs under clinical and preclinical investigation. In aggregate, mutated cancer genes were associated with cellular response to most currently available cancer drugs. Classic oncogene addiction paradigms were modified by additional tissue-specific or expression biomarkers, and some frequently mutated genes were associated with sensitivity to a broad range of therapeutic agents. By linking drug activity to the functional complexity of cancer genomes, systematic pharmacogenomic profiling in cancer cell lines provides a powerful biomarker discovery platform to guide rational cancer therapeutic strategies.[63]

1.4 Objective

Although converging in vivo evidences have advanced AAG8 as a pharmacological target for the treatment of neurological disorders, little has been investigated in detail about the roles of AAG8 in cancer. In contrast to the intensive investigation of AAG8 in neurology, few ligands have been tested for their anti-cancer property. Growth-inhibitory effects of the novel selective AAG8 antagonists in a breast cancer cell line has been documented, however, molecular explanation was lacking.[44] In this chapter, I discovered AAG8 antagonists as novel MEK inhibitors in melanoma cells and demonstrated the molecular mechanisms that: 1. AAG8 antagonism restricts melanoma cell growth by inactivation of the CARF-MEK signalling pathway; 2. AAG8 antagonist resistant melanoma cells obtain refractory CARF-MEK activity, which was not due to RAS activation. Finally, tandem AAG8 and MEK inhibition cooperatively and more efficiently kill the drug resistant melanoma cells.

2. Material and Methods

2.1 Cell line and reagents:

B16 cells were obtained from ATCC (CRL-6323) and were routinely cultured in Dulbecco's Modified Eagle's Medium (DMEM) (Nissui Pharmaceutical, Japan) supplemented with 10% fetal bovine serum (FBS, GIBCO 10099) and glutamine (SIGMA, G8540) (hereafter complete DMEM). Cell culture was maintained in a standard incubator at 37°C with 5% CO_2. B16 cells were seeded at a density of 5×10^5 per well in 6-well plates for BD1047, BD1063 (SANTA CRUZ, USA), and PD901 (WAKO, Japan) treatment. Matrigel^{TM} basement membrane matrix was from BD Bioscience.

2.2 3D culture.

3D on-top culture of melanoma cells was as described previously with some modifications.[67] Briefly, surface of 6-well plates was coated with pre-thawed Matrigel (500 μl/well) with a pipette tip. For each well, 10^5 cells were resuspended in 3 ml of complete DMEM containing 5% Matrigel and pipetted onto the pre-coated surface. AAG8 antagonists were added into the medium as indicated. Cells were then cultured for the indicated days before further assays.

2.3 Wound healing assay

Wound healing assay was performed as described elsewhere.[68] Briefly, cells were seeded at low confluency (15%) in 6-cm dishes in complete DMEM. Confluent cells monolayer was scraped with a P200 tip to obtain

a wound in each dish, and the medium was replaced with fresh serum-free medium. After 20 hr the cells were fixed with 4% paraformaldehyde and photographed. Pictures were taken at time 0 as reference.

2.4 SDS-PAGE and Western blot

Cells were plated 1 day before drug treatment in a 6-well plate at 5×10^5 cells per well for 2D culture, and were treated the next day. At the designated time points, cells were lysed with Laemmli buffer. Cytoplasmic and nuclear fractions were prepared with NE-PER Nuclear and Cytoplasmic Extraction Reagents (Thermo Scientific, USA) according to the manufacturer's instructions. RAS activity was examined with a RAS Activation Assay Kit (Millipore, Germany) as its manual instructed. Each lysate sample was loaded into two adjacent lanes of a 10% polyacrylamide gel for minimizing loading differences if indicated. Proteins were separated at 30 mA and transferred onto PVDF membranes (Millipore) using the Trans-Blot SD Semi-Dry Transfer Cell (BIORAD, USA). Membranes were blocked for 1 hr at room temperature using 5% skim milk or 5% BSA (for phosphorylation detection) in TBS-Tween (TBS-T). Western blot analysis was performed according to the antibody manufacturer's specifications. The membranes were incubated with primary antibodies overnight in either 5% BSA or 5% skim milk in TBS-T at 4 °C. The membranes were washed thrice in TBS-T. The appropriate HRP-conjugated secondary antibody was added into 5% skim milk in TBS-T, followed by three washes in TBS-T. The membranes were developed using a Luminata Crescendo Western HRP substrate (Millipore).

Antibodies used in this work are as follows: pCRAF (#9427), pMEK (#9154) and MEK (#8727) antibodies were from Cell Signaling Technology (MA, USA). BRAF (sc-55522), TPL2 (sc-373677) antibodies were from Santa Cruz Biotechnology (CA, USA). AAG8 (HPA018002), GAPDH (G9295) and the secondary HRP-conjugated anti-mouse IgG (A9044) antibodies were from Sigma (MO, USA). VIM (ab8978) antibody was from Abcam (MA, USA). The secondary HRP-conjugated anti-rabbit IgG antibody (G21234) was from Invitrogen (CA, USA).

2.5 Growth assay and apoptosis assay

Cells was seeded in 6-well plates with triplicate cultures and treated as indicated with according periods. Dead cells were stained with trypan blue and total cell number was evaluated with Countess^{TM} (Invitrogen). For apoptosis assay, cells were treated with indicated AAG8 antagonists for 48 hr in 3D Matrigel culture, and then stained with 1 nM ethidium bromide (EtBr) for 5 min. The stained DNA were observed and photographed under a fluorescence microscope (OLYMPUS, IX2-ILL100, Japan)

2.6 Statistics

All quantitative data were presented as means ± s.e.m.. Statistical significance between the control and treatment groups was assessed by using one way ANOVA followed by Tukey's test. Statistical significance was considered at the $p < 0.05$ level.

3. Results

3.1 AAG8-antagonism restricts melanoma cells

Dysregulation of signalling pathways by changes of gene expression contributes to hallmarks of cancer. A systematic study revealed AAG8 mRNA overexpression up to above 8-fold in melanoma versus normal skin (Figure 2-3),[69] indicating its vital roles in melanomagenesis. We wondered whether perturbing AAG8 function could affect melanoma cell growth by investigating AAG8 antagonism in B16F1 (B16) cells, derived from mouse melanoma. B16 cells express high level of AAG8 exclusively in the cytosol (Figure 2-4). Notably, B16 cells were sensitive to BD1047 (Figure 2-5), a specific AAG8 antagonist[70]. We observed dose-dependent suppressive phenotypes in 3D culture (Figure 2-6). To corroborate our results, BD1063 (Figure 2-5), another specific AAG8 antagonist, was used to treat B16 cells in 3D culture, and similar effects were obtained (Figure 2-7). We further found that BD1047 or BD1063 dose-dependently induced apoptosis of B16 cells in 3D culture (Figure 2-8). Confirming the growth regression, growth assay showed that BD1047 dose-dependently suppressed cell growth, and 100 μM BD1047, a routinely used concentration in vitro[70], dramatically decreased viable cells (Figure 2-9).

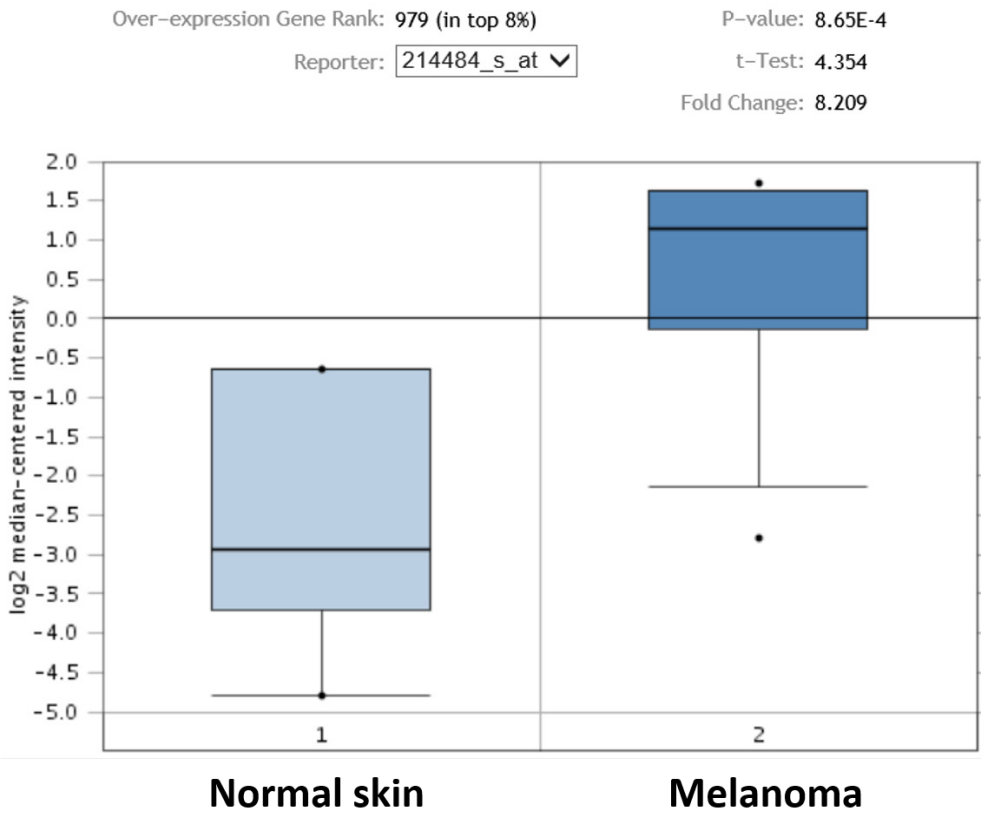

Figure 2-3 AAG8 mRNA is upregualted up to > 8 fold in melanoma comparing to normal skin tissues. (Talantov, D. *et al*. Clin Cancer Res, 2005)

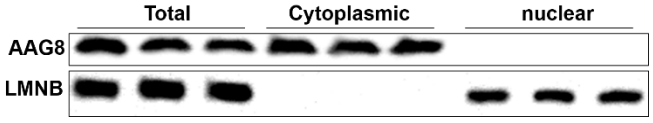

Figure 2-4 AAG8 cellular distribution. Immunoblot of AAG8 and LMNB in the indicated cellular fractions of B16 cells. LMNB serves as loading control.

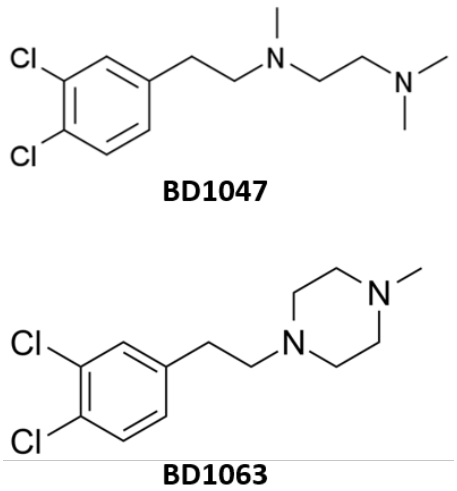

Figure 2-5 Chemical structures of AAG8 antagonists.

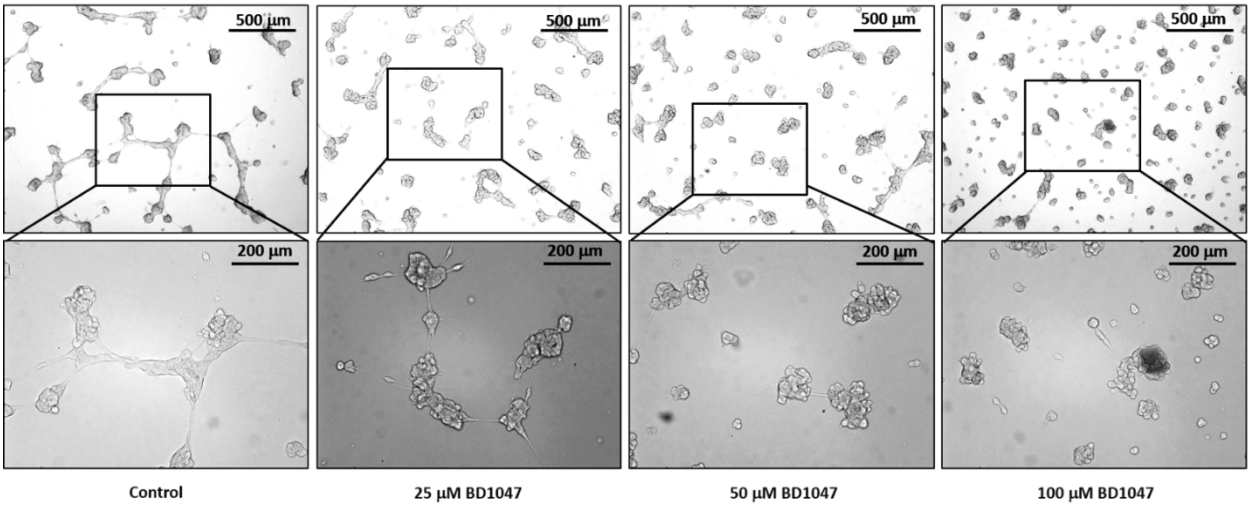

Figure 2-6 AAG8 antagonism in B16 cells of 3D culture. Phase contrast images showing B16 cells cultured in 3D Matrigel and treated with BD1047 of indicated concentration for 18 hr.

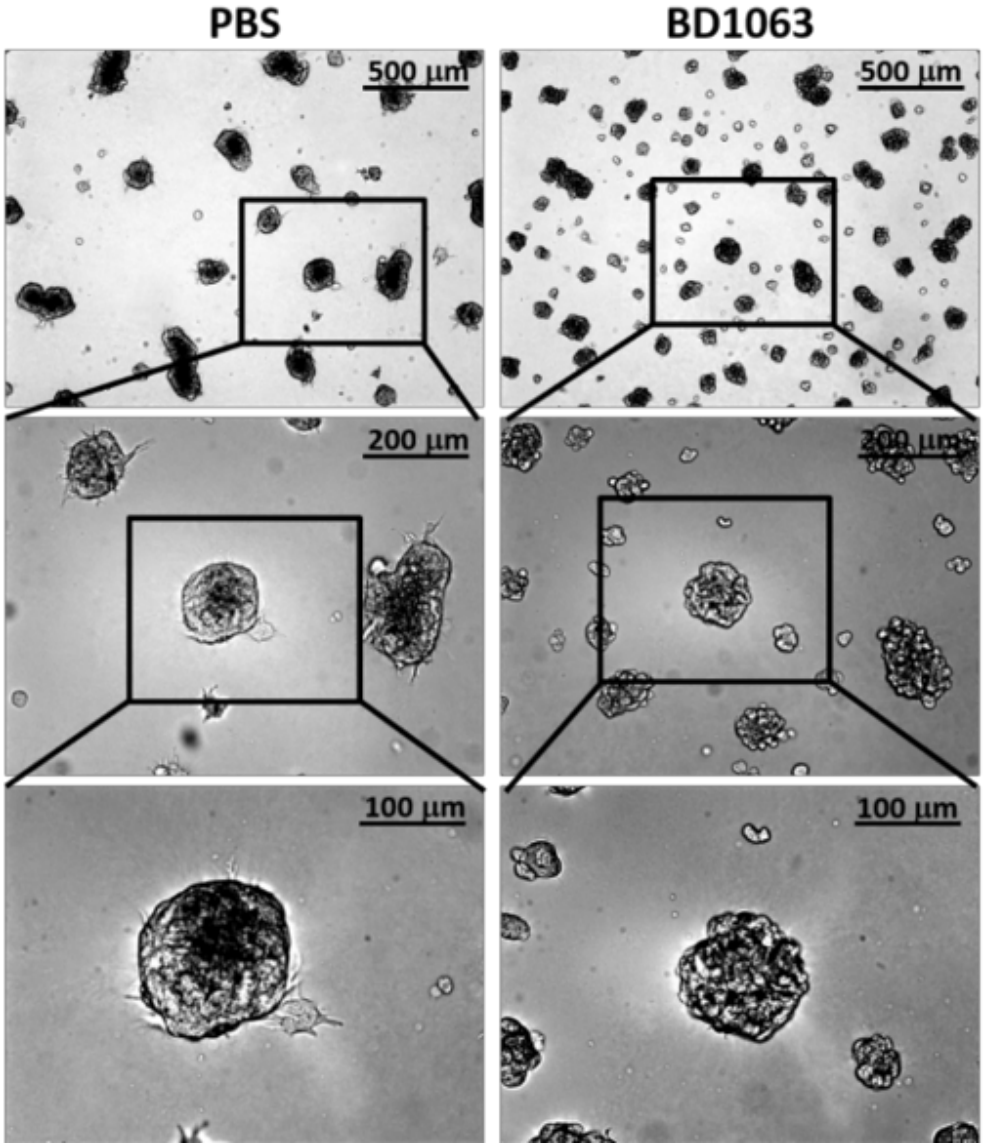

Figure 2-7 Phase contrast images showing B16 cells cultured in 3D Matrigel and treated with 50 µM BD1063 for 48 hr.

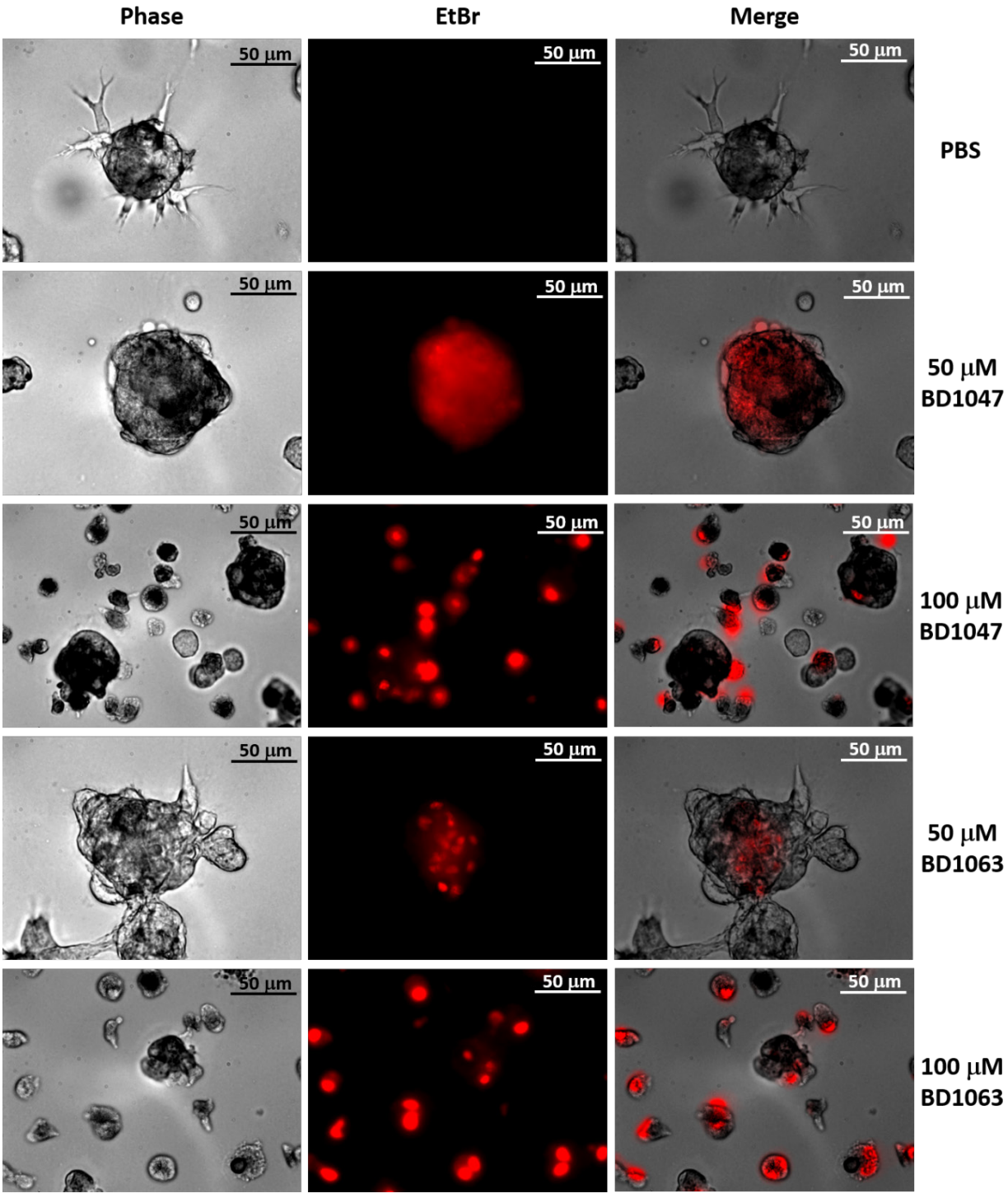

Figure 2-8 AAG8 antagonism induced apoptosis in B16 cells. B16 cells in 3D culture are treated with the indicated concentrations of BD1047 or BD1063 for 48 hr and stained with EtBr.

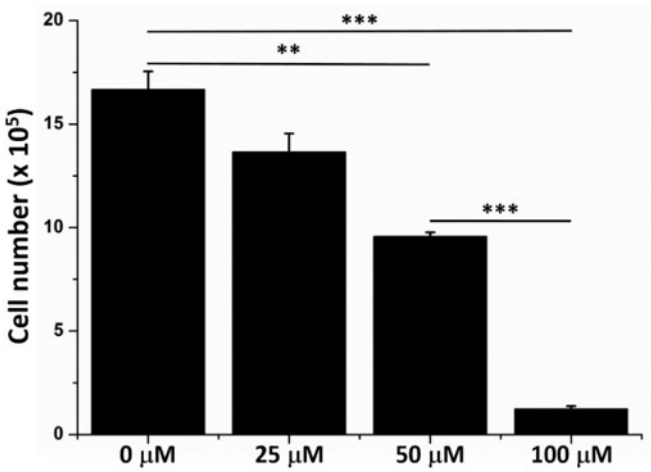

Figure 2-9 Growth assay with Countess™ (Invitrogen) of B16 cells of 2D culture treated with BD1047 of indicated concentration for 24 hr. Initial cell number = 3×10^5. n = 3. Error bars (s.e.m.) are indicated. Note: ** p <0.01, *** p <0.001 (one way ANOVA followed by Tukey's test).

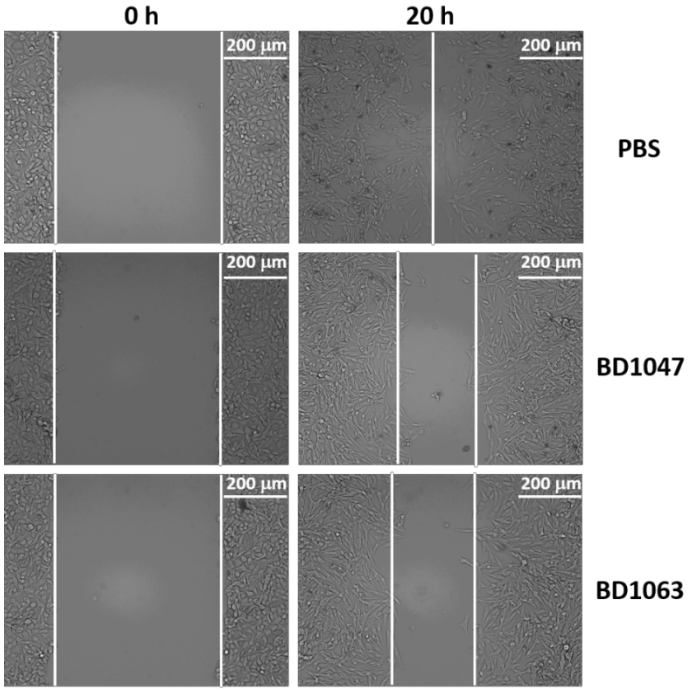

Figure 2-10 Representative images of wound healing assay of B16 cells treated with 100 μM BD1047 or BD1063. Experiments were performed three times with consistent results.

Additionally, metastatic progression of cancer is a complex and clinically daunting process. Metastatic growth in distant organs is the major cause of cancer mortality. It was observed that AAG8 antagonists dampened B16 cell migration, as indicated by wound healing assay. Cells treated with PBS healed the wound almost completely after 20 hr, in contrast, cells treated with antagonist could not (Figure 2-10). These data intimate the anti-tumor effects of AAG8 antagonism and highlight AAG8 antagonists as potential drugs for melanoma therapy.

3.2 AAG8 antagonism inhibits CRAF-MEK activity

Excessive MAPK pathway activation accounts for more than 90% of melanomas.[71] As MEK is a mediatory effector downstream of RAF, its inhibitors are being tested in clinical trials for melanoma and the other cancers.[45,59] I noticed the dose-dependent inactivation of MEK in BD1047-treated B16 cells (Figure 2-11). I further showed that the MEK activity decreased significantly after 3 hr of BD1047 treatment (Figure 2-12). Similar inhibitory effect on MEK activity was also observed with BD1063 (Figure 2-13). Furthermore, I found that both antagonists could lead to decreased activity of CRAF, the upstream kinase of MEK[45] (Figure 2-11, 2-13). These results suggest that AAG8 antagonism restricts B16 cells through, at least partly, the suppression of CRAF-MEK signaling. A recent study demonstrated a positive feedback loop in which CRAF phosphorylation is dependent on MEK activity[72]. I thus speculate that AAG8 antagonism blocks this loop and lead to the inactivation of both of these two kinases.

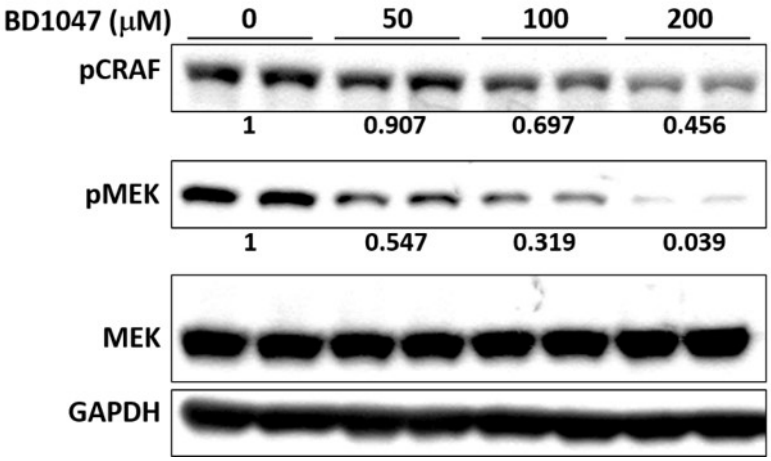

Figure 2-11 Immunoblot of pCRAF and pMEK in B16 cells treated with the indicated concentrations of BD1047 for 20 hr shows dose-dependent inhibition of CRAF and MEK. Mean values of pCRAF and pMEK versus MEK levels were labeled with control cells as standard.

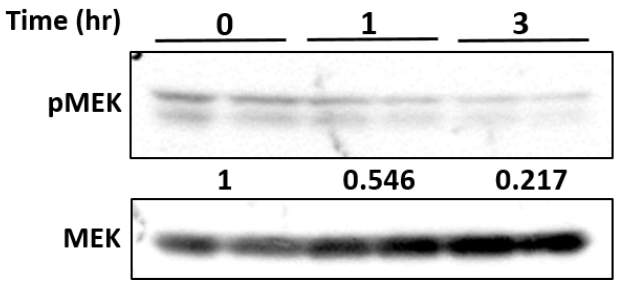

Figure 2-12 Immunoblot of pMEK and total MEK in B16 cells treated with 100 μM BD1047 for indicated time. Mean values of pMEK versus MEK levels were labeled with control cells as standard.

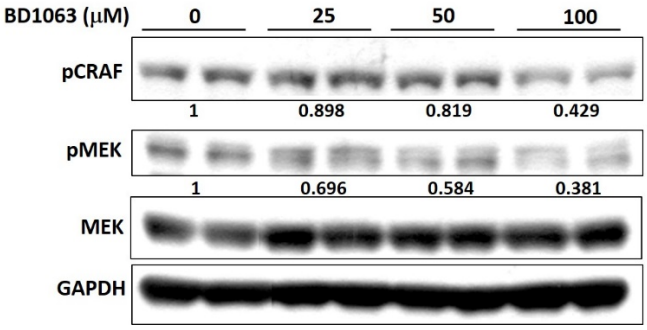

Fggure 2-13 Immunoblot of pCRAF and pMEK in B16 cells treated with the indicated concentrations of BD1063 for 20 hr. Mean values of pCRAF and pMEK versus MEK levels were labeled with control cells as standard.

3.3 B16 cells can generate drug resistance to AAG8 antagonists

To model the emergence of BD1047 resistance, B16 cells were continuously exposed to 100 μM BD1047, an approach that more closely represents the clinical situation.[73] A BD1047-resistant B16 cell line (termed B16BR) was established after 57 days. B16BR cells expressed comparable AAG8 level with B16 cells (Figure 2-14), however, these cells exhibited altered morphology in both 2D and 3D cultures (Figure 2-15, 16). For validating whether these BD1047-resistant cells are also less sensitive to BD1063, both cell lines were queried for sensitivity to BD1063 and BD1047, respectively. Importantly, BD1063, as well as BD1047, significantly suppressed B16 cell growth as compared with B16BR cells, confirming the refractory of B16BR cells to AAG8 antagonists (Figure 2-17). Consistently, AAG8 antagonist treatment failed to restrict B16BR cell migration (Figure 2-18). These data depict an AAG8 antagonist-resistant model which is valuable for further exploration of mechanisms of resistance.

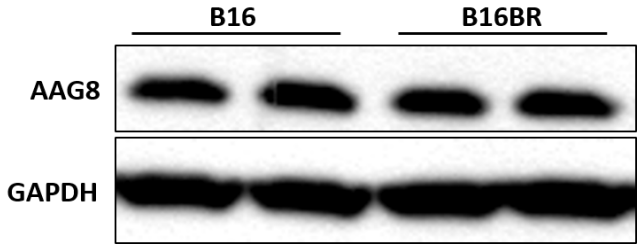

Figure 2-14 Immunoblot of AAG8 in B16BR cells versus B16 cells.

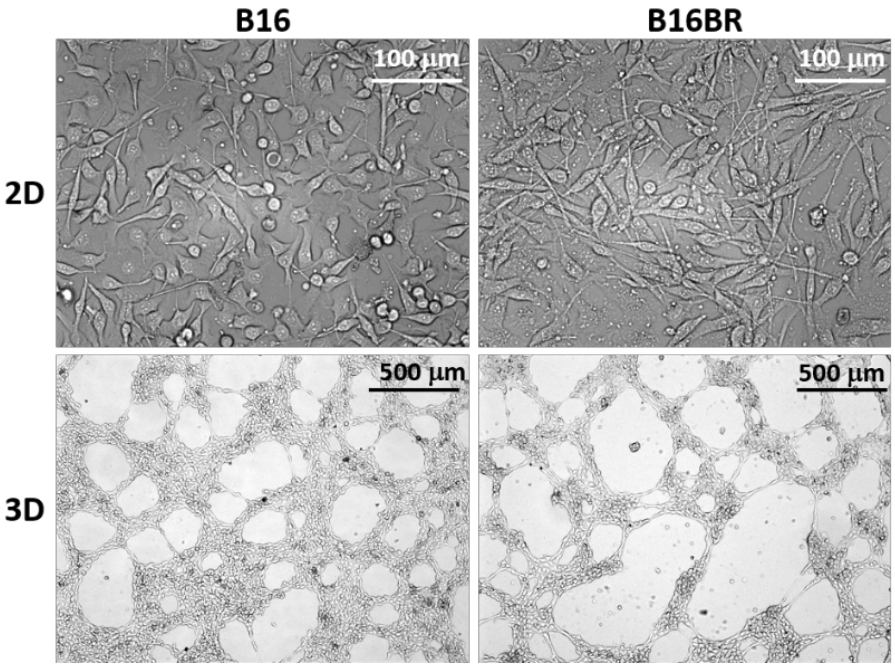

Figure 2-15 Phase contrast images showing different phenotypes of B16 and B16BR cells in 2D (upper) and 3D (lower) cultures, respectively.

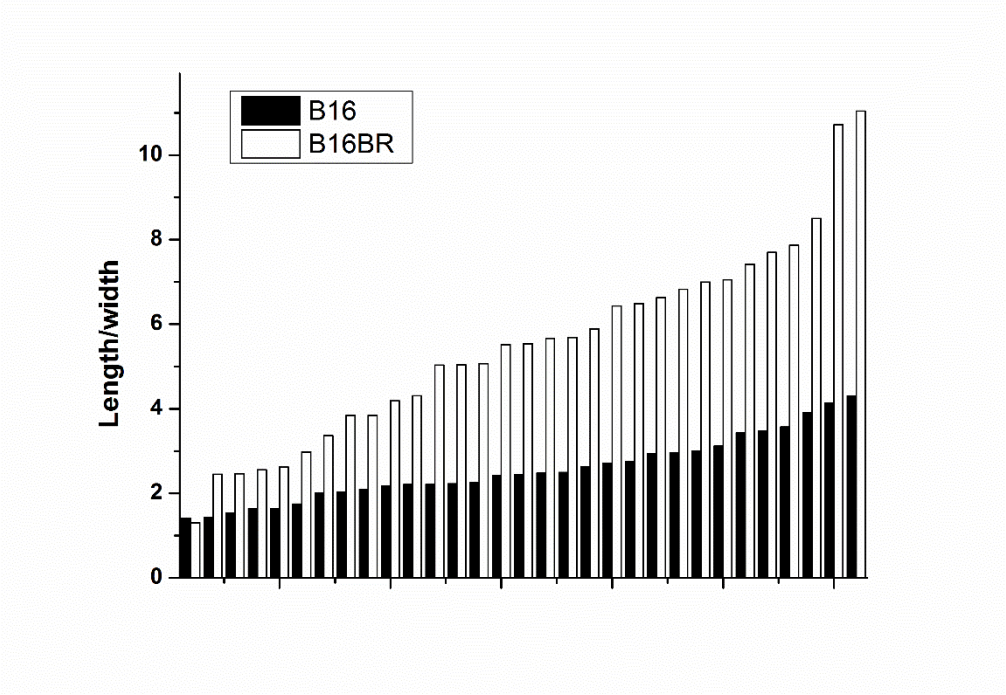

Figure 2-16 Comparision of the length/width ratio of B16 versus B16BR cells in 2D culture. 30 cells were randomly selected from the photo in Figure 2-15 (2D) and analyzed with ImageJ software.

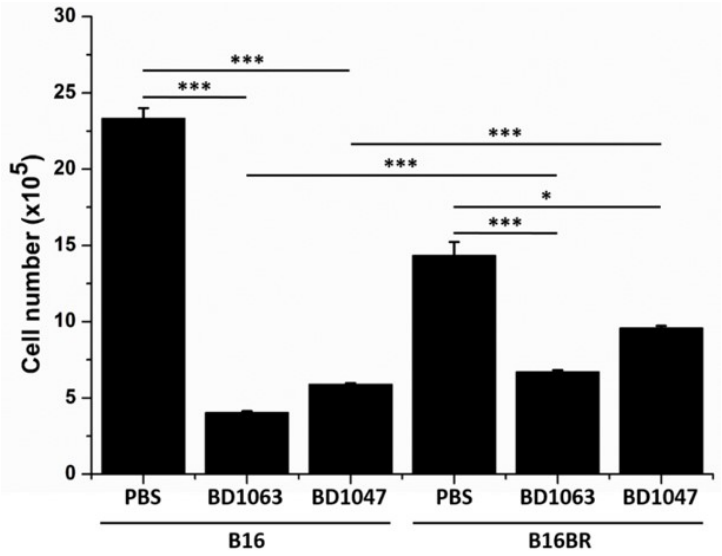

Figure 2-17 Growth assay with Countess™ (Invitrogen) of B16 or B16BR cells treated with 100 μM BD1047 or BD1063 for 96 hr. Initial cell number = 10^5. n = 3. Error bars (s.e.m.) are indicated. Note: * p <0.05, *** p <0.001 (one way ANOVA followed by Tukey's test).

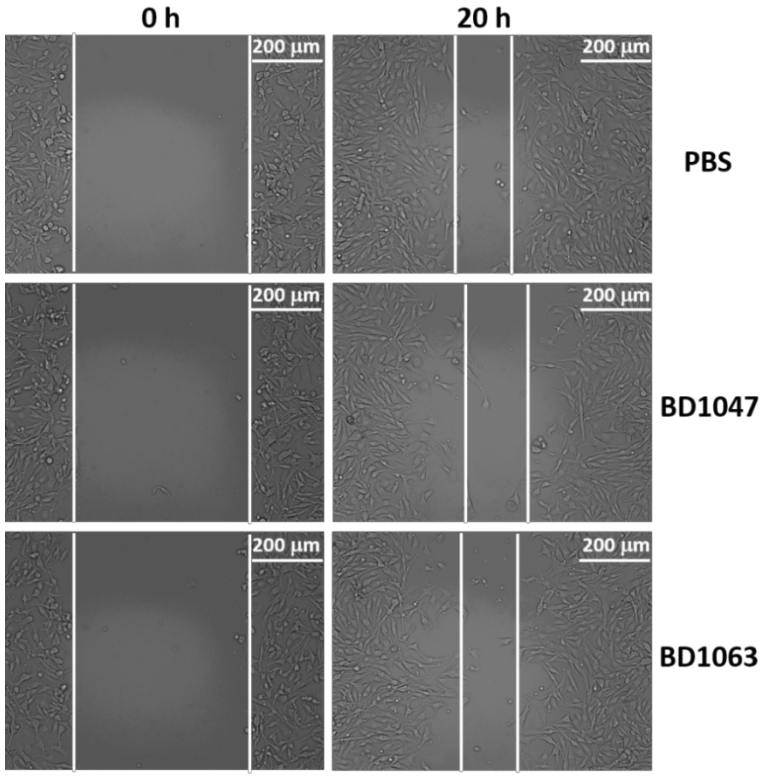

Figure 2-18 Representative images of wound healing assay of B16BR cells treated with 100 μM BD1047 or BD1063. Experiments were performed three times with consistent results.

3.4 MEK confers B16BR cells to AAG8 antagonist resistance

Various drug resistant mechanisms in melanoma have been argued recently.[45,59,60,73,74] Although upregulation and spliced variants of BRAF are often reported in drug-resistant melanoma models,[59,73] I did not detect the aberrant expression of BRAF (Figure 2-19), excluding the possibility of BRAF expression-related resistance. To determine the resistant mechanisms in our model, I tested whether it is associated with decreased sensitivity of MEK activity to AAG8 antagonists. I evaluated the difference between B16 and B16BR cells by measuring pMEK level 6 hr after BD1047 treatment. Whereas pMEK was suppressed in B16 cells, it was almost unaffected in B16BR cells (Figure 2-19). Concurrently, as I observed the mesenchymal-like phenotype of B16BR cells (Figure 2-15), the mesenchymal marker Vimentin (VIM) was compared between these cell lines, indicating there might be epithelial-to-mesenchymal transition (EMT) during the generation of the drug resistance. Neither BD1047 nor BD1063 treatment affected VIM expression, however, VIM expression increased in B16BR cells apparently (Figure 2-19). I conclude that B16BR cells are aggressive mesenchymal melanoma cells and are resistance due to the refractory MEK activity. Given that Johannessen *et al.* identified TPL2 as a MAPK pathway agonist that activates MEK independent of RAF signaling and drives resistance to RAF inhibition in melanoma,[75] I hypothesized that TPL2 might be upregulated in B16BR cells. Strikingly, I found a dramatically diminished expression level of TPL2 in these cells (Figure 2-19). This unanticipated and disparate finding means that TPL2 is not essential for the enhanced MEK activity in AAG8 antagnosts-resistant melanoma but might serve as a tumor suppressor under this circumstance.

Regarding the suppression of CRAF-MEK activity by AAG8 antagonism, I tested whether the upstream CRAF is also refractory to AAG8 antagonism. BD1047 or BD1063 treatment resulted in decreased CRAF phosphorylation in B16 cells, albeit modestly, but not in B16BR cells (Figure 2-19). Considering this modest change might be due to the shorter time (6 hr) treatment, I increased the treatment period to 20 hr for both cell lines. Apparently, B16BR cells did respond to BD1047 treatment at higher dose (300 μM), however, the degree of pCRAF and pMEK inhibition was less profound versus B16 cells under the same

conditions (Figure 2-20). These data confirmed that refractory CRAF-MEK activity confers B16BR cell resistance to AAG8 antagonism.

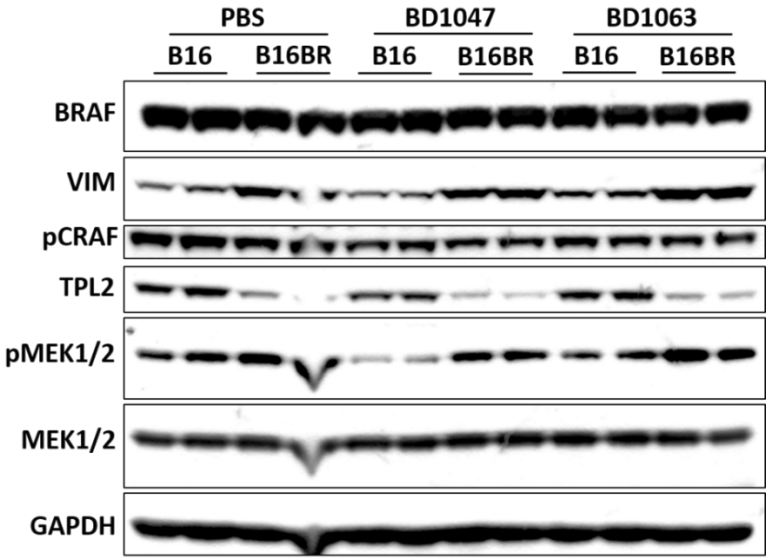

Figure 2-19 Immunoblot comparing the indicated proteins in B16 and B16BR cells treated with PBS, 100 μM BD1047 or 100 μM BD1063 for 6 hr.

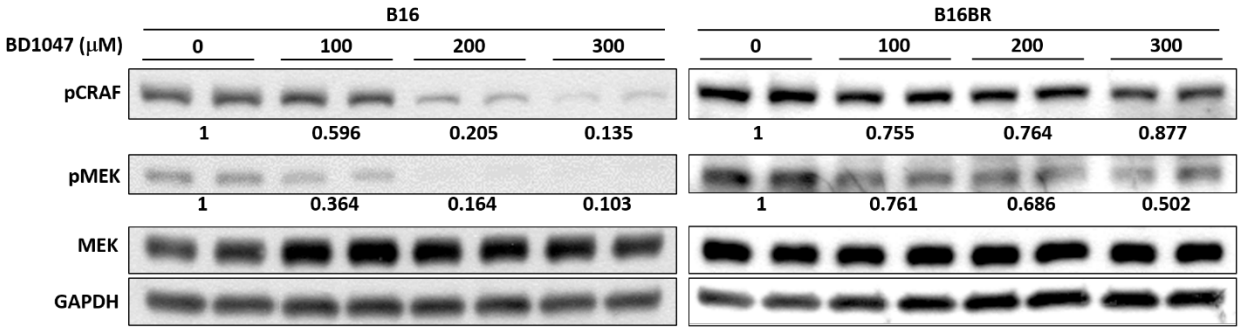

Figure 2-20 Immunoblot of pCRAF and pMEK shows the refractory CRAF and MEK activity in B16BR cells versus B16 cells treated with indicated concentrations of BD1047 for 20 hr. Mean values of pCRAF and pMEK versus MEK levels were labeled with control cells as standard.

RAS activity was next examined to investigate whether the reactivation of CRAF-MEK signaling is due to RAS reactivation. Surprisingly though, while BD1047 dramatically reduced RAS-GTP level in B16 cells, RAS activation was largely abrogated in B16BR cells (Figure 2-21). These data suggest that while RAS-CRAF-MEK signaling is efficiently suppressed by AAG8 antagonism in B16 cells, some other pathways, rather than RAS, have been triggered to substitute the function of RAS and maintain the refractory CRAF-MEK activity, which contributes to the drug resistance of B16BR cells (Figure 2-22). Though mutationally activated RAS is a common event in carcinogenesis[76,77], our findings suggest that RAS mutation might not be involved in AAG8 antagonists-induced drug resistance. These data also reveal the tricky mechanisms which cancer cells lacking oncogenetic RAS employ to generate drug resistance.

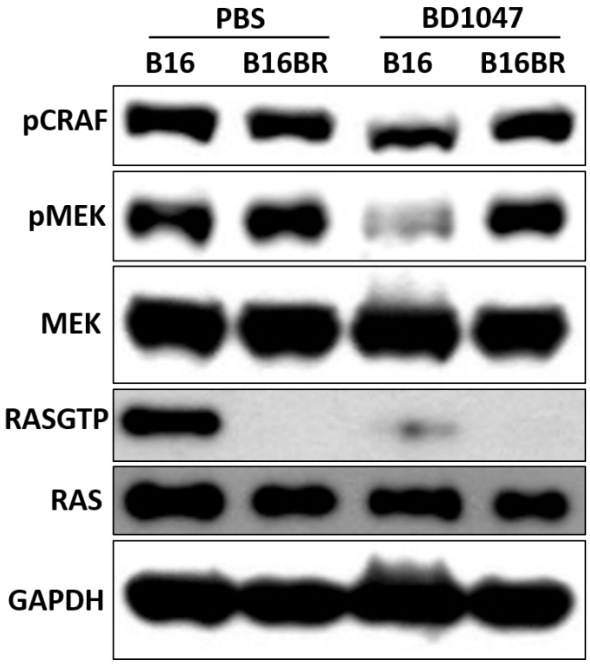

Figure 2-21 Immunoblot of pCRAF, pMEK, MEK, RASGTP, RAS and GAPDH in B16 versus B16BR cells treated with PBS or 100 μM BD1047 for 12 hr.

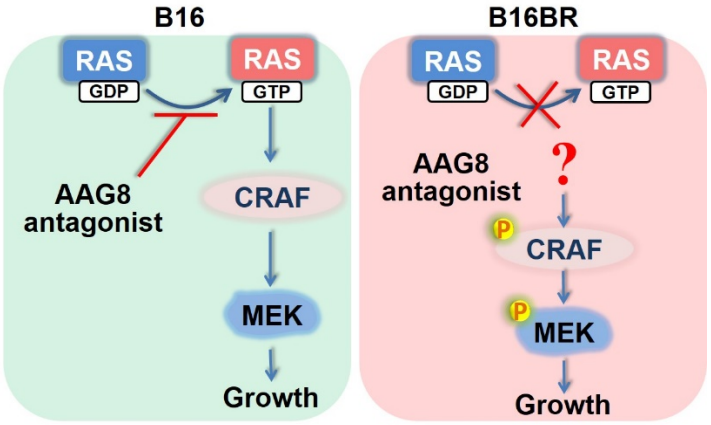

Figure 2-22 A hypothetic model that illustrates the mechanisms of AAG8 antagonism in melanoma cells.

3.5 Tandem AAG8-MEK inhibition in B16BR cells

Based on the finding that B16BR cells maintain refractory MEK activity, I supposed that combined inhibition of AAG8 and MEK could limit B16BR cell growth more efficiently. Substantiating this conjecture, I combined BD1047 and PD901 (hereafter PD901), a selective MEK inhibitor currently in clinical cancer trials which blocks MEK1 at values of 1 μM in vitro.[78] However, MEK inhibitors have often been reported for drug resistance and dose-limiting side effects, resulting the compromised efficacy.[71] To more closely mimic the clinical situation and decrease the cytostatic activity, I used a much lower dose at 50 nM PD901 for modeling our drug combination strategy. Intriguingly, whereas PD901 showed similar growth inhibitory effect with BD1047, combined treatment significantly decreased cell numbers, comparing with either BD1047 or PD901 treatment (Figure 2-23, 24). Because upregulation of counteracting signaling cascades as a direct response to MEK inhibition limits the efficacy of MEK inhibitors in melanoma patients,[74] our results pinpoint the collaborative effect of AAG8 antagonism and MEK inhibition and suggest AAG8 plus MEK inhibitory combination therapy as a potential therapeutic strategy for melanoma. This drug combination uses very low dose of MEK inhibitor and has critical implications for reducing the drug side effects during clinical melanoma prevention.

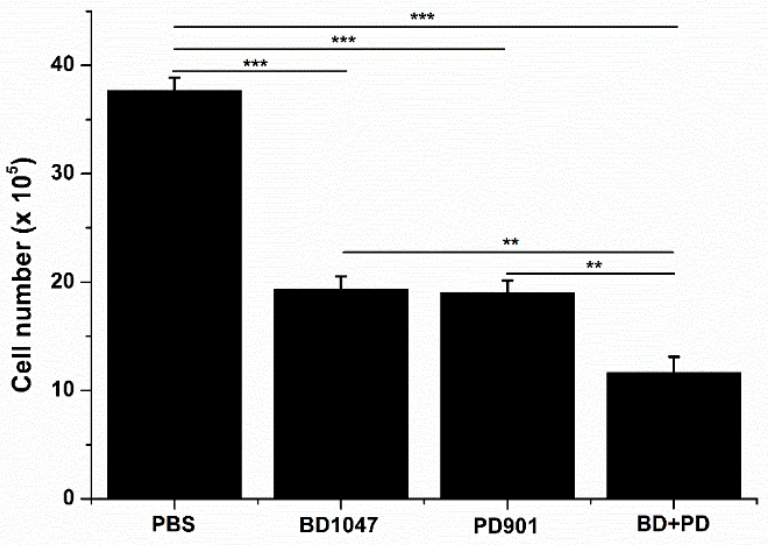

Figure 2-23 Tandem AAG8-MEK inhibition in B16BR cells treated with 100 μM BD1047 and/or 50 nM PD901 for 65 hr. Initial cell number = 5×10^5. n = 3. Error bars (s.e.m.) are indicated. Note: ** p <0.01, *** p <0.001 (one way ANOVA followed by Tukey's test).

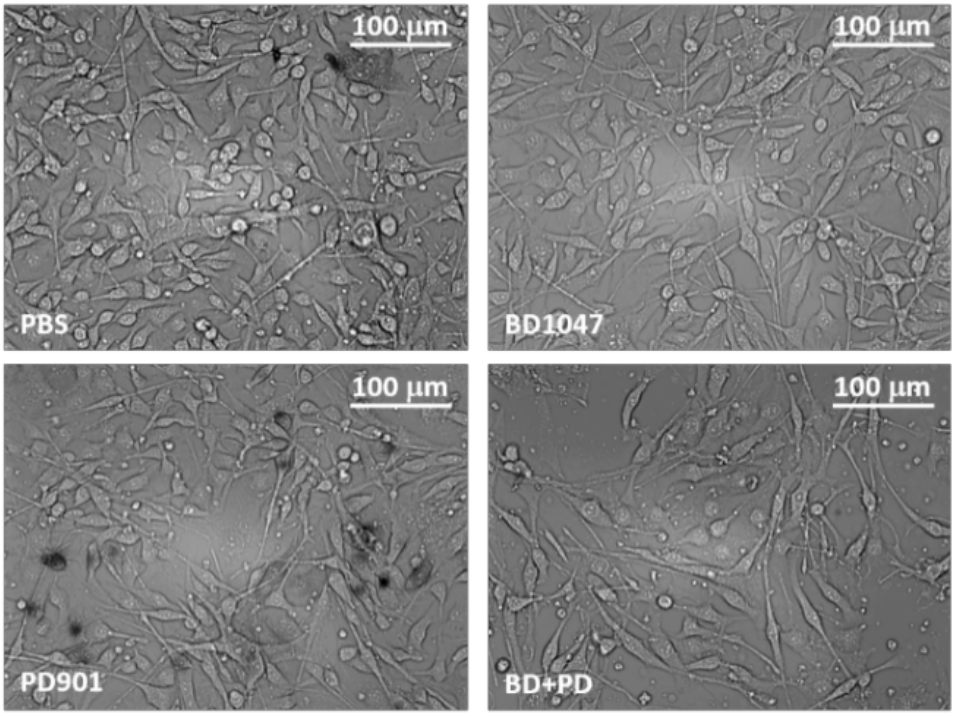

Figure 2-24 Phase contrast images of B16BR cells as described in (B).

4. Discussion

AAG8 is a protein profoundly investigated in neurology.[34] Previous studies have shown its ER-associated functions in lens[37] and mouse Leydig cells[15], however, how AAG8 correlates with carcinogenesis remains unidentified. Our studies uncover the molecular clue that AAG8 antagonism exhibits anti-melanoma effects through inhibition of the RAS-CRAF-MEK signaling activity. In agreement with the recent notion that CRAF S338 phosphorylation is dependent on MEK activity, I theorize that AAG8 antagonism could block this positive feedback loop to restrict melanoma cell growth. I also found that the melanoma cells got resistant during a consistent exposure to AAG8 antagonist. This is noteworthy as it implies that melanoma is incurable due to the acquisition of drug resistance, and the B16BR cell line provide a proper model for investigation of resistance mechanisms.

I employed two specific AAG8 antagonists in the micromolar range, the routinely used concentrations in vitro[69], for modeling the AAG8 antagonism and drug resistance in melanoma cells, though it is a higher dose comparing to current anti-tumor drugs[45]. Promisingly, other synthesized AAG8 ligands have been reported to specifically bind to AAG8 in the nanomolar range[15]. Further efforts are needed to determine whether the anti-tumor ability of AAG8 antagonists and the resistance could be translated in vivo, because this may have implications for developing AAG8 antagonists as novel anti-cancer drugs.

I further demonstrated the underlying resistance mechanisms of B16BR cells. I found that these cells are much less sensitive to AAG8 antagonists, and this is due to, at least partly, the refractory CRAF-MEK activity in these cells. This finding is consistent with the melanoma model that is resistant to RAF inhibitor,[73] suggesting MEK as a common culprit in maintaining melanoma survival in drug-existing microenvironment. Nevertheless, beyond our expectation, B16BR cells harbor little, rather than redundant, RAS activity, despite their sustained CRAF-MEK signaling. Consistent with previous rationales,[74,75,79] our findings suggest the existence of alternative signaling cascades which have been triggered in B16BR cells

to maintain the refractory CRAF-MEK activity. Our data reveal the exquisite modulation mechanisms of cancer cells for survival in response to harsh microenvironment (such as chemotherapeutic drugs).

Based on these molecular findings, I proposed a drug combination strategy, i.e. BD1047-PD901 combination, for tandem AAG8-MEK inhibition in melanoma cells. This combination efficiently limits the growth of B16BR cells, indicating the cooperative effects of these two inhibitors. In addition, despite efficient suppression of MEK activity by MEK inhibitors, cytostatic side effects restrict their efficacy for clinical trial.[71] I showed that AAG8 antagonist combined with even very low concentration (50 nM) of PD901 can significantly decrease the viability of refractory B16BR cells, suggesting that tandem AAG8-MEK inhibition is a powerful therapeutic approach for increasing the antitumor efficacy and decreasing the drug resistance of each single inhibitor.

This research has focused on the mechanistic insights into AAG8 antagonists-induced MEK inhibition and drug resistance. The importance of this study is to provide precise concept and methodology for preliminarily investigating the pharmacological and drug-resistant mechanisms of cancer in vitro. AAG8 antagonists BD1047 and its analogue BD1063 were used for in vitro modeling the AAG8 functions in melanoma. Moreover, our findings provide implications and encourage the medical chemists to improve the specificity and binding affinity of these antagonists for the further feasible clinical use.

Chapter 3 AAG8 Promotes Carcinogenesis through STAT3 Activation

1. Introduction

The STAT (signal transducer and activator of transcription) family consists of seven members: STAT1, STAT2, STAT3, STAT4, STAT5A, STAT5B, and STAT6. STATs are pivotal in modulating cellular functions in response to cytokines, interferons, and various growth factors, which activate JAKs (Janus kinases), leading to key tyrosine phosphorylation on their receptors. JAKs activation allows the binding of STATs via their SH2 domains to these phosphotyrosine docking sites. STATs are in turn tyrosine phosphorylated, thus allowing their dimerization and activation. STATs have been shown to be controlled by several negative regulatory mechanisms. Notably, the SOCS (suppressor of cytokine signalling) family negatively regulates STATs activation [80]. STAT3 is a well-known transcription factor that has been intensively investigated in cancer and immunity [81,82]. Upon phosphorylation at Y705, activated STAT3 translocates into the nucleus to initiate transcription. STAT3 hyperactivation is a feature of the majority of solid cancers. However, how STAT3 activation is regulated is not fully understood.

Despite the previous notably described findings of AAG8 in neuroscience, the importance of AAG8 in cancer has rarely been noticed. In chapter 2, I discovered that AAG8 antagonists potentially inhibits melanoma cells growth, however, the lack of gain- or loss-of-function studies has so far precluded a clear understanding of the rationale of AAG8 in carcinogenesis. In this chapter, I explored the intrinsic roles of AAG8 in cancer cells and found that AAG8 promoted carcinogenesis both in vitro and in vivo. We further characterized AAG8, for the first time to our knowledge, as a STAT3 activator and demonstrated that it alternatively activated STAT3 in addition to IL6/JAK pathway.

2. Materials and methods

2.1 Cell lines and reagents

DLD-1, HCT116, PANC1, AGS, MKN7, MSTO211H and B16 cell lines were obtained from American Type Culture Collection (USA). COLO205 cell line was purchased from RIKEN Cell Bank (Japan). Cell culture was maintained in Dulbecco's Modified Eagle's Medium (DMEM) supplemented with 10% fetal bovine serum (FBS, Life Technologies, Carlsbad, CA, USA) in a standard incubator at 37°C with 5% CO_2. AAG8 antagonists BD1047 and BD1063, and AAG8 agonist PRE084 were purchased from Santa Cruz Biotechnology (Santa Cruz, CA, USA). Matrigel^{TM} basement membrane matrix was from BD Bioscience (Bedford, MA, USA). Recombinant human IL-6 was from Genzyme-Techne (Minneapolis, MN, USA). Gemcitabine was from SIGMA (St Louis, MO, USA). JSI124, YM155, Ruxolitinib, JAK Inhibitor I and JAK Inhibitor VI were included in the SCADS Inhibitor Kits.

2.2 3D culture

3D on-top culture of cancer cells was as described previously with some modifications [67]. Briefly, surface of 6-well plates was coated with pre-thawed Matrigel (500 µl/well) with a pipette tip. For each well, 3×10^5 or 10^6 cells were resuspended in 3 ml of complete Dulbecco's Modified Eagle's Medium containing 5% Matrigel and pipetted onto the pre-coated surface. Chemicals were added into the medium as indicated. Cells were then cultured for the indicated days before further assays. Cells were observed and photographed under a phase contrast microscope (OLYMPUS, Tokyo, Japan).

2.3 Establishing stable cell lines

For AAG8 overexpression, *SIGMAR1* gene was cloned from the cDNA of DLD-1 cells with the forward primer 5'-ACCCAAGCTGGCTAGAATGCAGTGGGCCGTG-3' and reverse primer 5'-GTGGATCCGAGCTCGTCAAGGGTCCTGGCCAAAG-3', and subcloned into pcDNA3.1 vector (Life Technologies) between *Nhe*I and *Kpn*I sites. DLD-1 and AGS cells were transfected with empty vector or the plasmid expressing AAG8 with Lipofectamine LTX with Plus reagent (Life Technologies) according to the manufacture's instructions. 48 h after transfection, cells were selected by 700 μg/ml G418 (WAKO, Wako, Japan). For gene knockdown, we employed the RNA polymerase II promoter U6 in pLKO.1 vector to express shRNA targeting the 5'-CCTCAACCCAGCAGCAATTTG-3' sequence of *SIGMAR1* gene. Lentivirus incorporating with shRNA was generated in HEK293T cells by combining packing plasmid pCMV-dR8.91, envelope plasmid VSV-G (gifts from Dr. Kenneth Rock, University of Massachusetts Medical School, Worcester, MA) and the pLKO.1 plasmids. DLD-1 cells were infected with the lentivirus and selected by 3 μg/ml puromycin (SIGMA). HCT116 and AGS cells were transfected directly with the shRNA plasmids with Lipofectamine LTX with Plus reagent (Invitrogen) according to the manufacture's protocol. 48 h after transfection, cells were selected by 1 μg/ml puromycin (SIGMA). A scramble shRNA plasmid (kindly provided by Dr. David Sabatini, Addgene plasmid 1864) was used as control [83].

2.4 Transient API4 knockdown

DLD-1 cells were transfected with the pLKO.1 shRNAs targeting the 5'-CGTCCGGTTGCGCTTTCCTTT-3' sequence (shAPI4-1) and the 5'-CCGCATCTCTACATTCAAGAA-3' sequence (shAPI4-2) of *BIRC5* (API4) gene, respectively, with Lipofectamine LTX with Plus reagent (Invitrogen) according to the manufacture's protocol. A scramble shRNA plasmid was used as control. Seventy-two hours after transfection, cells were treated as indicated.

2.5 Growth assay and apoptosis assay

For growth assay, dead cells were stained with trypan blue and total cell number was evaluated with Countess™ (Life Technologies). For apoptosis assay, cells were treated with chemicals as indicated in 3D Matrigel culture, and then stained with 1 nM ethidium bromide (EtBr) for 5 min. The stained DNA were observed and photographed under a fluorescence microscope (OLYMPUS).

2.6 Xenografts

Animal experiments were performed in accordance with the policies of the Animal Ethics Committee of the University of Tokyo. Female BALB/c *nu/nu* mice (4 weeks of age) were purchased from the Sankyo Labo Service Corporation. Three million cells with Matrigel in 100 μl were injected into the flank of each mouse subcutaneously and tumors were measured as described previously [84].

2.7 Western blot

Cells were lysed with Laemmli buffer and each lysate sample was loaded into two adjacent lanes, if indicated, of a 10% polyacrylamide gel for minimizing loading differences. For PKM2 detection, cytoplasmic and nuclear fractions were prepared with NE-PER Nuclear and Cytoplasmic Extraction Reagents (Thermo Scientific, Rockford, RL, USA) according to the manual's instructions. Proteins were separated at 30 mA and transferred onto PVDF membranes (Millipore, Darmstadt, Germany). Membranes were blocked for 1 h at room temperature using 5% skim milk or 5% BSA (for phosphorylation detection) in TBS-Tween (TBS-T). Western blot analysis was performed according to the antibody manufacturer's

specifications. The membranes were incubated with primary antibodies overnight in either 5% BSA or 5% skim milk in TBS-T at 4 °C. The membranes were washed thrice in TBS-T. The appropriate HRP-conjugated secondary antibody was added into 5% skim milk in TBS-T, followed by three washes in TBS-T. The membranes were developed using a Luminata Crescendo Western HRP substrate (Millipore).

Antibodies used in this work are as follows: pSTAT3 (#9145) antibodies were from Cell Signalling Technology (Danvers, MA, USA). STAT3 (sc-482), antibodies were from Santa Cruz Biotechnology. AAG8 (HPA018002) and GAPDH (G9295) antibodies were from SIGMA. API4 (NB500-201H) and LMNB (NBP1-19804) antibodies were from NOVUS (Littleton, CO, USA). PKM2 (ab150377) antibody was from abcam (Cambridge, MA, USA). The secondary HRP-conjugated anti-rabbit IgG antibody (G21234) was from Life Technologies.

2.8 Statistical analysis

All statistical analysis was performed using Origin 8 Software. Error bars indicate standard errors of the mean (S.E.M.). Time courses or dose dependence were analyzed by two-tailed unpaired t-test or one-way ANOVA followed by appropriate post hoc test.

3. Results

3.1 Oncogenetic AAG8

We firstly observed that specific AAG8 antagonist BD1047 induced growth-suppressive phenotype of colorectal COLO205 cancer cells (Figure 3-1), pancreatic PANC1 cancer cells and gastric AGS cancer cells (Figures 3-2, 3-3) in 3D Matrigel culture. Moreover, BD1047 potently suppressed mesothelioma MSTO211H cell growth in 3D culture, by contrast, AAG8 agonist PRE084 failed to suppress their growth and tube formation, though different phenotype was observed (Figure 3-4). In addition, BD1047 induced apoptosis of 3D-cultured COLO205 cells (Figure 3-5). BD1047 also dose-dependently suppressed the growth of colorectal COLO205 and DLD-1 cancer cells, as well as gastric MKN7 cancer cells (Figure 3-6).

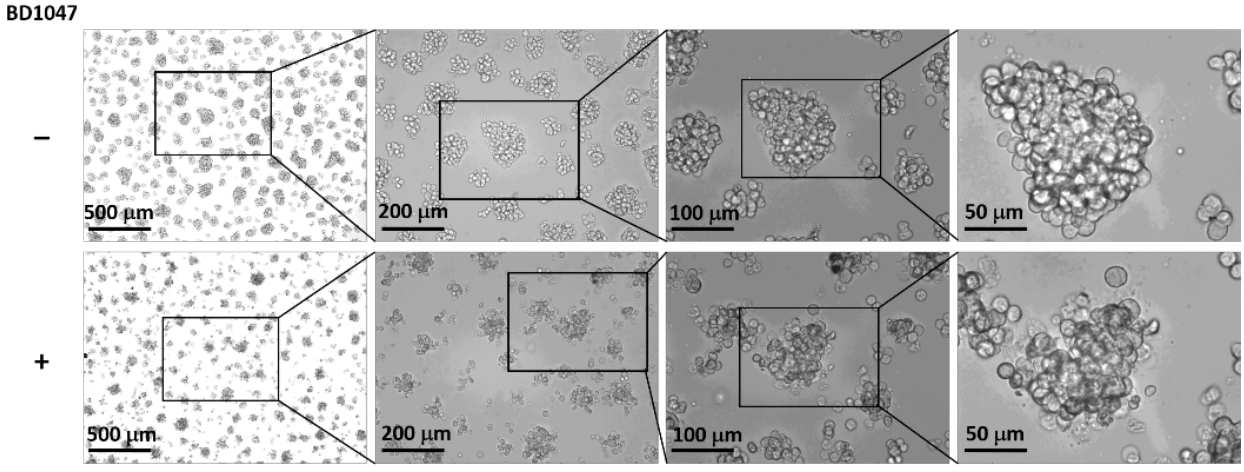

Figure 3-1 Phase contrast images showing COLO205 cells cultured in 3D Matrigel and treated with or without 100 μM BD1047 (AAG8 antagonist) for 48 h.

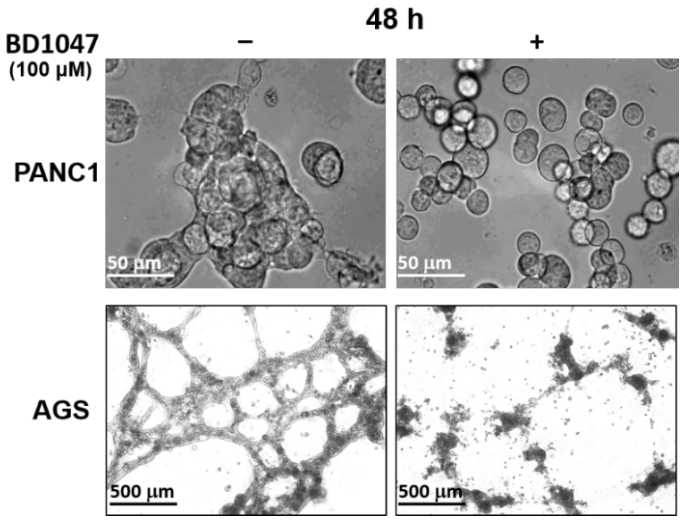

Figure 3-2 Phase contrast images of PANC1 and AGS cells cultured in 3D Matrigel and treated as indicated.

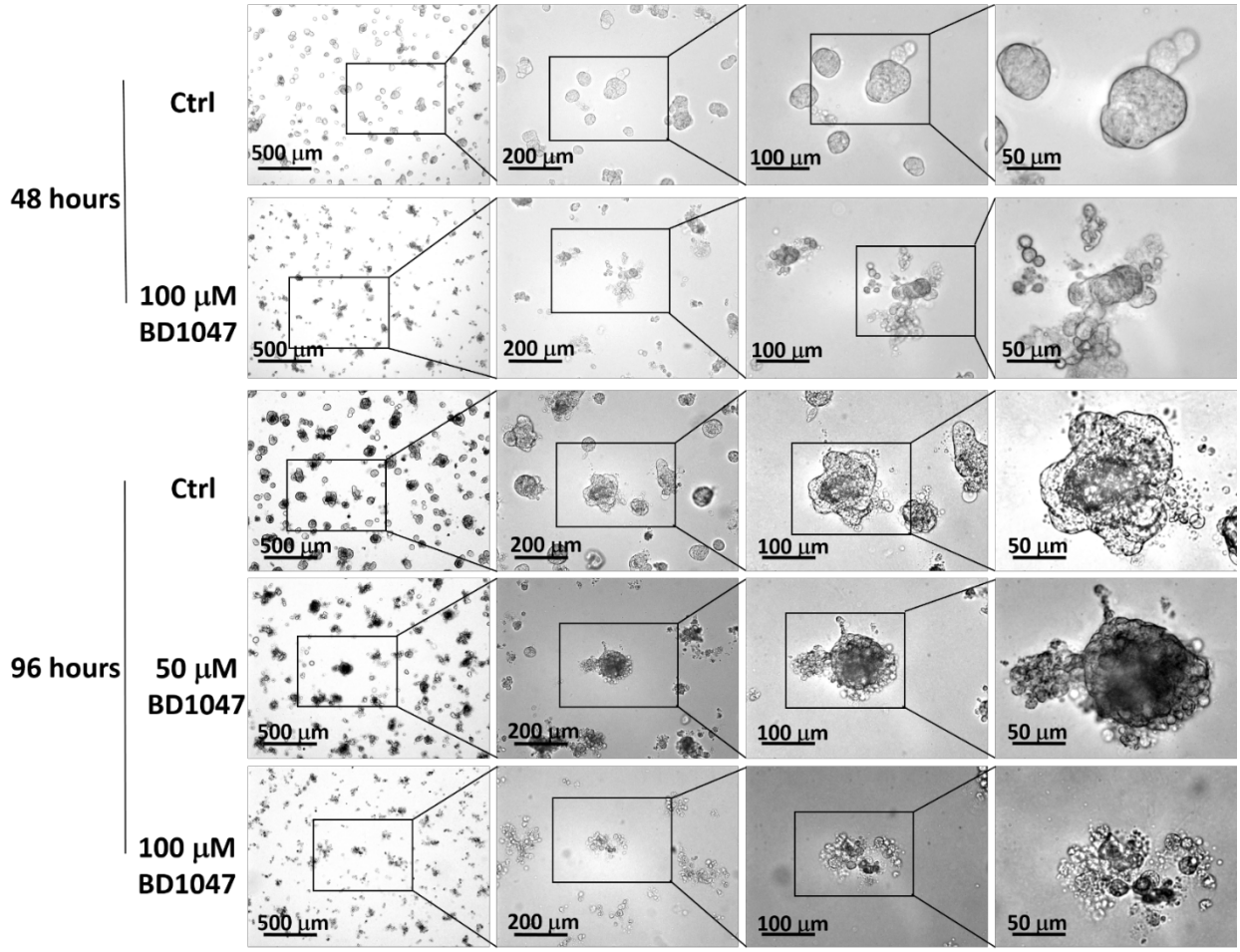

Figure 3-3 Phase contrast images of AGS cells cultured in 3D Matrigel and treated as indicated.

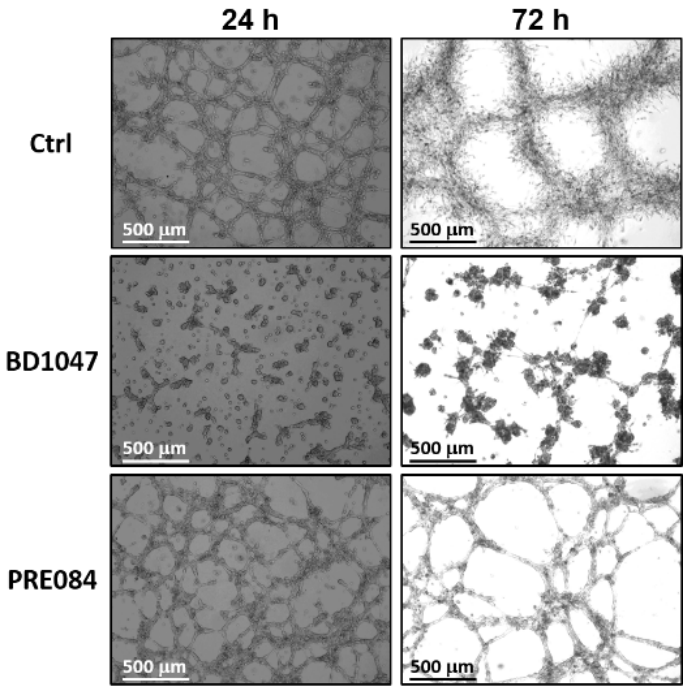

Figure 3-4 Phase contrast images MSTO-211H cells cultured in 3D Matrigel and treated as indicated.

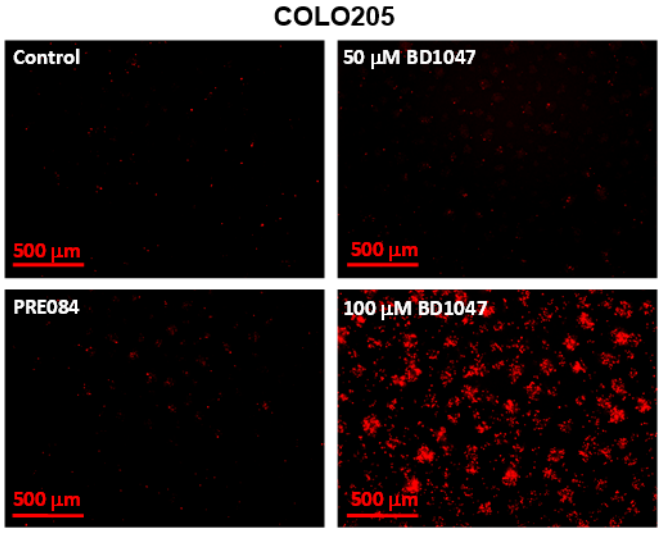

Figure 3-5 COLO205 cells in 3D culture were treated with 10 µM PRE084 (AAG8 agonist) or BD1047 of indicated concentrations for 72 h and stained with EtBr for indicating apoptosis.

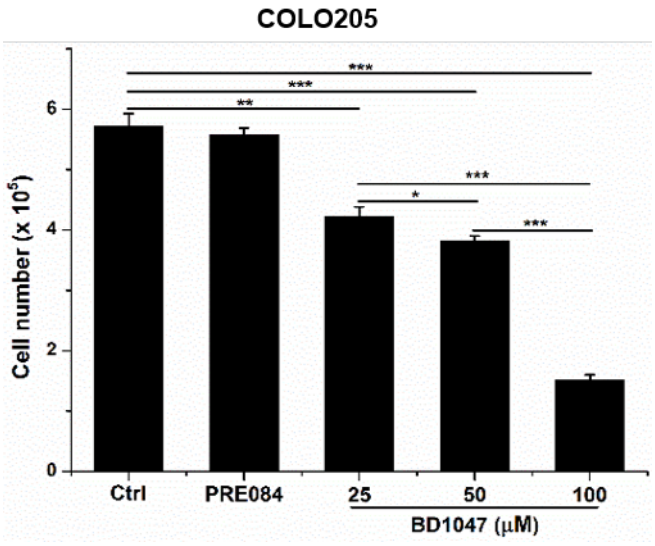
COLO205
Cell number (x 10^5)
0
2
4
6
***
***
**
***
*
***
Ctrl
PRE084
25
50
100
BD1047 (μM)

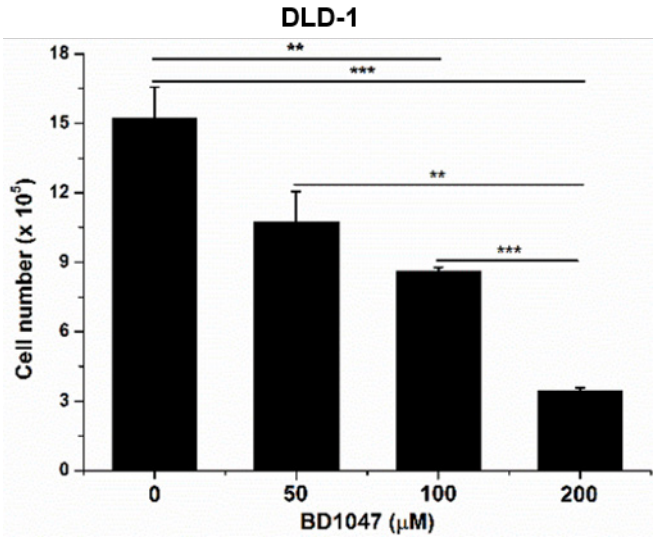
DLD-1
Cell number (x 10^5)
0
3
6
9
12
15
18
**
***
**
***
0
50
100
200
BD1047 (μM)

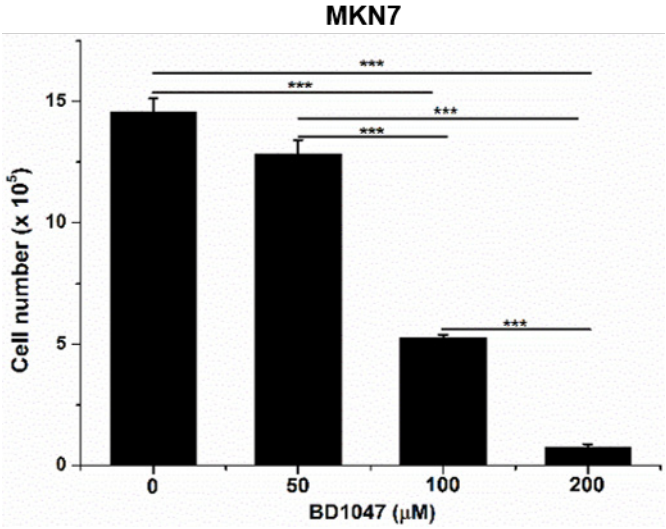
MKN7
Cell number (x 10^5)
0
5
10
15
***
***
***
***
***
0
50
100
200
BD1047 (μM)

Figure 3-6 Growth assay with Countess^{TM} (Invitrogen) of COLO205, DLD-1 and MKN7 cells in 2D culture treated with BD1047 of indicated concentrations or 10 μM PRE084 for 50 h. DLD-1: initial cell number = 5×10^5; n = 4. COLO205: initial cell number = 2×10^5. n = 4; MKN7: initial cell number = 5×10^5. n = 3. Error bars (s.e.m.) are indicated. * $p < 0.05$, ** $p < 0.01$, *** $p < 0.001$ (one way ANOVA followed by Tukey's test).

Gain- and loss-of-function approaches were next employed for further confirmation. AAG8 overexpression promoted proliferation of both DLD-1 (Figure 3-7) and gastric AGS (Figure 3-8) cancer cells. In line with this, AAG8 knockdown with short hairpin RNA (shRNA) delayed DLD-1 cell proliferation (Figure 3-9), and suppressed AGS cell growth in 3D culture (Figures 3-10, 3-11), which closely mimicked the phenotype changes observed with AAG8 antagonist (Figure 3-2). Interestingly, although AAG8 knockdown resulted in little to no alternations to the morphogenesis of colorectal HCT116 cancer cells in 3D culture, it increased their sensitivity to gemcitabine, a clinical cancer drug (Figures 3-12, 3-13). In agreement with the data in vitro, AAG8 knockdown slowed xenograft tumor formation of DLD-1 cells in vivo (Figure 3-14). These results collectively illustrate the tumor-promoting roles of AAG8 and imply that AAG8 serves as an oncoprotein and indicate AAG8 as a potential target for tumor chemotherapy.

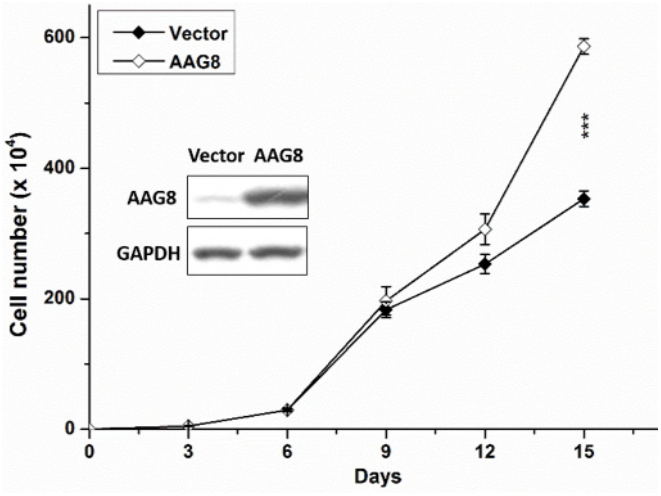

Figure 3-7 Immunoblot of AAG8 and proliferation assay of DLD-1 cells with stable overexpression. Total lysates from control and stable cell lines were immunoblotted with AAG8 antibody; GAPDH served as loading control. Cell number was counted every 3 days. Initial cell number = 5×10^3. n = 3. Error bars (s.e.m.) are indicated. * $p < 0.05$, *** $p < 0.001$ (two-tailed unpaired t-test).

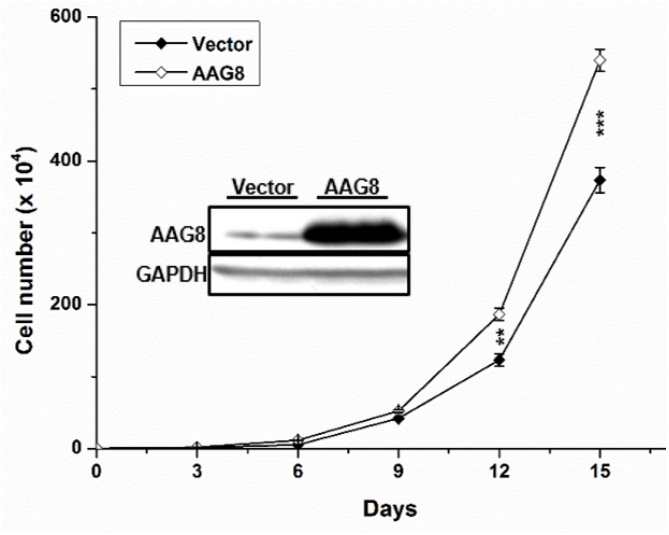

Figure 3-8 Enhanced AGS cell proliferation by AAG8 overexpression. Immunoblot of AAG8 and proliferation assay of AGS cells with stable AAG8 overexpression. Total lysates from control and stable overexpression cell lines were immunoblotted with AAG8 antibody; GAPDH served as the loading control. Cell number was counted every 3 days. Initial cell number = 5×10^3. n = 3. Error bars (s.e.m.) are indicated. ** $p < 0.01$, *** $p < 0.001$ (two-tailed unpaired t-tests).

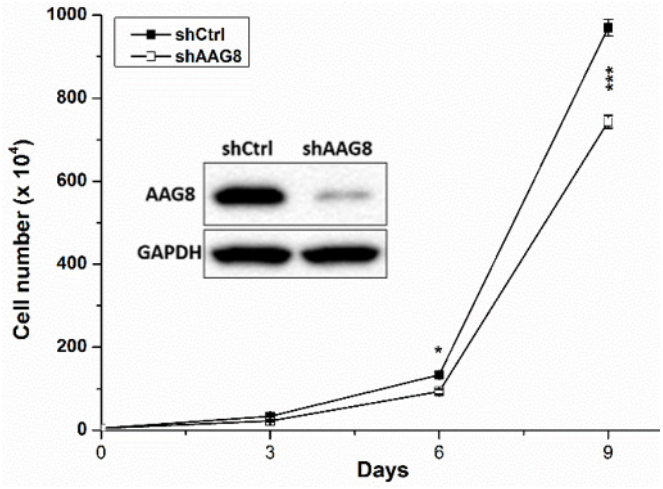

Figure 3-9 Immunoblot of AAG8 and proliferation assay of DLD-1 cells with stable AAG8 knockdown (right). Total lysates from control and stable knockdown cell lines were immunoblotted with AAG8 antibody; GAPDH served as loading control. Cell number was counted every 3 days. Initial cell number = 5×10^4. n = 3. Error bars (s.e.m.) are indicated. * $p < 0.05$, *** $p < 0.001$ (two-tailed unpaired t-test).

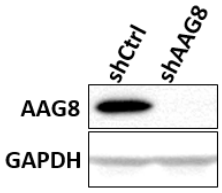

Figure 3-10 Immunoblot of AAG8 in stable AAG8-knockdown AGS cells. Total lysates from control and stable knockdown cell lines were immunoblotted with AAG8 antibody; GAPDH served as the loading control.

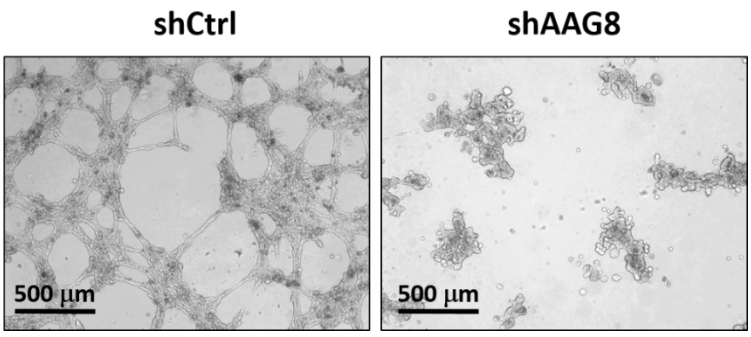

Figure 3-11 Phase contrast images showing AAG8-knockdown AGS cells cultured in 3D Matrigel.

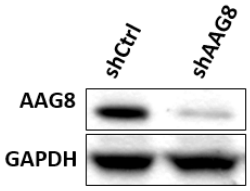

Figure 3-12 Immunoblot of AAG8 in stable AAG8-knockdown HCT116 cells. Total lysates from control and stable knockdown cell lines were immunoblotted with AAG8 antibody; GAPDH served as the loading control.

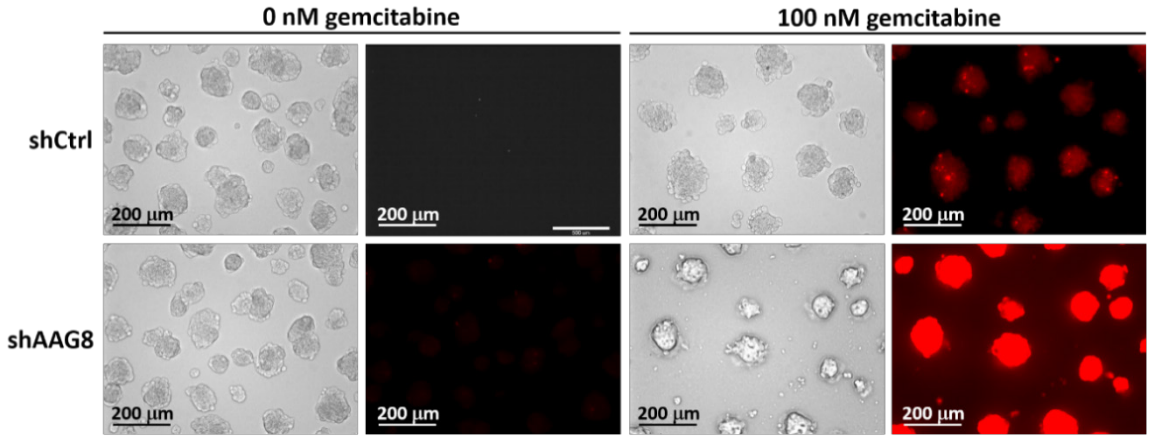

Figure 3-13 Phase contrast and immunofluorescence images of HCT116 cells treated with or without 100 nM gemcitabine for 72 h and then stained with EtBr for indicating apoptosis.

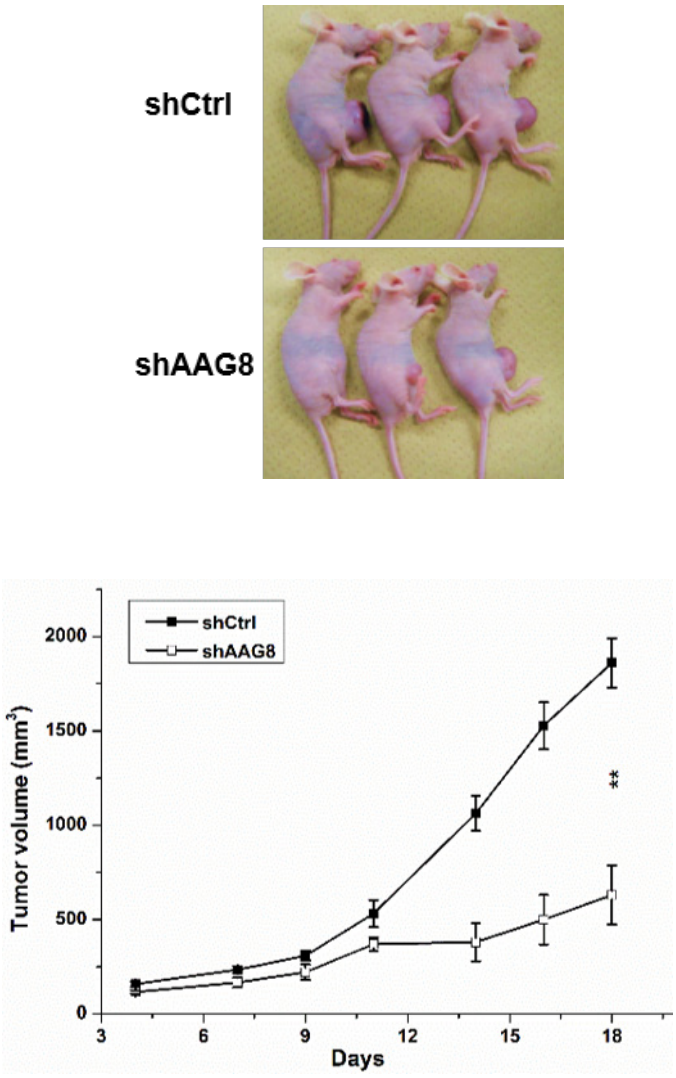

Figure 3-14 Three million DLD-1 cells were injected subcutaneously into athymic nude mice. Representative pictures of mice are shown in left panel and quantitative measurements are shown in right. n = 7 (shCtrl), n = 8 (shAAG8). Error bars (s.e.m) are indicated. ** p <0.01 (one way repeated ANOVA followed by Tukey's test).

3.2 Identification of AAG8 as a STAT3 activator

For explaining the underlying molecular mechanisms of AAG8 in promoting carcinogenesis, I unanticipatedly discovered STAT3 inactivation in both PANC1 (Figure 3-15) and AGS cells treated with BD1047 in a dose-dependent manner (Figure 3-16). Time-dependent assay revealed that STAT3 activity began to decrease 3 hours after BD1047 treatment and was largely suppressed after 6 hours in mouse melanoma B16 cells (Figure 3-17). I supposed that AAG8 may act as a STAT3 activator to enhance cancer cell proliferation. Supporting this hypothesis, I found that STAT3 Y705 phosphorylation level was increased by ectopic AAG8 expression in DLD-1 cells (Figure 3-18, left). Consistently, AAG8 knockdown decreased STAT3 activation in both DLD-1 cells (Figure 3-18, right), as well as in AGS cells (Figure 3-19). These findings convincingly indicate AAG8 as an upstream STAT3 activator.

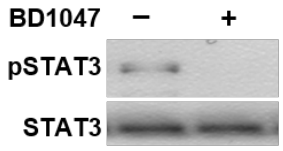

Figure 3-15 Immunoblot of pSTAT3 and STAT3 in PANC1 cells in 3D culture treated with 100 μM BD1047 for 48 h.

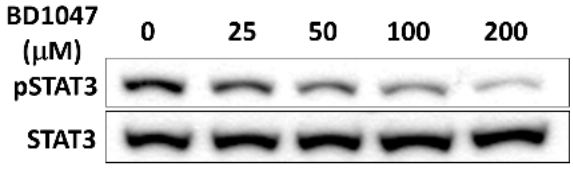

Figure 3-16 Immunoblot of pSTAT3 and STAT3 in AGS cells in 2D culture treated with BD1047 of indicated concentrations for 24 h.

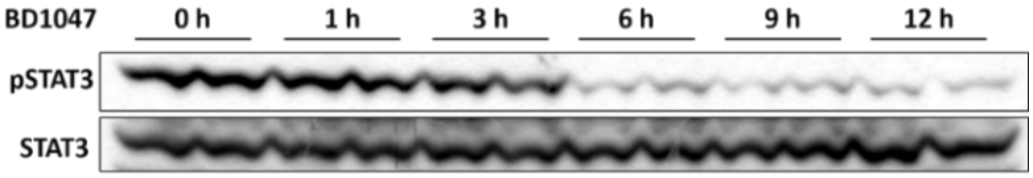

Figure 3-17 Immunoblot of pSTAT3 and STAT3 in B16 cells in 2D culture treated with 100 μM BD1047 for different periods of time (0, 1, 3, 6, 9 and 12 h). Total lysates from control and treated cells were immunoblotted with pSTAT3 antibody; STAT3 served as loading control.

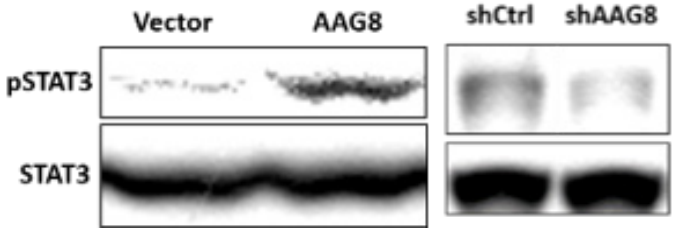

Figure 3-18 Immunoblot of pSTAT3 and STAT3 in DLD-1 cells with stable AAG8 overexpression (left panel) or stable AAG8 knockdown (right panel). Mean values of pSTAT3 versus STAT3 levels were labeled with control cells as standard.

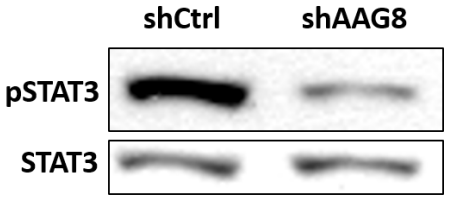

Figure 3-19 Immunoblot of pSTAT3 and STAT3 in stable AAG8-knockdown AGS cells. Mean values of pSTAT3 versus STAT3 levels were labeled with control cells as standard. Total lysates from control and treated cells were immunoblotted with pSTAT3 antibody; STAT3 served as loading control.

3.3 Dual STAT3 activation by AAG8 and JAK signalling

I next performed a SCADS (screening committee of anticancer drugs) screening using DLD-1 cells stably expressing both AAG8 and a luciferase STAT3 reporter, in which STAT3 activity could be monitored after drug treatment. Among 364 chemicals with 232 targets (Table 1), an API4 (apoptosis inhibitor 4) inhibitor, YM155, was found to dramatically (fold change > 20) decrease STAT3 activity in these cells (Figure 3-20). This is consistent with the published data that YM155 reduced STAT3 phosphorylation in PANC1 cells [85], and suggested that YM155 might block STAT3 activation either dependent on or independent of AAG8-related signalling. To further disentangle this event, DLD-1 cells with stable AAG8 knockdown were treated with or without YM155 for 12 h, followed by IL6 stimulation, because the IL6-JAK-STAT3 pathway has been well established previously. As a result, IL6-induced robust STAT3 activation was largely abolished by YM155 treatment (Figure 3-21), confirming the STAT3 inhibitory effect of YM155 in SCADS screening and suggesting that YM155 disturbs the signalling activities which are indispensable for IL6-induced STAT3 activation. In contrast, AAG8 knockdown contributes no change to IL6-induced STAT3 phosphorylation level (Figure 3-21), meaning that AAG8 activates STAT3 beyond IL6-dependent manner. Substantiating this conjecture, specific AAG8 antagonists BD1047 or its analog BD1063 failed to decrease IL6-induced STAT3 activation in DLD-1 cells (Figure 3-22). Surprisingly, AAG8 knockdown further diminished the remaining pSTAT3 in YM155-treated cells (Figure 3-21). Based on the above findings, I hypothesized that AAG8 knockdown could also decrease STAT3 activity in cells with inhibition of IL6/JAK pathway. As expected, similar results to Figure 3-21 was obtained with two JAK inhibitors, JAK inhibitor I and Ruxolitinib, respectively (Figure 3-23).

Target	Compound
antitumor (thymidylate synthetase)	5-FU
antitumor (aminopeptidase B)	Bestatin
antitumor (DNA)	Bleomycin sulfate
antitumor (DNA)	Cisplatin
antitumor (DHFR)	Methotrexate
antitumor (DNA)	Mitomycin C
antitumor (tubulin)	Vinblastine sulfate
antitumor (tubulin)	Paclitaxel
antitumor (AR)	Flutamide
antitumor (DNA)	Daunorubicin, HCl
antitumor (DNA)	Doxorubicin, HCl
antitumor (ER)	Tamoxifen, citrate
antitumor (RNA)	Actinomycin D
antitumor (topo I)	Camptothecin
antitumor (topo I/II)	Aclarubicin
antitumor (topo II)	Etoposide (VP-16)
actin filament	Cytochalasin D
adenylcyclase	2',5'-dideoxyadenosine
AKT	AKT inhibitor
AKT	NL-71-101
Bcr-Abl	AG957
CAMKII	KN93
caspase	Z-VAD-FMK
CDC2	Kenpaullone
CDK2	Purvalanol A
CDK4	3-ATA
CDKs	Olomoucine
CKII	TBB
COX-1	Sulindac sulfide
COX-1	Valeryl salicylate
COX-2	NS-398
COX	Sodium salicylate
cyclicphosphodiesterase	Theophylline
DNA methyltransferase	Azacytidine
DNA polymerase	Aphidicolin
EGFR	AG1478
EGFR, topoII	Genistein
farnesyltransferase	Manumycin A
farnesyltransferase	FTI-276
Flk-1	SU1498
geranylgeranyltransferase I	GGTI-286

GR	Dexamethasone
GSK-3	GSK-3 inhibitor II
HDAC	Scriptaid
HDAC	Trichostatin A
HER2 (erbB2/neu), EGFR	AG825
protein synthesis	Cycloheximide
HMG-CoA reductase	Lovastatin
HSP90	Radicicol
HSP90	17-AAG
IGF-1R	AG1024
iNOS	1400W, HCl
iNOS	AMT, HCl
Jak-2	AG490
Jak-2	Cucurbitacin I
JNK	SP600125
lck (p56), TYK	Damnacanthal
MEK	PD 98059
MEK	U0126
methionine aminopeptidase	Fumagillin
MMP	GM 6001
NF-kB	N-Acetyl-L-cysteine
NOS	Aminoguanidine, HCl
NOS	L-NMMA
p38 (MAPK)	PD169316
p38 (MAPK)	SB 203580
p70 S6K	Rapamycin
PARP	NU1025
PARP-1	Benzamide
PC-PLC	D609
PDE	IBMX
PDE (cAMP)	Ro-20-1724
PDE (cGMP)	Zaprinast
PDGFR	AG1296
PI3K	LY294002
PI3K	Wortmannin
PKA	H-89, HCl
PKC	Bisindolymaleimide I, HCl
PKC, PKA	H-7
PKC, PKA, PKG, MLCK	Staurosporine
PLA2	cPLA2inhibitor
PLA2	OBAA
PP2A	Cantharidin
PP2A	Cytostatin

PP2B/cyclophilin	Cyclosporin A
PP2B/FKBP	FK-506
proteasome	MG-132
proteasome	Lactacystin
ribonucleotide reductase	Hydroxyurea
ROCK	HA1077
ROCK	Y27632
Src, Fyn, Lck	PP1 (analog)
Src, Fyn, Lck	PP-H
tubulin depolymerization	Nocodazole
tyr phosphatase (PTP)	Dephostatin
p53	Pifithrin-a (cyclic)
p53 activator	PRIMA-1
5α-reductase	Finasteride
aromatase	Aminoglutethimide
aromatase	Formestane
progesterone receptor	Mifepristone
acetyl-CoA carboxylase (ACC)	TOFA
aminopeptidase A	Amastatin
aminopeptidase M	Actinonin
F1-ATPase	Oligomycin
V-ATPase	Bafilomycin A1
Bcl-2	HA 14-1
Bcl-XL	BH3I-1
Burton's tyrosine kinase(BTK)	LFM-A13
Burton's tyrosine kinase(BTK)	Terreic acid
calpain	E-64d
calpain, cathepsin B, L	ALLN
cathepsin B	CA-074
cathepsin D	Pepstatin A
cathepsin G	Z-GLF-CMK
CCR2	RS 102895
CCR3	SB 328437
CXCR2	SB 225002
CXCR4	AMD3100 octahydrochloride
Cdc25	NSC95397
Cdc25A	SC-αασ9
Na channel	Amiloride
Na channel	Lidocaine
Na ionophore	Monensin
Na/K ATPase	Ouabain
Na/K/Mg ATPase	Sanguinarine
K channel	Glibenclamide

K channel	Dequalinium
K channel opener	Diazoxide
K ionophore	Valinomycin
K ionophore	Nigericin
Ca channel	Diltiazem
Ca channel	Nifedipine
Ca channel, MDR	Verapamil
MDR	PGP-4008
BCRP	Fumitremorgin C
Ca ionophore	A23187
Ca ionophore	Ionomycin
Ca-ATPase	Thapsigargin
Ca-ATPase	t-Butylhydroquinone (BHQ)
Cl channel	N-phenylanthranilic acid
Cl channel	DIDS
Chk 1	SB 218078
Chk 1, 2	Debromohymenialdisine (DBH)
mitochondrial complex I	Rotenone
mitochondrial complex III	Antimycin A1
CRM1	Leptomycin B*
DAG kinase	R59022
DAG kinase	Dioctanoylglycol
DAG lipase	RHC80267
DAG acyltransferase (DGAT)	Xanthohumol
fatty acid synthase (FAS)	C75
FAS	Cerulenin
glycosylation	Tunicamycin
glucosidase I, II	Deoxynojirimycin
a-mannosidase	Swainsonine
guanylate cyclase	LY 83583
guanylate cyclase	ODQ
HAT	Anacardic acid
HIF	Chetomin
HIF-1a hydroxylase	Dimethyloxalylglycine
kinesin Eg5	HR22C16
kinesin Eg5	Monastrol
lipoxygenase	Nordihydroguaiaretic acid (NDGA)
12, 15-lipoxygenase	ETYA
12-lipoxygenase	Baicalein
Mdm2	Nutlin-3
Mdm2	MDM2 inhibitor
monoamine oxidase	Phenelzine
monoamine oxdase B	Deprenyl

mitochondrial permeability transition pore (MPTP)	Decylubiquinone
MPTP	Ro 5-4864
MPTP opener	Lonidamine
myosin light chain kinase	ML-7
O6-methylguanine-DNA methyltransferase (MGMT)	Benzylguanine
ornithine decarboxylase (ODC)	DFMO
PKG	KT 5823
PKG	Rp-8-CPT-cGMPS
PPAR-a	MK 886
PPAR-a activator	Clofibrate
PPAR-g	BADGE
PPAR-g activator	Troglitazone
reverse transcriptase	AZT
reverse transcriptase	Nalidixic acid
RNA polymerase	a-Amanitin
telomerase	MST-312
telomerase	b-Rubromycin
TGF-b receptor	SB 431542
spermidine/spermine N1-acetyltransferase (SSAT) activator	N1,N12-Diethylspermine (BESpm)
sphingosine N-acyltransferase	Fumonisin B1
AK	ABT-702
AKT	Akt Inhibitor IV
AKT	Akt Inhibitor VIII, Isozyme-Selective, Akti-1/2
AKT	Akt Inhibitor XI
AMPK	compound C
ATM	ATM/ATR kinase inhibitor
ATM	ATM kinase inhibitor
Aurora	Aurora kinase/cdk inhibitor
Aurora	Aurora kinase inhibitor II
Aurora	Aurora kinase inhibitor III
Bcr-abl	AG957
BTK	LFM-A13
BTK	Terreic acid
CAMKII	KN-93
CAMKII	KN-62
CAMKII	Lavendustin C
CDK	Kenpaullone
CDK	purvalanol A
CDK	Olomoucine
CDK	Alsterpaullone, 2-cyanoethyl
CDK	Cdk1/2 inhibitor III
CDK	Cdk2/9 inhibitor

CDK	NU6102
CDK	Cdk4 inhibitor
CDK	NSC625987
Chk	SB218078
Chk	isogranulatimide
Chk	Chk2 inhibitor
Chk	Chk2 inhibitor II
CK	Ellagic acid
CK	TBB
CK	DMAT
CK	D4476
Clk	TG003
DGK	Diacylglycerol kinase inhibitor II
DNA-PK	IC60211
eEF2	TX-1918
EGFR	BPIQ-Ⅱ
EGFR	AG1478
EGFR	AG490
FGFR	SU4984
FGFR	SU5402
Flt-3	Flt-3 Inhibitor
Fms	cFMS Receptor Tyrosine Kinase Inhibitor
Fyn	SU6656
GSK	GSK-3 inhibitor IX
GSK	1-Azakenpaullone
GSK	indirubin-3'-monoxime
HER2	AG825
IGF-IR	AG1024
IGF-IR	AGL 2263
IKK	BMS-345541
IKK	IKK-2 inhibitor VI
IRAK	IRAK-1/4 inhibitor
Jak	JAK Inhibitor I
Jak	JAK3 Inhibitor VI
JNK	SP600125
JNK	JNK inhibitor VIII
Lck	Damnacanthal
Lck	PP2
MAPK	ERK inhibitor II
MEK	PD98059
MEK	U-0126
MEK	MEK inhibitor I

Met	SU11274
MLCK	ML-7
p38	SB202190
p38	SB239063
PDGFR	AG1296
PDGFR	SU11652
PDGFR	PDGF receptor tyrosine kinase inhibitor V
PDGFR	PDGF receptor tyrosine kinase inhibitor IV
PI3K	LY-294002
PI3K	Wortmannin
PKA	H-89
PKA	4-cyano-3-methylisoquinoline
PKC	Bisindolymaleimide I, HCl
PKC	Go7874
PKG	Rp-8-CPT-cGMPS
PKG	KT5823
PKR	PKR inhibitor
Raf	RAF1 kinase inhibitor I
Raf	ZM 336372
ROCK	H-1152
ROCK	Y-27632
Hsp90	radicicol
Src	PP1 analog
Syk	Syk inhibitor
TGF-βRI	SB431542
TGF-βRI	TGF-b RI kinase inhibitor II
Tpl2	Tpl2 kinase inhibitor
TrKA	TrkA inhibitor
VEGFR	VEGFR receptor tyrosine kinase inhibitor II
VEGFR	VEGF recptor 2 kinase inhibitor I
VEGFR	SU1498
Bcr-Abl	nilotinib
Multi-kinases	sorafenib
mTOR	temsirolimus
EGFR/Her2	lapatinib
Bcr-Abl/Kit	imatinib mesylate
Multi-kinases	sunitinib malate
EGFR	gefitinib
HDAC	vorinostat
EGFR	erlotinib
Proteasome	bortezomib
Bcr-Abl/Src	dasatinib
mTOR	everolimus

Multi-kinases	pazopanib
Rho/SRF	CCG-1423
PIM	PIM1/2 Kinase Inhibitor V
PIM	PIM1 Inhibitor II
Hedgehog	AY 9944
Hedgehog	cyclopamine
Hedgehog	Jervine
STAT3	WP1066
STAT3	5,15-DPP
Wnt	IWP-2
Wnt	IWR-1-endo
Wnt	FH535
Notch	DAPT
tankyrase-selective PARP	XAV939
pan-PARP	PJ-34
PARP-1/2-selective	Olaparib
antipsychotic drug	chlorpromazine hydrochloride
depression treatment	desipramine hydrochloride
golgi inhibitor	brefeldin A
stress inducer	anisomycin
thalidomide family	thalidomide
thalidomide family	lenalidomide
retinoids	tretinoin
retinoids	tamibarotene
DNA alkylation	temozolomide
EML4-ALK	crizotinib
mTOR	Torkinib
lipase	orlistat
AR	MDV3100
caspase activator	PAC-1
blc-2	ABT-737
G9a	UNC0638
G9a	BIX01294
LSD1	S2101 (LSD1 inhibitor II)
PRMT1	AMI-1
p300	C646
SIRT1	SIRT1 inhibitor III
SIRT1/2	Tenovin-6
HDAC8	PCI-34051
BRD4 bromodomain	(+)-JQ1
Telomerase	TMPyP4
PARP	BSI-201 (Iniparib)
PARP	ABT-888 (Veliparib)

PARP	AG014699 (Rucaparib)
PARP	MK-4827 (Niraparib)
Aurora	ENMD-2076
Aurora	MLN8237
Survivin	YM155
PDK1	OSU-03012
IGF-IR	OSI-906
c-Met	PF-04217903
DNMT	Decitabine
Multi-kinases	Vandetanib
Multi-kinases	Axitinib
BRAF	Vemurafenib
JAK	Ruxolitinib
Hedgehog	Vismodegib
GLI1	Gant61
FGFR	PD173074
ALK	A83-01
GSK-3	BIO
GSK-3	TWS119
GSK-3	CT99021
TGFb-R	LY2157299
TGFb-R	SD208
ALK	LDN193189
ROCK	Thiazovivin

Table 1 SCADS screening. Totally 364 chemicals with 232 targets were examined in this screening.

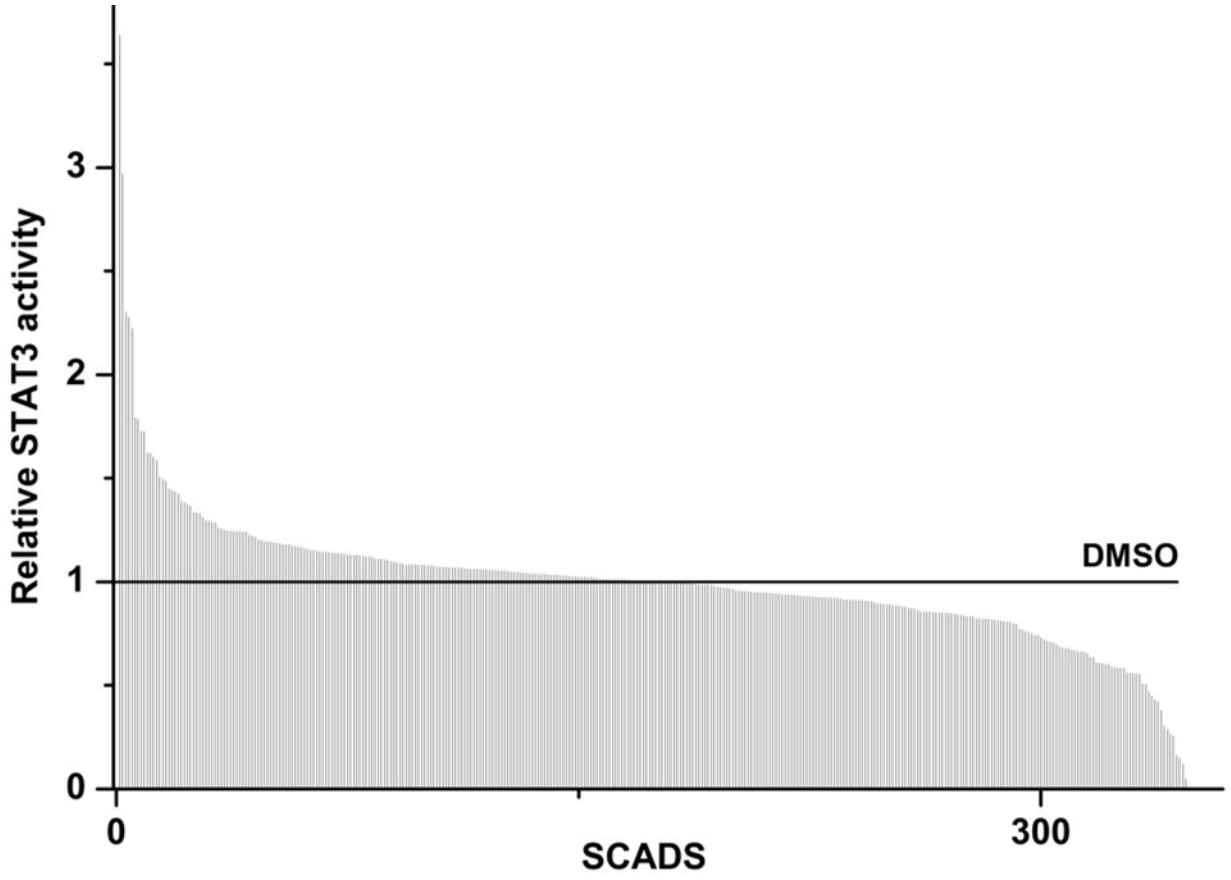

Figure 3-20 SCADS screening. The most right inhibitor is YM155, which dereases STAT3 activity by > 20 fold.

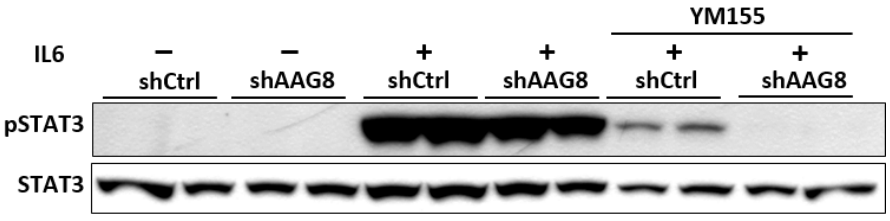

Figure 3-21 AAG8-knockdown DLD-1 cells were treated with or without 100 nM YM155 for 12 h, followed by PBS or 10 ng/ml IL6 treatment for 1 h. Total lysates from control and stable knockdown cell lines were immunoblotted with pSTAT3 antibody; STAT3 served as loading control.

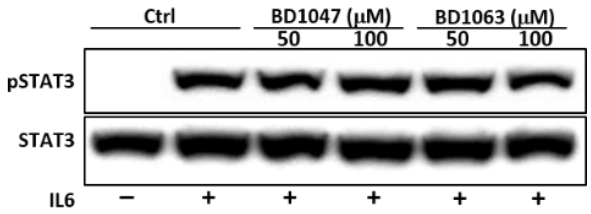

Figure 3-22 Immunoblot of pSTAT3 and STAT3 in DLD-1 cells treated with BD1047 or BD1063 for 12 h, followed by PBS or 10 ng/ml IL6 treatment for 1 h. Total lysates were immunoblotted with pSTAT3 antibody; STAT3 served as loading control.

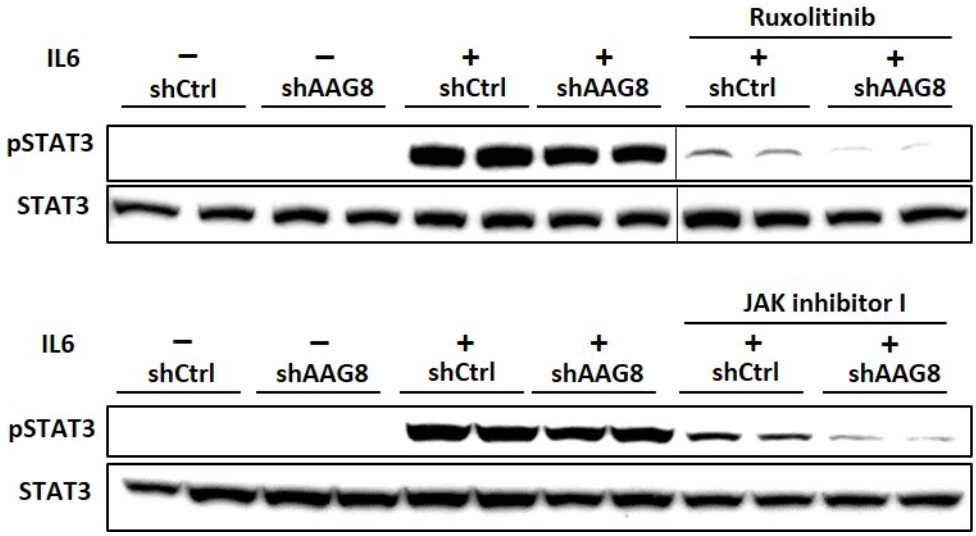

Figure 3-23 Upper: AAG8-knockdown DLD-1 cells were treated with or without 1 μM Ruxolitinib for 20 h, followed by PBS or 10 ng/ml IL6 treatment for 1 h. Juxtaposed lanes that were non-adjacent in the gel is indicated by a vertical black line. Lower: AAG8-knockdown DLD-1 cells were treated with or without 100 nM JAK inhibitor I for 24 h, followed by PBS or 10 ng/ml IL6 treatment for 1 h. Total lysates from control and stable knockdown cells were immunoblotted with pSTAT3 antibody; STAT3 served as loading control. Mean values of pSTAT3 versus STAT3 levels in Ruxolitinib- or JAK inhibitor I-treated cells were labeled with shCtrl cells as standard.

To interrogate the temporal regulation of STAT3 by YM155 in AAG8-knockdown cells, I decreased the time of YM155 treatment to 6 h or increased it to 18 h, respectively (Figure 3-24). YM155 treatment for 6 h affected little to API4, however, AAG8 knockdown led to decreased STAT3 activity in YM155-treated cells. In contrast, YM155 treatment for 18 h led to decreased API4 expression, dramatically decreased STAT3 activity and even decreased total STAT3 level. Notably, AAG8 knockdown further abolished STAT3 activation and reduced API4 in YM155-treated cells. These data exclude the possibility that YM155 inhibits STAT3 activation dependent on AAG8-related signallings. These results together give rise to the conclusion that AAG8 alternatively activates STAT3 in addition to IL6/JAK pathway.

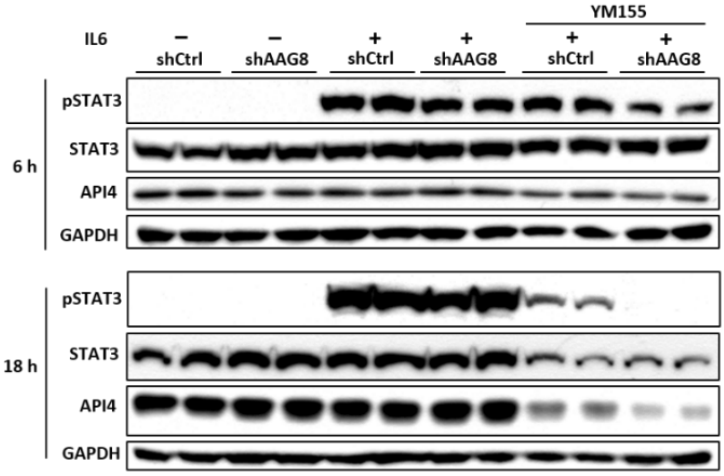

Figure 3-24 Temporal STAT3 regulation by YM155. Immunoblot of pSTAT3, STAT3 and API4 in AAG8-knockdown DLD-1 cells treated with or without YM155 for the indicated time, followed by PBS or 10 ng/ml IL6 treatment for 1 h. Total lysates were immunoblotted with pSTAT3, STAT3 and API4 antibodies; GAPDH served as loading control.

API4 is an anti-apoptotic protein and its transcription can be concurrently modulated by several transcription factors such as STAT3 [86], β-Catenin and YAP1 [87]. We could not establish the stable API4 knockdown DLD-1 cell line, with the similar report elsewhere [88], due to its cytotoxicity. To investigate

whether API4 is required for IL6-induced STAT3 activation, I transiently knocked down API4 in DLD-1 cells with two specific shRNAs (Figure 3-25). To our surprise, API4 depletion was dispensable for IL6-induced STAT3 phosphorylation in these cells (Figure 3-25). Although YM155 has been principally regarded as an API4 inhibitor, its specificity remains uncertain. As YM155 dramatically decreased IL6-induced STAT3 activation while API4 knockdown did not, I supposed that YM155 might employ other inhibition mechanisms for this inactivation. There are at least two pieces of evidences supporting this argument: Firstly, in Figure 3-24, while YM155 treatment for 6 h did not decrease API4 expression, it had already cooperated with AAG8 knockdown to cooperatively decrease STAT3 activation; Secondly, YM155 directly targets ILF3 (interleukin enhancer-binding factor 3), a transcription factor, to suppress API4 expression [89]. Apparently, some other proteins, in addition to API4, could also be suppressed by ILF3-dependent YM155 treatment. In summary, YM155 appears to be a potent STAT3 inhibitor independent of its suppression on API4.

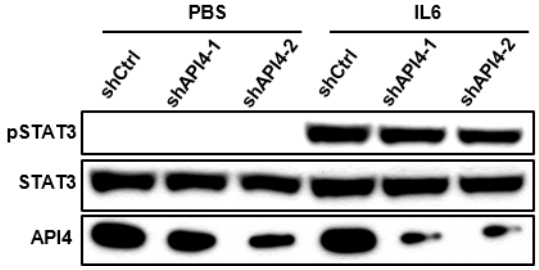

Figure 3-25 Effect of API4 knockdown on IL6-induced STAT3 activation. Immunoblot of pSTAT3, STAT3 and API4 in transient API4-knockdown DLD-1 cells treated with PBS or 10 ng/ml IL6 treatment for 1 h. Total lysates were immunoblotted with pSTAT3, STAT3 and API4 antibodies; STAT3 served as loading control.

Furthermore, though PKM2 (pyruvate kinase M2) was reported to translocate into nucleus and function as a direct kinase for STAT3 phosphorylation at Y705 [90], I could not detect the changes in both expression level and cellular distribution of PKM2 upon AAG8 overexpression or knockdown (Figures 3-26, 3-27),

suggesting that PKM2 might not be involved in AAG8-induced STAT3 activation. Taken together, our data identified AAG8 as an alternative STAT3 activator in addition to JAKs and PKM2 kinases.

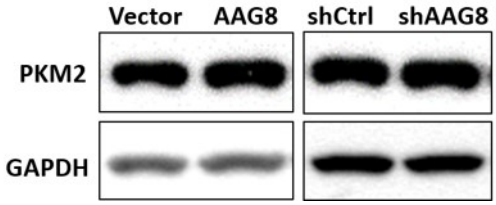

Figure 3-26 Immunoblot of PKM2 in DLD-1 cells with either AAG8 overexpression (left) or knockdown (right). Total lysates were immunoblotted with AAG8 antibody; GAPDH served as loading control.

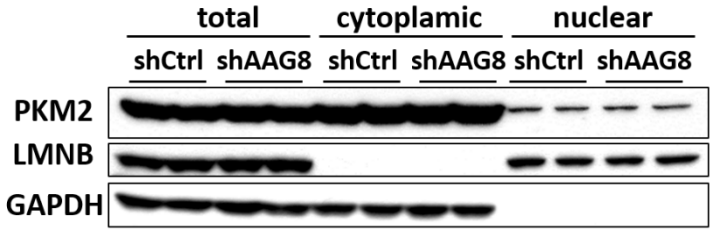

Figure 3-27 Immunoblot of PKM2 of total, cytoplasmic and nuclear fractions in AAG8-knockdown HCT116 cells. Lysates of indicated fractions were immunoblotted with PKM2 antibody. LMNB served as loading control for the nuclear fraction. GAPDH served as loading control for total and cytoplasmic fractions.

3.4 Combined inhibition of AAG8 and JAK signalling

I then supposed that combining YM155 and AAG8 knockdown could cooperatively suppress STAT3 activation and cancer cell growth. Accordingly, I observed that YM155 treatment significantly limited DLD-1 cell growth in 3D culture, which was enhanced by AAG8 knockdown (Figure 3-28), suggesting the collaborative antitumor effects by the combined inhibition. Similarly, AAG8 knockdown significantly slowed the proliferation of DLD-1 cells treated with the JAK inhibitor JSI-124 (Figure 3-29) and JAK3 Inhibitor VI (Figure 3-30), respectively.

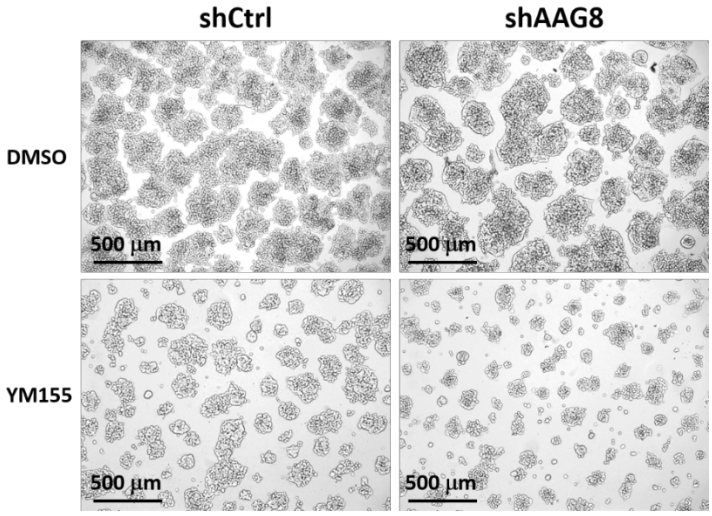

Figure 3-28 Phase contrast images showing acinar morphology of the indicated DLD-1 cells in 3D culture on day 5 after treatment with or without 100 nM YM155.

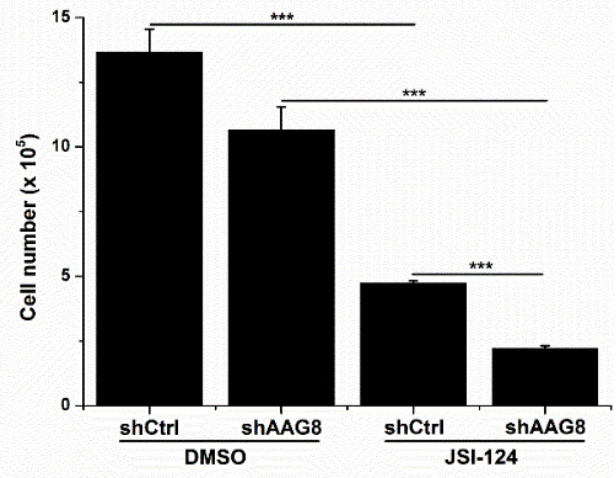

Figure 3-29 Growth assay of AAG8-knockdown DLD-1 cells treated with 1 μM JSI-124 (JAK inhibitor) for 24 h. Initial cell number = 6×10^5. n = 3. Error bars (s.e.m.) are indicated. *** $p < 0.001$ (one way ANOVA followed by Tukey's test).

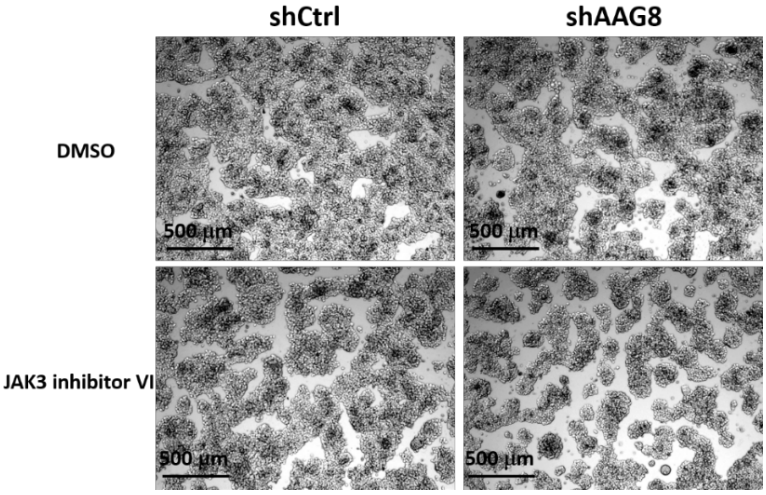

Figure 3-30 Phase contrast images showing acinar morphology of the indicated DLD-1 cells in 3D culture on day 10 after treatment with or without 100 nM JAK3 inhibitor VI.

4. Discussion

In this study, I showed that AAG8, a chaperon protein, promotes carcinogenesis by activating STAT3. Inhibition of AAG8 by antagonists or shRNA efficiently suppressed cancer cell growth in vitro and tumor formation in vivo. Furthermore, from analysis using a drug screening, I pinpoint AAG8 as an alternative STAT3 activator in addition to IL6/JAK signalling. This study elucidates, for the first time, the critical roles of AAG8 in regulating JAK/STAT3 signalling pathway, though previous studies demonstrated that AAG8 associated with several ion channels and/or receptors to regulate cellular ion signalling.[34,35]

Although an AAG8 antagonist has been assessed for pain treatment in phase I studies [91], few have been tested for their anti-cancer property. I evaluated the anti-tumor effects of AAG8 antagonists, thus suggested the novel use of classical neurological drugs on cancer treatment. Some synthesized AAG8 ligands have been reported to specifically bind to AAG8 in the nanomolar range [15]. Further efforts are needed to determine whether the anti-cancer ability of AAG8 antagonists could be translated in vivo.

At present, the exact mechanisms by which AAG8 activates STAT3 is uncertain. STAT3 phosphorylation on Y705 is concurrently and tightly controlled by multiple kinases and protein tyrosine phosphatases, which are a large and structurally diverse family of enzymes that catalyze the dephosphorylation. I demonstrated that STAT3 kinases are dispensable in AAG8-induced STAT3 activation. However, there is possibility that dephosphorylation might account for AAG8-related regulation. For instance, PTPMeg2 is a physiologic STAT3 phosphatase that can directly dephosphorylate STAT3 at the Tyr705 residue [92]. This possibility merits future detailed evaluation.

Despite great efforts focusing on STAT3 for cancer therapy, few efficient strategies have been developed [93]. Single usage of chemical drugs targeting upstream kinases of STAT3, such as JAK2 inhibitors, often results in drug insensitivity due to acquired resistance [94]. In the anticancer drugs screening, I identified YM155 as a potent STAT3 suppressant, suggesting that YM155 blocks the signalling activities which are absolutely required for IL6-induced STAT3 activation. I further illustrated that combined inhibition of

AAG8 and IL6/JAK signalling more efficiently limits cancer cell growth. As single use of both JAK inhibitors and API4 inhibitor YM155 has clinical limitations [94,95], our drug combination strategy provides a promising therapeutic approach for increasing the antitumor efficacy and decreasing drug resistance.

At least five lines of evidences have supported the notion that AAG8 antagonists have overwhelmingly higher specificity in cancer cells than in normal cells:

Evidence 1: AAG8 knockout mouse.

AAG8 knockout mice were created in 2009 and with this knockout mouse model, the hallucinogen N,N-Dimethyltryptamine (DMT) has been identified as an endogenous agonist of AAG8.[96] Strangely, the mice demonstrated no overt phenotype. As expected, however, they did lack locomotor response to the AAG8 ligand (+)-SKF-10,047 and displayed reduced response to formalin-induced pain. These findings indicate that loss of AAG8 affects little on normal body cells except for the neurology system.

Evidence 2: Clinical study of AAG8 antagonist.

The safety, tolerability and pharmacokinetics of an AAG8 antagonist, S1RA, have been assessed in the clinical phase I studies for pain treatment. As a result, S1RA exhibited an acceptable safety, tolerability, pharmacodynamic and pharmacokinetic profile in healthy subjects over the dose range studied, though the most common side effects were headache and dizziness.[91]. These clinical data support the great potential of AAG8 antagonists as drugs for feasible application.

Evidence 3: 100 μM BD1047 did not affect mouse hippocampal cells.

Exogenously, a plethora of ligands of AAG8 have been synthesized.[37,38] BD1047 and its analogue BD1063 are the two specific AAG8 antagonists which have been widely used to elaborate the functions of AAG8, especially in neuroscience. Consistent with the tiny changes of phenotype in AAG8 knockout mice, 100 μM BD1047 (the routinely used concentration in vitro, I also used this concentration in my studies)

treatment of mouse organotypic hippocampal slice cultures (normal cells) for 24 h did not affect cell growth (Figure 3-31).[97]

Percent control PI uptake in CTRL, CTRL + BD1047, 100 μM METH w/d, 100 μM METH w/d + BD1047 treated tissue in the CA1 region of the hippocampus.

CA1	Percent CTRL PI uptake
CTRL	100 ± 5.215
CTRL + BD1047	99.9 ± 5.477
100 μM METH w/d	129.4940 ± 4.3210
100 μM METH w/d + BD1047	126.7 ± 9.107

Figure 3-31 Mouse organotypic hippocampal slice cultures treated with or without 100 μM BD1047 and cell viability was indicated by propidium iodide (PI) staining. (Smith, K. J. *et al.* Neuroscience letters, 2010)

Evidence 4: 100 μM BD1047 did not affect human retinal cells.

AAG8 stimulation is reported to protect against oxidative stress. AAG8 expression is markedly increased in response to H_2O_2 in human lens cells. Application of AAG8 agonist significantly inhibited the H_2O_2 induced cell death and also suppressed the oxidative stress induced reduction of pro-caspase 12 and suppressed the induction of the ER stress proteins BiP and EIF2α. On the other hand, AAG8 agonist protects human lenses against apoptotic cell death, LDH release and against H_2O_2 induced opacification.[37] In agreement with the nontoxicity to mouse organotypic hippocampal slice cellls,[97] one study also showed that treatment with the same concentration of BD1047, as well as another AAG8 antagonist, NE-100, did not decrease the cell viability of human retinal pigment epithelial cells (Figure 3-32).[98] As the figure indicates, BD1047 treatment even increased the percentage of cell viability, indicating the nontoxicity of AAG8 antagonists on normal cells.

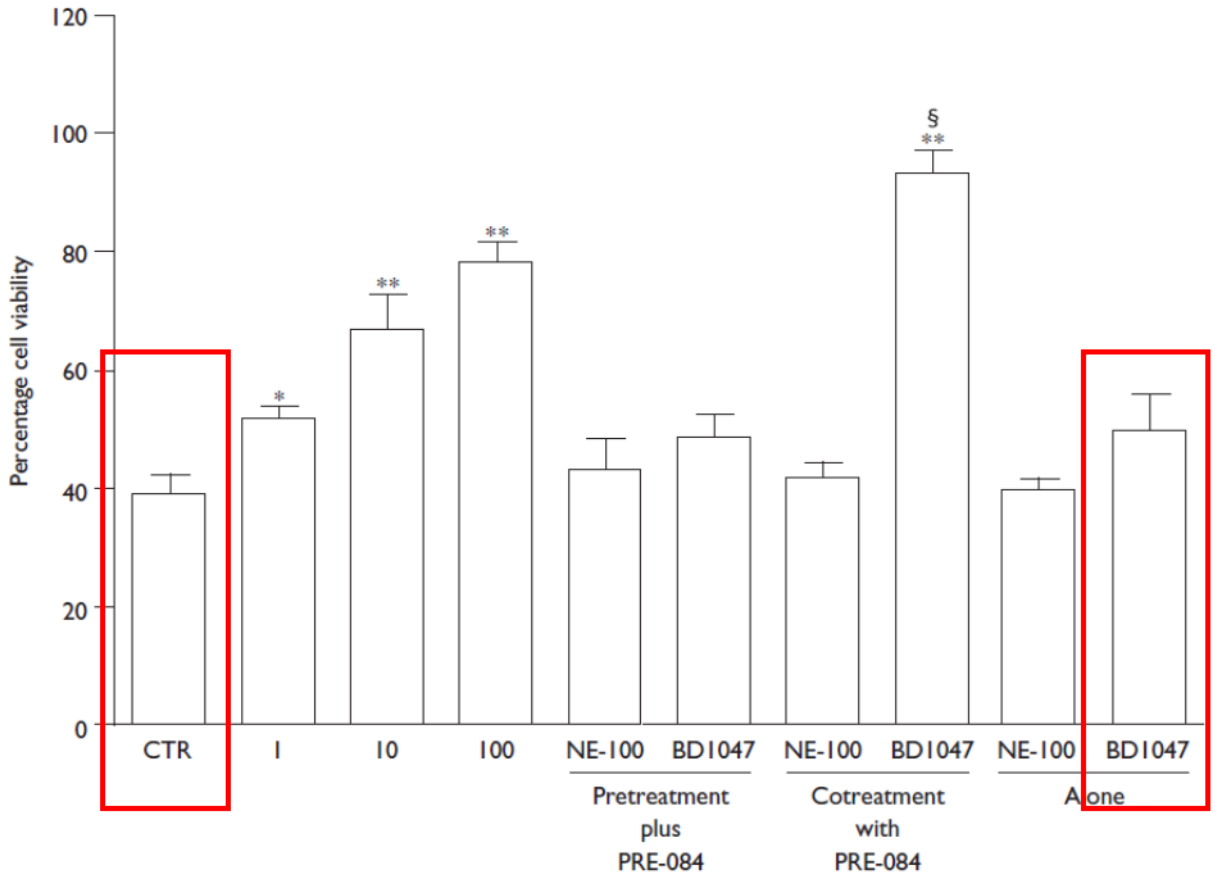

Figure 3-32 Effects of 100 μM BD1047 on death of ARPE-19 cells (human retinal pigment epithelium cells). (Bucolo, C. *et al*. Neuroreport, 2006)

Evidence 5: AAG8 overexpression in cancer serves as the antagonist target.

As AAG8 is overexpressed in the majority of cancer types, especially for melanoma. The upregulated AAG8 in cancer cells presents a preferential target for AAG8 antagonists. Accordingly, in all the cancer cells we tested (Table 2), AAG8 antagonists showed dramatic growth inhibitory effects on these cells. Importantly, all the results from gain- or loss-of-function studies, both in vitro and in vivo, are consistent. Our investigation of AAG8 in cancer cells, integrated with the published data, demonstrated that while AAG8 impacts little on normal body cells, it particularly play vital roles in carcinogenesis, Conclusively, specifically targeting AAG8 can be an efficient way for cancer therapy with minor side effects.

Cell line	Cancer type	Antagonist	Overexpression	Knockdown	Xenograft	STAT3
DLD1	Colon	◯	◯	◯	◯	◯
COLO205	Colon	◯				
AGS	Gastric	◯	◯	◯		◯
MKN7	Gastric	◯				
PANC1	Pancreatic	◯				◯
MSTO-211H	Mesothelioma	◯				
B16	Melanoma	◯				◯

◯: Experiment performed in this study

Table 2 Summary of the cancer cell lines and investigative methods used in this study.

Chapter 4 Conclusion and Perspective

Drug resistance presents a challenge to the treatment of cancer patients, especially for melanomas, most of which are caused by the hyperactivation of MAPK signaling pathway. Innate or acquired drug-resistant relapse calls for the investigation of the resistant mechanisms and new anti-cancer drugs to provide implications for the ultimate goal of curative therapy. This study discovered AAG8 antagonists as new MEK inhibitors in melanoma cells and propose a novel drug combination strategy by presenting the experimental evidences. Specific antagonism of AAG8, efficiently suppresses melanoma cell growth and migration through, at least in part, the inactivation of the RAS-CRAF-MEK signaling pathway. We further demonstrate that melanoma cells that are resistant to AAG8 antagonist harbor refractory CRAF-MEK activity. MEK acts as a central mediator for anti-cancer effects and also for the resistance mechanism, leading to my proposal of tandem AAG8-MEK inhibition in melanoma cells. Combination of AAG8 antagonist and very low concentration of a MEK inhibitor cooperatively restricts the growth of drug-resistant cells.

In addition, the present study characterized AAG8 as an oncoprotein in multiple types of cancers through investigating its cancer-promoting effects and the underlying mechanisms. I uniquely uncovered the molecular clues that AAG8 is an alternative upstream STAT3 activator in addition to IL6/JAK signalling pathway. Tandem inhibition of AAG8 and JAK signalling cooperatively suppresses cancer cell growth. Taken together, these findings shed light on the fundamental evidences for identification of AAG8 as a potential target for cancer prevention, and highlight the importance of ER chaperon proteins in contributing to JAK/STAT signalling and carcinogenesis.

Despite my characterization of AAG8 as an oncoprotein and the elucidation of the molecular mechanisms of AAG8 and it antagonists in cancer cells, how AAG8 directly regulates RAS and STAT3 activity has been currently unsolved. Further efforts should be made to seek the direct interacting partners of AAG8 or investigate the related involvement of AAG8 in some singalling cascades to clarify the activation

mechanisms. It is also unclear whether AAG8-induced RAS activation and STAT3 activation could interplay with each other. Since proteins fulfill their functions by protein-protein interactions, generating an in vivo AAG8 interactome[99] would be valuable for further explaining the mechanisms. The protein(s) that interact with AAG8 might serve as the common mediator(s) for the activation of the oncogenetic signalling pathways such as MAPK and JAK/STAT, and this would also explain the possible connections between AAG8-induced RAS activation and STAT3 activation. In such cases, AAG8 antagonists would disturb the interactions of AAG8 and its partners, and therefore inhibit AAG8 functions.

In addition to AAG8, the sigma-2 receptor (σ2R) is a sigma receptor subtype which preferentially binds to siramesine. Unlike sigma-1 receptor, it has not yet been cloned. Since the AAG8 knockout mice show no obvious phenotypic change, this might be due to the genetic redundancy. However, knowledge of σ2R is extremely limited and the fundamental research of σ2R, such as cloning of this gene, should be addressed firstly to further test the hypothesis of genetic redundancy.

Cellar distribution or translocation is another promising topic for illustrating the proper functions of proteins.[100] Previous investigations have also points out the importance of the translocation of AAG8 between ER membrane and cell membrane in the neurologic response.[34] It has been well believed that AAG8 is a membrane-tethered protein that shuffles among the membrane structures in the cells, and this may provide a possible clue that AAG8 may interact with the membrane proteins, especially the receptor complexes on cell membrane, to impact on the oncogenetic signalling pathways. Supporting this, it was found that AAG8 directly bound to the Kv1.2 potassium channel on cell membrane to facilitate the K^+ current.[34] Future work should be aiming at the discovery of the constant or dynamic interactions between AAG8 and other membrane proteins or complexes.

Moreover, since my studies imply that AAG8 might be a promising target for cancer therapy, especially in melanoma and colon cancer, and according drug combination strategies have been proposed based on the fundamental data, further in vivo and preclinical trials should be made to confirm their efficacy. Importantly, AAG8 antagonists with higher binding affinity and specificity should be designed and synthesized to decrease the using dosage and their side effects, these antagonists would become promising

useful drugs in the combination with the current used clinical chemicals for cancer therapy and even other disease control.

References

1 Yoshimoto, S. *et al.* Obesity-induced gut microbial metabolite promotes liver cancer through senescence secretome. *Nature* **499**, 97-+, doi:Doi 10.1038/Nature12347 (2013).

2 Hanahan, D. & Weinberg, R. A. Hallmarks of cancer: the next generation. *Cell* **144**, 646-674, doi:10.1016/j.cell.2011.02.013 (2011).

3 Wilson, T. R. *et al.* Widespread potential for growth-factor-driven resistance to anticancer kinase inhibitors. *Nature* **487**, 505-U1652, doi:Doi 10.1038/Nature11249 (2012).

4 Muller, F. L. *et al.* Passenger deletions generate therapeutic vulnerabilities in cancer. *Nature* **488**, 337-+, doi:Doi 10.1038/Nature11331 (2012).

5 Castets, M. *et al.* DCC constrains tumour progression via its dependence receptor activity. *Nature* **482**, 534-U259, doi:Doi 10.1038/Nature10708 (2012).

6 Krimpenfort, P. *et al.* Deleted in colorectal carcinoma suppresses metastasis in p53-deficient mammary tumours. *Nature* **482**, 538-U134, doi:Doi 10.1038/Nature10790 (2012).

7 Maddocks, O. D. K. *et al.* Serine starvation induces stress and p53-dependent metabolic remodelling in cancer cells. *Nature* **493**, 542-+, doi:Doi 10.1038/Nature11743 (2013).

8 Hsieh, A. C. *et al.* The translational landscape of mTOR signalling steers cancer initiation and metastasis. *Nature* **485**, 55-U196, doi:Doi 10.1038/Nature10912 (2012).

9 Jeon, S. M., Chandel, N. S. & Hay, N. AMPK regulates NADPH homeostasis to promote tumour cell survival during energy stress. *Nature* **485**, 661-+, doi:Doi 10.1038/Nature11066 (2012).

10 Qin, J. *et al.* COUP-TFII inhibits TGF-beta-induced growth barrier to promote prostate tumorigenesis. *Nature* **493**, 236-U252, doi:Doi 10.1038/Nature11674 (2013).

11 Kumar, M. S. *et al.* HMGA2 functions as a competing endogenous RNA to promote lung cancer progression. *Nature* **505**, 212-+, doi:Doi 10.1038/Nature12785 (2014).

12 Ortega-Roldan, J. L., Ossa, F. & Schnell, J. R. Characterization of the Human Sigma-1 Receptor Chaperone Domain Structure and Binding Immunoglobulin Protein (BiP) Interactions. *J Biol Chem* **288**, 21448-21457, doi:DOI 10.1074/jbc.M113.450379 (2013).

13 Chu, U. B., Ramachandran, S., Hajipour, A. R. & Ruoho, A. E. Photoaffinity Labeling of the Sigma-1 Receptor with N-[3-(4-Nitrophenyl)propyl]-N-dodecylamine: Evidence of Receptor Dimers. *Biochemistry-Us* **52**, 859-868, doi:Doi 10.1021/Bi301517u (2013).

14 Hayashi, T. & Fujimoto, M. Detergent-Resistant Microdomains Determine the Localization of sigma-1 Receptors to the Endoplasmic Reticulum-Mitochondria Junction. *Mol Pharmacol* **77**, 517-528, doi:DOI 10.1124/mol.109.062539 (2010).

15 Marriott, K. S. C., Prasad, M., Thapliyal, V. & Bose, H. S. sigma-1 Receptor at the Mitochondrial-Associated Endoplasmic Reticulum Membrane Is Responsible for Mitochondrial Metabolic Regulation. *J Pharmacol Exp Ther* **343**, 578-586, doi:DOI 10.1124/jpet.112.198168 (2012).

16 Hayashi, T., Hayashi, E., Fujimoto, M., Sprong, H. & Su, T. P. The Lifetime of UDP-galactose: Ceramide Galactosyltransferase Is Controlled by a Distinct Endoplasmic Reticulum-associated Degradation (ERAD) Regulated by Sigma-1 Receptor Chaperones. *J Biol Chem* **287**, 43156-43169, doi:DOI 10.1074/jbc.M112.380444 (2012).

17 Mori, T., Hayashi, T., Hayashi, E. & Su, T. P. Sigma-1 Receptor Chaperone at the ER-Mitochondrion Interface Mediates the Mitochondrion-ER-Nucleus Signaling for Cellular Survival. *Plos One* **8**, doi:ARTN e76941DOI 10.1371/journal.pone.0076941 (2013).

18 Al-Saif, A., Al-Mohanna, F. & Bohlega, S. A mutation in sigma-1 receptor causes juvenile amyotrophic lateral sclerosis. *Ann Neurol* **70**, 913-919, doi:Doi 10.1002/Ana.22534 (2011).

19 Luty, A. A. *et al.* Sigma Nonopioid Intracellular Receptor 1 Mutations Cause Frontotemporal Lobar Degeneration-Motor Neuron Disease. *Ann Neurol* **68**, 639-649, doi:Doi 10.1002/Ana.22274 (2010).

20 Ruscher, K. *et al.* The sigma-1 receptor enhances brain plasticity and functional recovery after experimental stroke. *Brain* **134**, 732-746, doi:Doi 10.1093/Brain/Awq367 (2011).

21 Navarro, G. *et al.* Direct involvement of sigma-1 receptors in the dopamine D-1 receptor-mediated effects of cocaine. *P Natl Acad Sci USA* **107**, 18676-18681, doi:DOI 10.1073/pnas.1008911107 (2010).

22 Tsai, S. Y. *et al.* Sigma-1 receptors regulate hippocampal dendritic spine formation via a free radical-sensitive mechanism involving Rac1.GTP pathway. *P Natl Acad Sci USA* **106**, 22468-22473, doi:DOI 10.1073/pnas.0909089106 (2009).

23 Sabino, V. *et al.* The sigma-Receptor Antagonist BD-1063 Decreases Ethanol Intake and Reinforcement in Animal Models of Excessive Drinking. *Neuropsychopharmacol* **34**, 1482-1493, doi:Doi 10.1038/Npp.2008.192 (2009).

24 Yao, H. H. *et al.* Cocaine Hijacks sigma 1 Receptor to Initiate Induction of Activated Leukocyte Cell Adhesion Molecule: Implication for Increased Monocyte Adhesion and Migration in the CNS. *J Neurosci* **31**, 5942-5955, doi:Doi 10.1523/Jneurosci.5618-10.2011 (2011).

25 Ishikawa, M. *et al.* High occupancy of sigma(1) receptors in the human brain after single oral administration of donepezil: a positron emission tomography study using [C-11]SA4503. *Int J Neuropsychoph* **12**, 1127-1131, doi:Doi 10.1017/S1461145709990204 (2009).

26 Fu, Y. M. *et al.* Sigma-1 receptors amplify dopamine D1 receptor signaling at presynaptic sites in the prelimbic cortex. *Bba-Mol Cell Res* **1803**, 1396-1408, doi:DOI 10.1016/j.bbamcr.2010.08.005 (2010).

27 Yang, Z. J., Carter, E. L., Torbey, M. T., Martin, L. J. & Koehler, R. C. Sigma receptor ligand 4-phenyl-1-(4-phenylbutyl)-piperidine modulates neuronal nitric oxide synthase/postsynaptic density-95 coupling mechanisms and protects against neonatal ischemic degeneration of striatal

neurons. *Experimental neurology* **221**, 166-174, doi:DOI 10.1016/j.expneurol.2009.10.019 (2010).

28 Toussaint, M. *et al.* Tic hydantoin sigma-1 agonist: Pharmacological characterization on cocaine-induced stimulant and appetitive effects. *Eur Neuropsychopharm* **19**, 504-515, doi:DOI 10.1016/j.euroneuro.2009.01.008 (2009).

29 Paschos, K. A., Veletza, S. & Chatzaki, E. Neuropeptide and Sigma Receptors as Novel Therapeutic Targets for the Pharmacotherapy of Depression. *Cns Drugs* **23**, 755-772 (2009).

30 Hiramatsu, N. *et al.* Synergistic effect of 5-HT1A and sigma(1) receptor activation on prefrontal dopaminergic transmission under circulating steroid deficiency. *Neuropharmacology* **75**, 53-61, doi:DOI 10.1016/j.neuropharm.2013.06.026 (2013).

31 Sanchez-Fernandez, C. *et al.* Potentiation of morphine-induced mechanical antinociception by sigma(1) receptor inhibition: Role of peripheral sigma(1) receptors. *Neuropharmacology* **70**, 348-358, doi:DOI 10.1016/j.neuropharm.2013.03.002 (2013).

32 Yang, R. *et al.* Anti-amnesic effect of neurosteroid PREGS in A beta(25-35)-injected mice through sigma(1) receptor- and alpha 7nAChR-mediated neuroprotection. *Neuropharmacology* **63**, 1042-1050, doi:DOI 10.1016/j.neuropharm.2012.07.035 (2012).

33 Roh, D. H. *et al.* Spinal neuronal NOS activation mediates sigma-1 receptor-induced mechanical and thermal hypersensitivity in mice: involvement of PKC-dependent GluN1 phosphorylation. *Brit J Pharmacol* **163**, 1707-1720, doi:DOI 10.1111/j.1476-5381.2011.01316.x (2011).

34 Kourrich, S. *et al.* Dynamic Interaction between Sigma-1 Receptor and Kv1.2 Shapes Neuronal and Behavioral Responses to Cocaine. *Cell* **152**, 236-247, doi:DOI 10.1016/j.cell.2012.12.004 (2013).

35 Balasuriya, D. *et al.* The Sigma-1 Receptor Binds to the Nav1.5 Voltage-gated Na+ Channel with 4-Fold Symmetry. *J Biol Chem* **287**, 37021-37029, doi:DOI 10.1074/jbc.M112.382077 (2012).

36 Balasuriya, D., Stewart, A. P. & Edwardson, J. M. The sigma-1 Receptor Interacts Directly with GluN1 But Not GluN2A in the GluN1/GluN2A NMDA Receptor. *J Neurosci* **33**, 18219-18224, doi:Doi 10.1523/Jneurosci.3360-13.2013 (2013).

37 Wang, L. X. *et al.* Sigma 1 receptor stimulation protects against oxidative damage through suppression of the ER stress responses in the human lens. *Mech Ageing Dev* **133**, 665-674, doi:DOI 10.1016/j.mad.2012.09.005 (2012).

38 Hyrskyluoto, A. *et al.* Sigma-1 receptor agonist PRE084 is protective against mutant huntingtin-induced cell degeneration: involvement of calpastatin and the NF-kappa B pathway. *Cell Death Dis* **4**, doi:ARTN e646DOI 10.1038/cddis.2013.170 (2013).

39 Gomez-Soler, M. *et al.* Predicting the Antinociceptive Efficacy of sigma(1) Receptor Ligands by a Novel Receptor Fluorescence Resonance Energy Transfer (FRET) Based Biosensor. *J Med Chem* **57**, 238-242, doi:Doi 10.1021/Jm401529t (2014).

40 Choi, S. R. *et al.* Spinal sigma-1 receptors activate NADPH oxidase 2 leading to the induction of pain hypersensitivity in mice and mechanical allodynia in neuropathic rats. *Pharmacol Res* **74**, 56-67, doi:DOI 10.1016/j.phrs.2013.05.004 (2013).

41 Moon, J. Y. *et al.* Sigma-1 receptor-mediated increase in spinal p38 MAPK phosphorylation leads to the induction of mechanical allodynia in mice and neuropathic rats. *Experimental neurology* **247**, 383-391, doi:10.1016/j.expneurol.2013.01.004 (2013).

42 Tagashira, H. *et al.* Stimulation of sigma(1)-receptor restores abnormal mitochondrial Ca2+ mobilization and ATP production following cardiac hypertrophy. *Bba-Gen Subjects* **1830**, 3082-3094, doi:DOI 10.1016/j.bbagen.2012.12.029 (2013).

43 Schrock, J. M. *et al.* Sequential Cytoprotective Responses to Sigma1 Ligand-Induced Endoplasmic Reticulum Stresss. *Mol Pharmacol* **84**, 751-762, doi:DOI 10.1124/mol.113.087809 (2013).

44 Piergentili, A. *et al.* Novel Highly Potent and Selective sigma(1) Receptor Antagonists Related to Spipethiane. *J Med Chem* **53**, 1261-1269, doi:Doi 10.1021/Jm901542q (2010).

45 Hatzivassiliou, G. *et al.* Mechanism of MEK inhibition determines efficacy in mutant KRAS- versus BRAF-driven cancers. *Nature* **501**, 232-236, doi:Doi 10.1038/Nature12441 (2013).

46 Barretina, J. *et al.* The Cancer Cell Line Encyclopedia enables predictive modelling of anticancer drug sensitivity. *Nature* **483**, 603-607, doi:Doi 10.1038/Nature11003 (2012).

47 Perez-Mancera, P. A. *et al.* The deubiquitinase USP9X suppresses pancreatic ductal adenocarcinoma. *Nature* **486**, 266-+, doi:Doi 10.1038/Nature11114 (2012).

48 Son, J. *et al.* Glutamine supports pancreatic cancer growth through a KRAS-regulated metabolic pathway. *Nature* **496**, 101-+, doi:Doi 10.1038/Nature12040 (2013).

49 Ostrem, J. M., Peters, U., Sos, M. L., Wells, J. A. & Shokat, K. M. K-Ras(G12C) inhibitors allosterically control GTP affinity and effector interactions. *Nature* **503**, 548-+, doi:Doi 10.1038/Nature12796 (2013).

50 Zimmermann, G. *et al.* Small molecule inhibition of the KRAS-PDE delta interaction impairs oncogenic KRAS signalling. *Nature* **497**, 638-642, doi:Doi 10.1038/Nature12205 (2013).

51 Zaidi, M. R. *et al.* Interferon-gamma links ultraviolet radiation to melanomagenesis in mice. *Nature* **469**, 548-U129, doi:Doi 10.1038/Nature09666 (2011).

52 Bertolotto, C. *et al.* A SUMOylation-defective MITF germline mutation predisposes to melanoma and renal carcinoma. *Nature* **480**, 94-U259, doi:Doi 10.1038/Nature10539 (2011).

53 Bald, T. *et al.* Ultraviolet-radiation-induced inflammation promotes angiotropism and metastasis in melanoma. *Nature* **507**, 109-+, doi:Doi 10.1038/Nature13111 (2014).

54 Ceol, C. J. *et al.* The histone methyltransferase SETDB1 is recurrently amplified in melanoma and accelerates its onset. *Nature* **471**, 513-+, doi:Doi 10.1038/Nature09806 (2011).

55 White, R. M. *et al.* DHODH modulates transcriptional elongation in the neural crest and melanoma. *Nature* **471**, 518-522, doi:Doi 10.1038/Nature09882 (2011).

56 Karreth, F. A. *et al.* In Vivo Identification of Tumor-Suppressive PTEN ceRNAs in an Oncogenic BRAF-Induced Mouse Model of Melanoma. *Cell* **147**, 382-395, doi:DOI 10.1016/j.cell.2011.09.032 (2011).

57 Gaziel-Sovran, A. *et al.* miR-30b/30d Regulation of GalNAc Transferases Enhances Invasion and Immunosuppression during Metastasis. *Cancer Cell* **20**, 104-118, doi:DOI 10.1016/j.ccr.2011.05.027 (2011).

58 Prahallad, A. *et al.* Unresponsiveness of colon cancer to BRAF(V600E) inhibition through feedback activation of EGFR. *Nature* **483**, 100-U146, doi:Doi 10.1038/Nature10868 (2012).

59 Das Thakur, M. *et al.* Modelling vemurafenib resistance in melanoma reveals a strategy to forestall drug resistance. *Nature* **494**, 251-255, doi:Doi 10.1038/Nature11814 (2013).

60 Landsberg, J. *et al.* Melanomas resist T-cell therapy through inflammation-induced reversible dedifferentiation. *Nature* **490**, 412-+, doi:Doi 10.1038/Nature11538 (2012).

61 Kaplon, J. *et al.* A key role for mitochondrial gatekeeper pyruvate dehydrogenase in oncogene-induced senescence. *Nature* **498**, 109-+, doi:Doi 10.1038/Nature12154 (2013).

62 Dar, A. C., Das, T. K., Shokat, K. M. & Cagan, R. L. Chemical genetic discovery of targets and anti-targets for cancer polypharmacology. *Nature* **486**, 80-84, doi:10.1038/nature11127 (2012).

63 Garnett, M. J. *et al.* Systematic identification of genomic markers of drug sensitivity in cancer cells. *Nature* **483**, 570-U587, doi:Doi 10.1038/Nature11005 (2012).

64 Murtaza, M. *et al.* Non-invasive analysis of acquired resistance to cancer therapy by sequencing of plasma DNA. *Nature* **497**, 108-+, doi:Doi 10.1038/Nature12065 (2013).

65 Straussman, R. *et al.* Tumour micro-environment elicits innate resistance to RAF inhibitors through HGF secretion. *Nature* **487**, 500-U118, doi:Doi 10.1038/Nature11183 (2012).

66 Chen, Z. *et al.* A murine lung cancer co-clinical trial identifies genetic modifiers of therapeutic response. *Nature* **483**, 613-617, doi:Doi 10.1038/Nature10937 (2012).

67 Lee, G. Y., Kenny, P. A., Lee, E. H. & Bissell, M. J. Three-dimensional culture models of normal and malignant breast epithelial cells. *Nat Methods* **4**, 359-365, doi:Doi 10.1038/Nmeth1015 (2007).

68 Montagner, M. *et al.* SHARP1 suppresses breast cancer metastasis by promoting degradation of hypoxia-inducible factors. *Nature* **487**, 380-384, doi:Doi 10.1038/Nature11207 (2012).

69 Talantov, D. *et al.* Novel genes associated with malignant melanoma but not benign melanocytic lesions. *Clin Cancer Res* **11**, 7234-7242, doi:Doi 10.1158/1078-0432.Ccr-05-0683 (2005).

70 Amer, M. S. *et al.* Inhibition of endothelial cell Ca2+ entry and transient receptor potential channels by Sigma-1 receptor ligands. *Brit J Pharmacol* **168**, 1445-1455, doi:Doi 10.1111/Bph.12041 (2013).

71 Smith, M. P. *et al.* Effect of SMURF2 Targeting on Susceptibility to MEK Inhibitors in Melanoma. *J Natl Cancer I* **105**, 33-46, doi:Doi 10.1093/Jnci/Djs471 (2013).

72 Hu, J. C. *et al.* Allosteric Activation of Functionally Asymmetric RAF Kinase Dimers. *Cell* **154**, 1036-1046, doi:DOI 10.1016/j.cell.2013.07.046 (2013).

73 Poulikakos, P. I. *et al.* RAF inhibitor resistance is mediated by dimerization of aberrantly spliced BRAF(V600E). *Nature* **480**, 387-U144, doi:Doi 10.1038/Nature10662 (2011).

74 Ferguson, J., Arozarena, I., Ehrhardt, M. & Wellbrock, C. Combination of MEK and SRC inhibition suppresses melanoma cell growth and invasion. *Oncogene* **32**, 86-96, doi:Doi 10.1038/Onc.2012.25 (2013).

75 Johannessen, C. M. *et al.* COT drives resistance to RAF inhibition through MAP kinase pathway reactivation. *Nature* **468**, 968-U370, doi:Doi 10.1038/Nature09627 (2010).

76 Rosenfeldt, M. T. *et al.* p53 status determines the role of autophagy in pancreatic tumour development. *Nature* **504**, 296-+, doi:Doi 10.1038/Nature12865 (2013).

77 Misale, S. *et al.* Emergence of KRAS mutations and acquired resistance to anti-EGFR therapy in colorectal cancer. *Nature* **486**, 532-U131, doi:Doi 10.1038/Nature11156 (2012).

78 Jessen, W. J. *et al.* MEK inhibition exhibits efficacy in human and mouse neurofibromatosis tumors. *J Clin Invest* **123**, 340-347, doi:Doi 10.1172/Jci60578 (2013).

79 Johannessen, C. M. *et al.* A melanocyte lineage program confers resistance to MAP kinase pathway inhibition. *Nature* **504**, 138-+, doi:Doi 10.1038/Nature12688 (2013).

80 Yang, X. X. O. *et al.* The signaling suppressor CIS controls proallergic T cell development and allergic airway inflammation. *Nat Immunol* **14**, 732-+, doi:Doi 10.1038/Ni.2633 (2013).

81 Hatziapostolou, M. *et al.* An HNF4 alpha-miRNA Inflammatory Feedback Circuit Regulates Hepatocellular Oncogenesis. *Cell* **147**, 1233-1247, doi:DOI 10.1016/j.cell.2011.10.043 (2011).

82 Shui, J. W. *et al.* HVEM signalling at mucosal barriers provides host defence against pathogenic bacteria. *Nature* **488**, 222-+, doi:Doi 10.1038/Nature11242 (2012).

83 Sarbassov, D. D., Guertin, D. A., Ali, S. M. & Sabatini, D. M. Phosphorylation and regulation of Akt/PKB by the rictor-mTOR complex. *Science* **307**, 1098-1101, doi:DOI 10.1126/science.1106148 (2005).

84 Shirai, Y. *et al.* Bone Morphogenetic Protein-2 and-4 Play Tumor Suppressive Roles in Human Diffuse-Type Gastric Carcinoma. *Am J Pathol* **179**, 2920-2930, doi:DOI 10.1016/j.ajpath.2011.08.022 (2011).

85 Na, Y. S. *et al.* YM155 Induces EGFR Suppression in Pancreatic Cancer Cells. *Plos One* **7**, doi:ARTN e38625DOI 10.1371/journal.pone.0038625 (2012).

86 Sen, N. *et al.* Signal transducer and activator of transcription 3 (STAT3) and survivin induction by varicella-zoster virus promote replication and skin pathogenesis. *P Natl Acad Sci USA* **109**, 600-605, doi:DOI 10.1073/pnas.1114232109 (2012).

87 Rosenbluh, J. *et al.* beta-Catenin-Driven Cancers Require a YAP1 Transcriptional Complex for Survival and Tumorigenesis. *Cell* **151**, 1457-1473, doi:DOI 10.1016/j.cell.2012.11.026 (2012).

88 Sarthy, A. V. *et al.* Survivin depletion preferentially reduces the survival of activated K-Ras-transformed cells. *Mol Cancer Ther* **6**, 269-276, doi:Doi 10.1158/1535-7163.Mct-06-0560 (2007).

89 Nakamura, N. *et al.* Interleukin Enhancer-binding Factor 3/NF110 Is a Target of YM155, a Suppressant of Survivin. *Mol Cell Proteomics* **11**, doi:DOI 10.1074/mcp.M111.013243 (2012).

90 Gao, X. L., Wang, H. Z., Yang, J. J., Liu, X. W. & Liu, Z. R. Pyruvate Kinase M2 Regulates Gene Transcription by Acting as a Protein Kinase. *Mol Cell* **45**, 598-609, doi:DOI 10.1016/j.molcel.2012.01.001 (2012).

91 Abadias, M., Escriche, M., Vaque, A., Sust, M. & Encina, G. Safety, tolerability and pharmacokinetics of single and multiple doses of a novel sigma-1 receptor antagonist in three randomized phase I studies. *Brit J Clin Pharmaco* **75**, 103-117, doi:DOI 10.1111/j.1365-2125.2012.04333.x (2013).

92 Li, R. *et al.* Niclosamide Overcomes Acquired Resistance to Erlotinib through Suppression of STAT3 in Non-Small Cell Lung Cancer. *Mol Cancer Ther* **12**, 2200-2212, doi:Doi 10.1158/1535-7163.Mct-13-0095 (2013).

93 Sen, M. *et al.* First-in-Human Trial of a STAT3 Decoy Oligonucleotide in Head and Neck Tumors: Implications for Cancer Therapy. *Cancer Discov* **2**, 694-705, doi:Doi 10.1158/2159-8290.Cd-12-0191 (2012).

94 Koppikar, P. *et al.* Heterodimeric JAK-STAT activation as a mechanism of persistence to JAK2 inhibitor therapy. *Nature* **489**, 155-U222, doi:Doi 10.1038/Nature11303 (2012).

95 Kelly, R. J. *et al.* A phase I/II study of sepantronium bromide (YM155, survivin suppressor) with paclitaxel and carboplatin in patients with advanced non-small-cell lung cancer. *Ann Oncol* **24**, 2601-2606, doi:DOI 10.1093/annonc/mdt249 (2013).

96 Fontanilla, D. *et al.* The Hallucinogen N,N-Dimethyltryptamine (DMT) Is an Endogenous Sigma-1 Receptor Regulator. *Science* **323**, 934-937, doi:DOI 10.1126/science.1166127 (2009).

97 Smith, K. J., Butler, T. R. & Prendergast, M. A. Inhibition of sigma-1 receptor reduces N-methyl-D-aspartate induced neuronal injury in methamphetamine-exposed and -naive hippocampi. *Neuroscience letters* **481**, 144-148, doi:10.1016/j.neulet.2010.06.069 (2010).

98 Bucolo, C., Drago, F., Lin, L. R. & Reddy, V. N. Sigma receptor ligands protect human retinal cells against oxidative stress. *Neuroreport* **17**, 287-291, doi:10.1097/01.wnr.0000199469.21734.e1 (2006).

99 Han, K. *et al.* SHANK3 overexpression causes manic-like behaviour with unique pharmacogenetic properties. *Nature* **503**, 72-+, doi:Doi 10.1038/Nature12630 (2013).

100 Koyano, F. *et al.* Ubiquitin is phosphorylated by PINK1 to activate parkin. *Nature* **510**, 162-+, doi:Doi 10.1038/Nature13392 (2014).

Publications

1. **B. Sun** *et al.* AAG8 promotes carcinogenesis by activating STAT3. Cellular Signalling, (2014); published online 12 APR 2014 (DOI: 10.1016/j.cellsig.2014.04.001)
2. **B. Sun** *et al.* Modeling tandem AAG8-MEK inhibition in melanoma cells. Cancer Medicine, (2014); published online 14 MAR 2014 (DOI: 10.1002/cam4.233)
3. J. Du, **B. Sun** *et al.* Metabolites of Cerebellar Neurons and Hippocampal Neurons Play Opposite Roles in Pathogenesis of Alzheimer's Disease. Plos One 4, (2009); published online EpubMay 13 (Artn E5530 Doi 10.1371/Journal.Pone.0005530).
4. J. Du, **B. Sun** *et al.* Antagonist of peroxisome proliferator-activated receptor gamma induces cerebellar amyloid-beta levels and motor dysfunction in APP/PS1 transgenic mice. Biochem Bioph Res Co 384, 357-361 (2009); published online EpubJul 3 (DOI 10.1016/j.bbrc.2009.04.148).
5. J. Du, Y. Liang, F. Xu, **B. Sun** *et al.* Trehalose rescues Alzheimer's disease phenotypes in APP/PS1 transgenic mice. J Pharm Pharmacol 65, 1753-1756 (2013); published online EpubDec (Doi 10.1111/Jphp.12108).

Presentations

Oral Presentations

1. B. Sun, *et al.* Modeling tandem AAG8-MEK inhibition in melanoma cells, 2014 International Congress on Chemical, Biological and Environmental Sciences (ICCBES), Kyoto, 2014

Poster Presentations

1. B. Sun, *et al.* Translational Regulation of E-Cad Expression by SAV1 in Carcinogenesis， 13th Life Science Symposium of the University of Tokyo, 2013, Tokyo
2. B. Sun, *et al.*AAG8 promotes carcinogenesis by activating STAT3, 14th Life Science Symposium of the University of Tokyo, 2014, Tokyo

Acknowledgements

I would like to express my deep gratitude and honest respect to Professor Teruyuki NAGAMUNE (Department of Bioengineering, Department of Chemistry and Biotechnology, Graduate School of Engineering, the University of Tokyo) for his earnest instructions and critical suggestions on all of my research from my entrance to this lab. I would also be sincerely grateful to Dr. Masahiro KAWAHARA (Department of Chemistry and Biotechnology, Graduate School of Engineering, the University of Tokyo) who has directly supervised my entire work during the past three years with his tremendous devoted energies.

I greatly thank Professor Ung-il CHUNG, Professor Kazunori KATAOKA, Professor Yukiko GOTOH and Professor Shinsuke OHBA for their helpful suggestions as referees of this dissertation in spite of busy schedules.

I greatly appreciated the collaboration with Dr. Shigo EHATA (Department of Molecular Pathology, Graduate School of Medicine, the University of Tokyo). I thank Dr. Daizo KOINUMA (Department of Molecular Pathology, Graduate School of Medicine, the University of Tokyo) and Professor Kohei MIYAZONO (Department of Molecular Pathology, Graduate School of Medicine, the University of Tokyo) for their helpful suggestions and discussions.

I would also thank China Government for 3-year scholarship supporting my study in Tokyo. I also appreciate the University of Tokyo and Tsinghua University for providing me the chance to do my research here.

Finally, I thank my parents and friends for their continuous encouragement throughout my long studying life.